Preparation, Size Separation and Chiroptical Properties of Chiral Gold Nanoparticles

---

Thèse présentée à la Faculté des Sciences
Institut de Microtechnique
Université de Neuchâtel

Par

Cyrille Gautier

Acceptée sur proposition du jury :
Prof. T. Bürgi, directeur de thèse
Prof. H. M. Stoeckli-Evans, rapporteur
Prof. J. Lacour, rapporteur

Soutenue le 28 mars 2008

Université de Neuchâtel
2008

Université de Neuchâtel

FACULTE DES SCIENCES
Secrétariat-Décanat de la faculté
- Rue Emile-Argand 11
- CP 158
- CH-2009 Neuchâtel

IMPRIMATUR POUR LA THESE

Preparation, size separation and chiroptical properties of chiral gold nanoparticles

Cyrille GAUTIER

UNIVERSITE DE NEUCHATEL

FACULTE DES SCIENCES

La Faculté des sciences de l'Université de Neuchâtel,
sur le rapport des membres du jury

MM. T. Bürgi (directeur de thèse),
Mme H. Stoeckli-Evans et
J. Lacour (Genève)

autorise l'impression de la présente thèse.

Neuchâtel, le 29 avril 2008

Le doyen :
F. Kessler

UNIVERSITE DE NEUCHATEL
FACULTE DES SCIENCES
Secrétariat - décanat de la faculté
Rue Emile-Argand 11 - CP 158
CH-2009 Neuchâtel
Felix Kessler

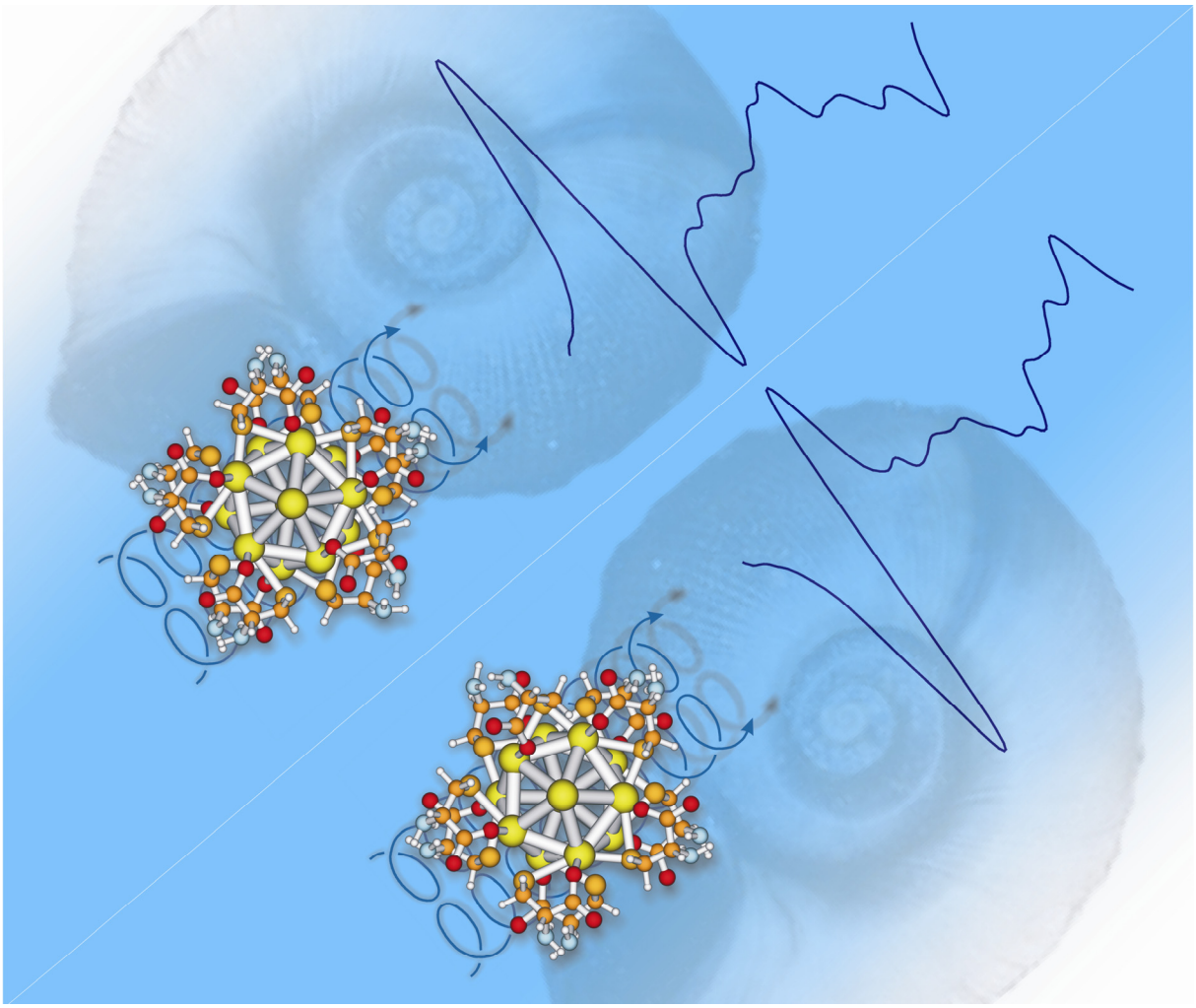

Previous page:

A pictorial illustration of chiral gold nanoparticles covered by the two enantiomers of cysteine.

Table of Contents

Appendix

Acknowledgments

I am deeply indebted to my advisor, Thomas Bürgi, for offering me the chance to join his group and to work in a fascinating field of research. His perpetual energy and enthusiasm (even at three o'clock in the morning) had motivated me throughout the last four years. In addition, he is always accessible and willing to help patiently his students with their research.

I would express my gratitude to my colleagues, Dr. Silvia Angeloni-Suter, Natalia Shalkevich, Dr. Qiaoling Li, Dr. Marco Bieri, Igor Dolamic, Julien Boudon and Dr. Si Satyabrata for all the good moments that we have shared and for their collaboration. I especially thank Julien and Natalia for the many TEM measurements and once again Julien for the nice group website and for his precious help in informatics.

I owe my sincere gratitude to the two apprentices, Joël Monnin and Marie-Josée Breguet and to the students; Rana Afshar, Sebastiano Guerra, Suzy Toscer and Frédéric Queloz who have greatly contributed to the work described in this thesis.

I also would like to thank the NMR services, Heinz Bursian and Dr. Julien Furrer, the staff of the chemical store, Maurice Binggeli and Claire-Lise Rosset, the MS services, Dr. Bernard Jean-Denis and Dr. Armelle Vallat and finally, the X-ray diffraction experts Dr. Antonia Neels and Olha Sereda. Their help and their kindness are greatly acknowledged.

Many thanks to Mrs. Tissot for aid in administrative problems and Philippe Stauffer, André Floreano and Mr. Duvoisin for help in technical problems.

I am grateful also to the Swiss Center for Electronics and Microtechnology (CSEM) in Neuchâtel and especially to Dr. Massoud Dadras for TEM measurements.

Many thanks to Gianni Gasparotto for informatic helps.

Cordial gratitude to the Swiss National Science Foundation for providing funds to support this research and the Swiss National Supercomputing centre (CSCS) for grants of computing time.

Sincere and special appreciation goes to my dearly beloved, Cathia and to Benjamin for their love and patience.

In final instance, this thesis is dedicated to my mother, Francine, and to the memory of my father, Roland, for their unselfish support and encouragement throughout my life.

Keywords

Nanoparticles • Gold • Chirality • Vibrational Circular Dichroism • Surfaces • Chiral Induction • ligand Exchange • Chiral Inversion

Mots Clés

Nanoparticules • Or • Chiralité • Dichroïsme Circulaire Vibrationnel • Surfaces • Induction de Chiralité • Echange de Ligand • Inversion de Chiralité

Summary

The knowledge of surface-molecule interactions is fundamental in order to understand and to take advantage of the physicochemical properties of organic-inorganic hybrid materials. How does a surface react when a molecule adsorbs? How does the molecule adsorb? What is the conformation of the molecule on the surface? This thesis is intended to give some insight on these phenomena.

Monolayer protected nanoparticles can be viewed as the nanometer size analogues of extended hybrid materials. These nanomaterials are furthermore interesting because their physical and chemical properties can easily be tuned for custom requirements by changing their size and their shape. Macro- and nano- hybrid materials have a wide range of potential applications in various fields such as catalysis, sensing, therapy, electronics, nanotechnology and optics.

Due to their solubility, nanoparticles can be manipulated and characterized as simple organic compounds and thus give some answers to our questions. Specifically, nanoparticles studied in this thesis are protected by chiral organic molecules. The chirality of these NPs allows one to use chiroptical techniques which are very sensitive to their three dimensional structures and to extend their wide range of potential application to chiral technologies such as enantioselective catalysis.

The first chapter of the thesis deals with the general properties, the preparation methods and the applications of nanoparticles before to focus in more detail on metallic nanoparticles protected by a monolayer of chiral organic molecules. This chapter also deals with optically active coordination clusters, which correspond to the inferior size limit of chiral metallic nanoparticles and with the very new and few studies of chiral organic nanoparticles. The subnanometer class of gold nanoparticles covered with chiral thiols shows optical activities both in the UV-vis and in the IR.

In this thesis, we have applied for the first time vibrational circular dichroism (VCD) spectroscopy and density functional theory calculations (DFT) to study the conformation of chiral thiols adsorbed on gold nanoparticles by comparison of the calculated and the experimental spectra. Specifically the chapters 2, 3 and 5 describe the preparation and the VCD studies of gold nanoparticles covered respectively with N-acetyl-*L*-cysteine (NAC), N-isobutyryl-cysteine (NIC) and 1,1'-binaphtyl-2,2'dithiol (BINAS). Typically the particles are small, with gold core diameters of about 2 nm and below as determined by transmission electron microscopy (TEM) and UV-vis spectroscopy. Whereas the IR spectra are identical for the gold nanoparticles covered by either N-isobutyryl-*L*-cysteine or N-isobutyryl-*D*-cysteine , the VCD spectra show mirror image relationship (chapter 3). VCD yields detailed structural information on the adsorption mode and on the conformation of the adsorbed thiol. The calculated conformations were in good agreement with those reported for self-assembled-monolayer on extended gold surfaces. The conformation of the two cysteine derivatives, NIC and NAC, is characterized by an interaction of the carboxylate with the gold cluster which represents a second anchoring point beside the strong gold – sulfur bond. Such information is

difficult to obtain by other methods but is thought to be essential for properties like enantiodifferentiation and molecular recognition.

The nanoparticles protected with NIC and BINAS were furthermore separated according to their size by electrophoresis and size exclusion chromatography, respectively. Whereas the optical activity in the IR remained unchanged (see chapter 5), the optical activity in the UV-vis was strongly size dependent (chapter 3 and 4). These results clearly demonstrate the power of chiroptical techniques to selectively probe the conformation of chiral adsorbates in the IR region and the structure of the metallic part in the UV-vis. Meanwhile, the origin of the optical activity located in the metal-based electronic transitions and whether the metal core is intrinsically chiral remain open questions due to the lack of direct structural information.

The size separated particles reveal well-quantized electronic structures in optical absorption spectra and a systematic red shift of the absorption onset as the size of the particle increases. This is due to the quantum size effects and it shows that these small nanoparticles are better described as semiconductor in state of metallic. Some compounds showed identical absorption spectra as analogous particles protected with *L*-glutathione. This shows that these particles have identical core size (Chapter 3) and indicates that the number and arrangement of the absorbed thiol are the same, independent of the two thiols, which have largely different size. Some separated compounds show strong optical activity in the UV-vis and mirror image relationship when covered with opposite enantiomers (Chapter 3, 4 and 6). The observations are consistent with a mechanism based on a chiral footprint on the metal core imparted by the adsorbed ligand. In particular, the VCD studies show that the ligands able to impart optical activity onto the metallic core are attached to the latter by at least two anchoring points. In

addition, BINAS which is a bidentate atropisomeric ligand is particularly well-suited to impart optical activity to the metallic core since the nanoparticles protected with this ligand show the largest anisotropy factors reported so far.

Finally, the last chapter describes thiolate-for-thiolate ligand exchange performed on well defined gold nanoparticles under inert atmosphere without any modification of the core-size. This reaction is faster than the well known core-etching. Surprisingly, if a chiral thiol is exchanged for its opposite enantiomer, the optical activity in the metal-based electronic transitions is reversed although the form of the ECD spectra remains largely unchanged. This shows that the chiral arrangement of metal atoms in the metal particle (surface) can not withstand the driving force imposed by the ligand of opposite absolute configuration. The extent of inversion corresponds to the overall ee of the chiral ligand in the system. If the incoming thiol has a different structure, the electronic transitions in the metal core are slightly modified whereas the absorption onset remains unchanged. These results emphasized the influence of the thiols on the structure of the gold nanoparticles and give insight on the ligand exchange pathways.

Résumé

La connaissance des interactions surface-molécule est fondamentale pour comprendre les propriétés physico-chimiques des matériaux hybrides et développer leurs applications. Comment réagit une surface quand une molécule s'adsorbe ? Comment s'adsorbe cette molécule ? Quelle est la conformation de cette molécule à la surface ? Les expériences décrites dans cette thèse permettent de mieux comprendre ces phénomènes.

Les nanoparticules métalliques protégées par une monocouche de molécules organiques peuvent être vues comme des analogues de ces matériaux hybrides à l'échelle nanométrique. Ces nanomatériaux sont par ailleurs très intéressants car leurs propriétés peuvent facilement être ajustées pour une application précise. Les matériaux hybrides de tailles macro-, micro- et nanométriques ont un large potentiel d'applications dans des domaines tels que la catalyse, la reconnaissance moléculaire, la médecine, l'optique, les micro- et nanotechnologies.

Grâce à leurs solubilités, les nanoparticules hybrides peuvent être manipulées et caractérisées comme de simples molécules organiques et ainsi apporter de nouvelles réponses à nos questions. Plus spécifiquement, les nanoparticules étudiées dans cette thèse sont recouvertes de molécules organiques chirales. Cette chiralité nous permet d'utiliser les techniques spectroscopiques chiroptiques qui sont très sensibles aux structures

tridimensionnelles et d'étendre le potentiel d'application aux technologies chirales comme par exemple la catalyse énantiosélective.

Le premier chapitre de cette thèse présente de façon générale les propriétés, les méthodes de préparation et de séparation ainsi que les applications des nanoparticules hybrides avant de discuter plus en détail des nanoparticules métalliques protégées par une monocouche de molécules organiques chirales. Ce chapitre d'introduction donne aussi un aperçu des clusters de coordination optiquement actifs qui représentent la limite inférieure des nanoparticules en terme de taille ainsi que des nanoparticules de molécules organiques chirales qui forment une nouvelle classe de nanomatériaux. Certaines nanoparticules d'or de taille nanométrique recouvertes par des thiols chiraux sont optiquement actives dans l'UV-visible et dans l'infrarouge.

Dans cette thèse, nous avons combiné pour la première fois le dichroïsme circulaire vibrationnel (VCD) et les calcules basés sur la théorie de la fonctionnelle de la densité (DFT) dans le but de déterminer la conformation des thiols chiraux adsorbés sur des nanoparticules d'or. Les chapitres 2, 3 et 5 décrivent la préparation de nanoparticules d'or protégées respectivement par l'acétylcystéine (NAC), l'isobutyryl-cystéine (NIC) et le 1,1'-binaphtyl-2,2'dithiol (BINAS). Le diamètre moyen de ces particules déterminé par microscopie électronique en transmission (TEM) est de l'ordre de un à deux nanomètres. Les spectres infrarouges des nanoparticules protégées par les deux énantiomères de la NIC sont identiques tandis que leurs spectres VCD montrent une relation de type image miroir (chapitre 3). Le VCD donne des informations structurelles détaillées sur le mode d'adsorption des thiols. Les conformations déterminées à partir de cette méthode corrèlent avec celles qui ont été déterminées pour des monocouches auto-assemblées (SAM) sur des surfaces d'or. Cette

conformation se distingue particulièrement par une interaction entre le carboxylate et l'or. De telles informations sont difficiles à obtenir avec d'autres méthodes spectroscopiques.

Les nanoparticules protégées avec la NIC ou le BINAS ont pu être fractionnées en fonction de leurs tailles par électrophorèse sur gel de polyacrylamide (PAGE) pour les premières et par chromatographie d'exclusion stérique (SEC) pour les secondes. Alors que l'activité optique dans l'infrarouge est similaire pour les différentes tailles de particules (chapitre 5), l'activité optique est très différente dans l'UV-visible (chapitre 3 and 4). Ces résultats montrent clairement que les méthodes chiroptiques sont des outils puissants pour déterminer sélectivement la conformation des molécules chirales adsorbées sur les nanoparticules dans l'infrarouge et la structure de la partie métallique dans l'UV-visible. Cependant, l'origine de l'activité optique basée sur les transitions électroniques métalliques ainsi que les structures (chirales ou achirales) restent indéterminées à cause du manque d'informations structurelles.

Les particules séparées par tailles exhibent des structures électroniques quantifiées dans leurs spectres d'absorption ainsi qu'un effet bathochrome lorsque la taille des particules augmente. Ces phénomènes sont dus aux effets quantiques de taille et montrent que ces particules ne sont pas métalliques mais semi-conductrices. Quelques fractions ont des spectres d'absorption optique identiques à ceux de nanoparticules analogues protégées avec la *L*-glutathion. Cela montre que ces particules ont des tailles comparables et que le nombre et l'arrangement des molécules adsorbées sont similaires malgré la différence de taille entre les deux thiols. Certaines tailles de particules ont une activité optique importante dans l'UV-vis avec une relation image miroir pour les spectres ECD des particules recouvertes avec des thiols de configuration absolue opposée (chapitre 3, 4 et 6). Les observations sont en accord

avec un mécanisme schématisé comme une « empreinte de pied chirale » imposée sur la surface métallique par le ligand. En particulier, les études VCD montrent que les ligands capables de conférer une activité optique au métal sont attachés par au moins deux points sur celui-ci. De plus, le BINAS qui est un ligand bidentate atropisomère est particulièrement bien approprié pour induire une forte activité optique dans les transitions métalliques avec notamment des facteurs d'anisotropie plus élevés que ceux reportés jusqu'à présent pour des nanoparticules d'or.

Finalement, le dernier chapitre décrit la réaction de substitution de thiol sur des nanoparticules de tailles bien définies. Sous conditions inertes, une rétention de la taille des particules est observée. Cette réaction est plus rapide que la réaction bien connue procédant par modification de la taille des particules (core-etching). Etonnamment, si un thiol chiral est échangé par son énantiomère, l'activité optique est inversée et la forme du signal reste quasiment inchangée. Cela démontre que l'arrangement chiral, « empreinte de pied chirale », des atomes d'or à la surface des particules ne supporte pas la force imposée par le nouvel énantiomère à la surface. Le taux d'inversion correspond à l'excès énantiomérique global du ligand dans le système. Si le thiol entrant possède une structure différente, les transitions électroniques à l'intérieur du corps métallique sont légèrement modifiées alors que la fréquence de début d'adsorption et par conséquent la taille des particules restent constantes. Ces résultats mettent en avant l'influence des thiols sur la structure des particules d'or et donnent de nouvelles informations sur les différents modes d'échange de ligand.

List of Abbreviations

A

ADF	Amsterdam Density Functional
APS	Ammonium PerSulfate

B

BINAP	2,2’-bis-(diphenylphosphino)-1-1’-binaphtyl
BINAS	1,1’-binaphthyl-2,2’-dithiol
BINAS-cyclic disulphide	Dinaphtho[2,1-c:1',2'-e][1,2]dithiin
Bis	N,N’-methylenebisacrylamide

C

CD	Cinchonidine
CN	Cinchonine
CN-MBE	1-cyano-trans-1,2-bis-(4’-methylbiphenyl)ethylene

D

DFT	Density Functional Theory
DH-CIN	Dihydrocinchonidine
DNBE	(*R*)-(+)-1,1’-bi-2-naphthol dimethyl ether

DNP	(*R*)-di-2-NaphthylProlinol

E

ECD	Electronic Circular Dichroism
ee	enantiomeric excess
ESI	ElectroSpray Ionization

I

IR	Infrared

L

LCs	Liquid Crystals

M

MBETs	Metal-Based Electronic Transitions
MD	Marks Decahedron
MPNs	Monolayer Protected Nanoparticles

N

NAC	N-acetyl-*L*-cysteine
NIC	N-isobutyryl-cysteine
NIDC	N-isobutyryl-*D*-cysteine
NILC	N-isobutyryl-*L*-cysteine
NMR	Nuclear Magnetic Resonance
NPs	Nanoparticles
NRDs	Nanorods

O

ONPs	Organic Nanoparticles

P

PAGE	PolyAcrylamide Gel Electrophoresis
PEM	PhotoElastic Modulator
pMBA	*p*-mercaptobenzoic acids
PVA	Poly(Vinyl Alcohol)

Q

QSE	Quantum Size Effect

R

R-BINAS	(*R*)-1,1'-binaphthyl-2,2'-dithiol
R-BTBN	(*R*)-(–)-2,21-bis-(*p*-toluenesulfonyloxy)-1,1'- binaphthalene

S

SAMs	Self-Assembled Monolayers
S-BINAS	(*S*)-1,1'-binaphthyl-2,2'-dithiol
SEC	Size Exclusion Chromatography
SP	Surface Plasmon

T

TEM	Transmission Electron Microscopy
TEMED	N,N,N',N'-tetramethylethylenediamine
THF	Tetrahydrofuran

TOAB	TetraOctylAmmonium Bromide
TPP	TriPhenylPhosphine
Tris	Tris(hydroxymethylaminomethane)

V

VCD	Vibrational Circular Dichroism
VOA	Vibrational Optical Activity

Z

ZORA	Zero Order Regular Approximation

1

Introduction

1.1 Chirality on Extended Surfaces

Chiral metal surfaces have gained increasing interest in fundamental research in the last ten years,[1, 2] mainly motivated by applications in the field of chiral technologies such as enantioselective heterogeneous catalysis and chiral recognition. The use of chiral metal surfaces is a promising strategy for the preparation of enantiopure compounds, for example as pharmaceutical. For technical applications it offers the advantages of a heterogeneous over a homogeneous process concerning catalyst handling, separation and reuse.

The different types of chirality observed for metal surfaces are illustrated in **Figure 1.1**. (A) High Miller index metal surfaces such as Cu(643)^{R} and Cu(643)^{S} are nonsuperimposable mirror images of one another. This intrinsic chirality is due to the presence of kinked steps with unequal step lengths on either side of the kinks.[3] Such surfaces have been shown to react differently with the two enantiomers of a chiral compound.[4, 5]

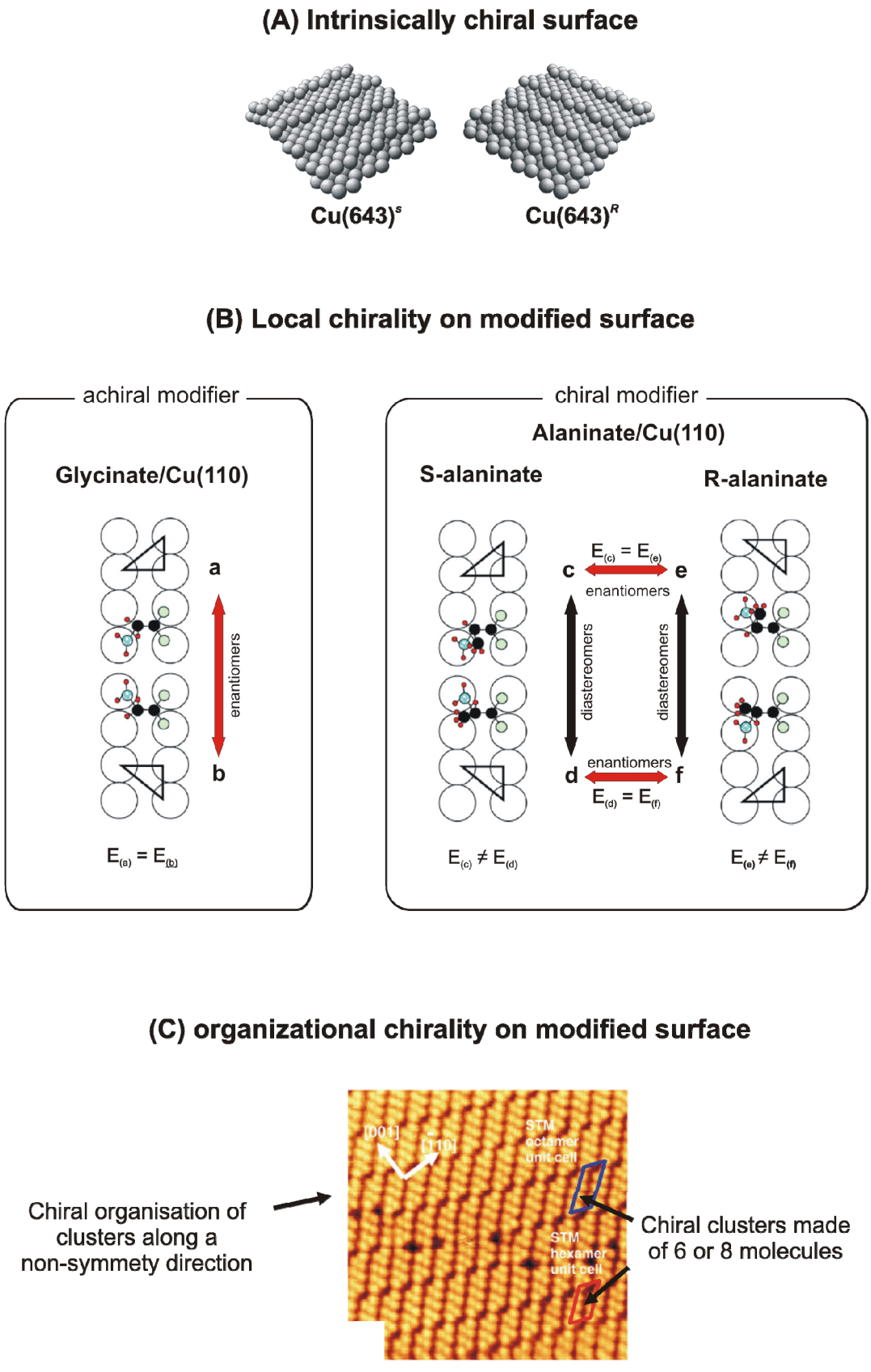
(A) Intrinsically chiral surface
Cu(643)S
Cu(643)R
(B) Local chirality on modified surface
achiral modifier
Glycinate/Cu(110)
a
b
enantiomers
E(a) = E(b)
chiral modifier
Alaninate/Cu(110)
S-alaninate
R-alaninate
E(c) = E(e)
c
e
enantiomers
diastereomers
diastereomers
enantiomers
d
f
E(d) = E(f)
E(c) ≠ E(d)
E(e) ≠ E(f)
(C) organizational chirality on modified surface
Chiral organisation of clusters along a non-symmety direction
[001]
[1̄10]
STM octamer unit cell
STM hexamer unit cell
Chiral clusters made of 6 or 8 molecules

Figure 1.1 : Chirality on extended metal surfaces. (A) Intrinsic chirality. (B) Local chirality on achiral modified surfaces. Achiral modifiers can form two enantiomer motifs which are energetically equivalent whereas chiral modifiers can form diastereomeric pairs from one enantiomer which can be energetically different and enantiomeric pairs from the racemic mixture. (C) Organizational chirality.

Local chirality can also be obtained on achiral surfaces through modification by chiral or even achiral molecules when the formation of the metal – molecule complex eliminates both molecular and surface reflection symmetry elements. This phenomena is illustrated in **Figure 1.1** (B) by the examples of the local chiral motifs created upon alaninate and glycinate adsorption on Cu(110).[6]

The adsorbed molecules can furthermore self-assemble and create different levels of organization, from small nanostructures that break local mirror symmetry to macroscale domains that destroy the reflection symmetry over the entire surface. This organizational chirality is depicted by the organization of *S*-alanine on Cu(110) in **Figure 1.1** (C). The scanning tunneling microscopy (STM) image reveals a first level of organizational chirality due to the formation of nanoclusters made of 6 or 8 molecules. These nanoclusters furthermore organize along a specific non symmetry direction and create a highly ordered and single handed chiral supramolecular assembly that extends across the entire surface.[6]

Interestingly it has recently been shown that such single handed surfaces are not exclusively obtained with enantiopure molecules. If achiral molecules and racemic mixtures of chiral molecules generally lead to a variety of domains with opposite handedness, small amounts of chiral molecules or small enantiomeric excess can induce further asymmetrization towards single handedness over the entire surface via cooperatively amplified interaction.[7, 8]

Two catalytic systems which are based on the chiral modification of a catalyst have been studied in details in the past mostly by surface sensitive experimetal techniques which in general do not probe the chiral information: (i) The Ni-tartrate system for the enantioselective hydrogenation of β-ketoesters and some other β-functionnalized ketones[9] and (ii) the Pt-cinchona system for the enantioselective hydrogenation of α-functionalized ketones.[10] However, the formation of the chiral organization of the modifiers on modified surfaces and the transfer of chirality from the surface to the substrates in enantioselective catalysis are not well understood The nature and the subtle interplay between (i) the formation of chemical bonds between modifiers and metals, (ii) the conformation of individual molecules after adsorption, (iii) the reconstruction of the surface upon adsorption, (iv) the intermolecular interactions, (v) the through metal interactions, (vi) the substrate - modifier interactions and finally, (vii) the substrate - metal interactions remain unclear.

1.2 Goal of the Thesis

The goal of the project was to gain a molecular level understanding of the local interactions between surfaces and molecules. Specifically, we seek to clarify how chiral molecules can impart chirality onto a surface. A special approach was applied in this thesis using size-selected gold nanoparticles protected with a chiral thiol monolayer which can be viewed as the nanometer size analogue of extended metal surfaces. Indeed, due to their high surface to volume ratio, a large proportion of the metal atoms belong to the surface and, in contrast to extended metal surfaces, these nanoparticles are amenable to chiroptical techniques such as electronic circular dichroism (ECD) and vibrational circular dichroism

(VCD). The comparison between experimental and calculated spectra will give detailed information on the chiral structure of the adsorbate layer and of the metal core of the particle and will reveal the relationship between the two.

Our research will help a more rational design of improved catalyst material. In addition, nanoparticles are fascinating materials as you will see by reading the following sections. This study will furthermore give insight on the evolution of properties with nanoparticle size.

1.3 Chirality at the Nanoscale – Chiral Nanoparticles

The future development of nanotechnology is likely to rely on the construction of new devices by self-assembly of nanoscale building blocks. This strategy is largely inspired by life, which relies on self-assembly of molecules, and which is dominated by homochirality. While the origin of homochirality remains unclear, the transcription and amplification of chirality from small chiral molecules such as *L*-amino acids to large biological materials like proteins inevitably played a crucial role in its evolution. Obviously, chirality of nanoparticles (NPs), which are promising building blocks for the bottom-up approach, will become an important parameter in the miniaturization race. The properties and structures of inorganic solids are usually catalogued without reference to their size. However, when dimensions of bulk materials are shrinking down to the nanoscale, intrinsic properties and geometry are turned upside down. New behaviors appear and the structure of nanomaterials may significantly differ from the highly symmetric structure found in bulk materials and in some cases, low symmetry chiral structures become more stable. Future technologies and

integration of NPs in new devices will rely on these size effects, which are briefly introduced in Section 1.4. NPs behaviors are easily tunable by playing on parameters such as composition, size, shape, organization and functionalization. During the last twenty years, new characterization tools such as electron and scanning probe microscopes have been developed that allow the investigation of materials with a resolution close to the atomic level. In parallel, a large variety of synthetic routes for the preparation of NPs have been developed, as will be described in Section 1.5. After a brief overview of general preparation routes special emphasis will be given on pathways yielding NPs which are optically active, which are asymmetric catalysts or which are simply observed to be chiral in pure or racemic forms by microscopy or X-ray diffraction. Ensembles of NPs produced by the best available techniques still suffer from inhomogeneous broadening due to impurities or to size and shape distribution. Therefore Section 1.5.2 deals with size and shape separation, which are essential in order to understand the chiroptical properties. Manifestation and origins of optical activity in metal-based electronic transitions (MBETs) of monolayer protected NPs are discussed in Section 1.6. The next section deals with optically active coordination clusters, which correspond to the inferior limit of optically active metallic NPs and which can serve as models for a better comprehension of larger particles. The very new and few studies of chiral organic nanoparticles (ONPs) are overviewed in Section 1.8. Despite their novelty, this type of nanomaterial seems to have a great potential in a wide range of applications.

NPs play an important role in catalysis. For example, Haruta has discovered that gold NPs dispersed across the surfaces of certain oxides are active catalysts for carbon monoxide oxidation at room temperature, whereas bulk gold is totally inactive.[11] Actually, the use of NPs in catalysis is in constant progress and recently, few examples of enantioselective

catalysis with NPs have been reported and are enumerated in Section 1.9. This section also discusses the potential applications of chiral NPs in various fields such as enantiodiscrimination but also to their possible integration and organization in liquid crystals (LCs). Finally, as will become evident by reading this chapter, the study of chiral NPs is still in its discovery phase. The last Section, will describe the perspectives of these types of materials.

1.4 Nanoparticles Properties

This section gives a short introduction on NPs properties in order to ease the understanding of asymmetric NPs properties. Several books and reviews describe this subject extensively.[12-15] NPs can be understood as intermediate between molecular (atomic) and bulk matter and their physical properties are neither those of molecules nor those of bulk material. From a physical point of view, most of these properties are related to two phenomena, which are illustrated in **Figure 1.2**, surface plasmon (SP) resonance and quantum size effect (QSE) for metallic and semiconducting NPs, respectively. SP resonance arises from the interaction between surface charges of metallic NPs and an electromagnetic field. SPs are waves that propagate along the surface of the conducting NPs. The free electrons respond collectively by oscillating in resonance with light giving rise to absorption and scattering. The resulting red color of gold NPs has been used for centuries in coloration of stained-glass windows. On the other hand, the QSE refer to electron confinement in NPs.

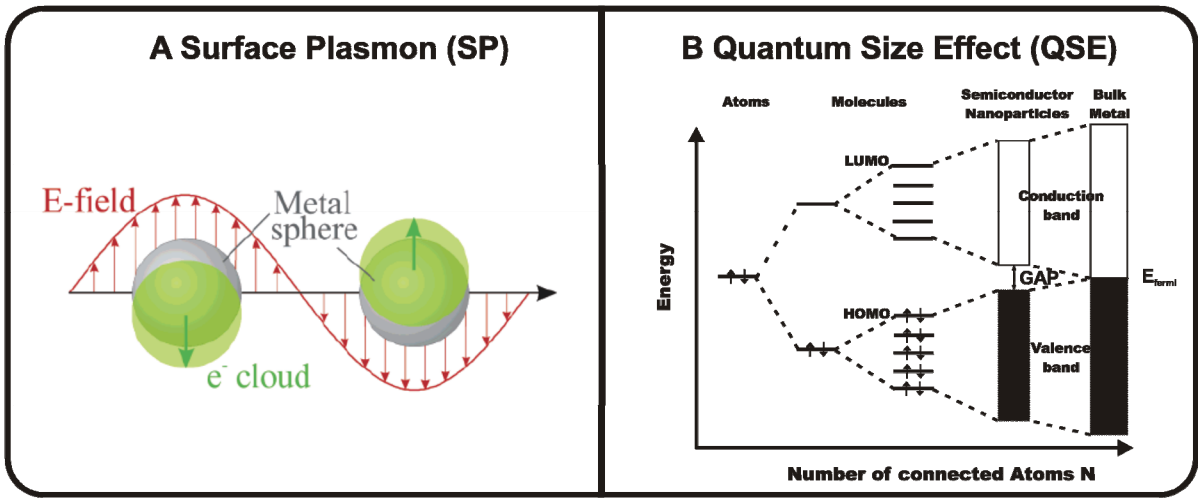

Figure 1.2 : A) A schematic representation of the plasmon oscillation for a sphere, showing the displacement of the conduction electron charge cloud relative to the nuclei. Reprinted with permission from ref. [16]. Copyright (2003) American Chemical Society. B) Schematic illustration of the electronic energy levels as a function of the number of connected atoms. From left to right, evolution of energy levels by binding more and more atoms together, the discrete energy levels merge into energy bands with a band gap for semiconductor NPs. The band gap progressively decreases and the NPs are becoming metallic as the corresponding bulk metal. Adapted from Figure 2.1 of ref. [13] with permission.

Both SP resonance and QSE of NPs are easily tunable. Important modifications of electrical and optical properties can be observed, which may be used for new applications such as fabrication of transistors, biosensors and catalysts. The physical behavior is dictated by the size, the shape, the nature, the composition, and even the organization of NPs. These physical characteristics can be combined with chemical and biological properties for hybrid NPs, which are surrounded with organic molecules or biological materials.

As illustrated in **Figure 1.3**, the most striking demonstration of QSE is the variation of color of NPs (A) as evidenced by their systematic bathochromic shift in absorption spectra as their size is increasing (B), or by their change in emission as a function of their size (C). Section 1.6 shows that the chiroptical properties of NPs are also dictated by QSE.

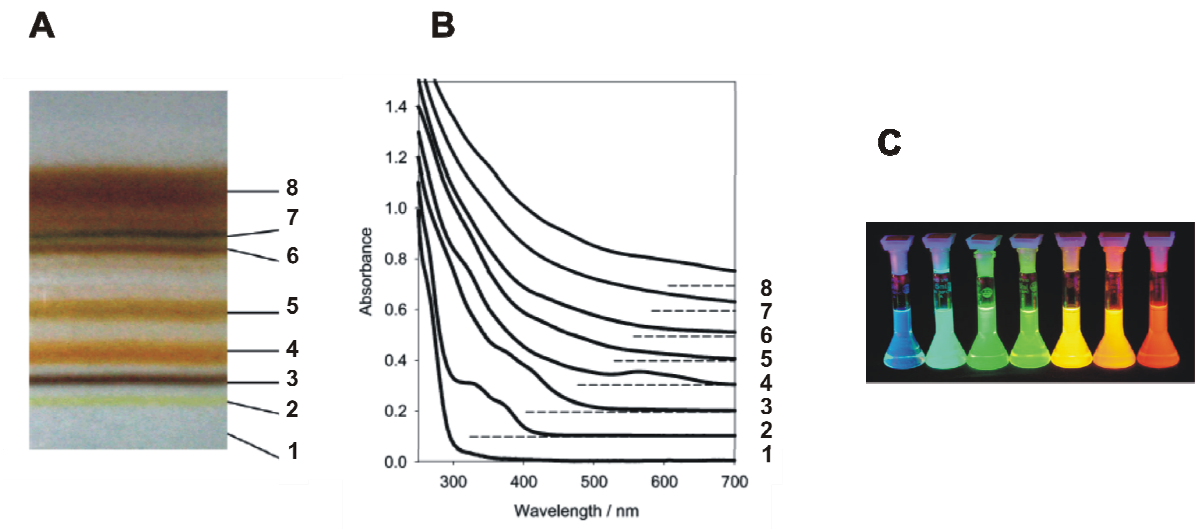

Figure 1.3 : A) Gold NPs separated according to their size by Polyacrylamide Gel Electrophoresis (PAGE). NPs are numbered according to their increasing size. B) UV-vis spectra of the size separated gold NPs. A clear red shift of the absorption onset is observed as the size of NPs increases. A and B are reprinted with permission from ref. [17]. Copyright (2006) American Chemical Society. C) Fluorescence induced by exposure to ultraviolet light of vials containing various sized Cadmium Selenide (CdSe) quantum dots.

When the size of particles is reduced, their dispersion, that is their fraction of surface atoms, increases, and so does the surface to volume ratio. At the nanoscale, the large contribution of the surface energy to the overall system is responsible for the large change in thermodynamic properties as for example the diminution of the melting temperature. This has also important consequences on the structure of NPs and could be a driving force for inducing chirality in the latter. The shape is also an important factor for the tuning of physical properties. For example the SP resonance band of spherical NPs splits into different bands for anisotropic NPs such as nanorods (NRDs).[18] The surface of nanocrystals exposes different crystallographic facets, which can grow at different rate or be selectively functionalized.[19, 20] This allows the preparation of NPs with a large panel of shapes such as NRDs, nanotripods and nanostars, which are ideal “building blocks” for the bottom-up preparation of

new nanodevices through self-assembling of NPs directed by functional groups within their organic shell.[19, 21] Recently, chiral single-walled nanotubes of Pt and Au were observed by ultra high vacuum-transmission electron microscopy.[22, 23] They consist of five or six atomic rows that coil helically around the axis of the tube.

Organization of NPs has a large impact on their electronic and optical properties. For example arrays of pairs of parallel NRDs have been shown to have a negative refractive index at the optical communication wavelength. Such metamaterials have been predicting to act as perfect lenses.[24] Due to a coupling of the SP resonance the formation of a polymeric network of gold NPs in solution is observable through a color change from red to blue. This can be used for colorimetric sensing of biomolecules.[19, 21, 25] The controlled coupling of SPs of well ordered NP lattices is promising for preparing optoelectronic devices.[26] Experiments and calculations have shown that arrays of chiral micro- and nano- metallic particles with subwavelength-period can rotate the polarization plane azimuth of the transmitted wave at normal incidence.[27, 28] This behavior is similar to the one observed for chiral LCs and opens the possibility to create planar polarization-sensitive devices via self-assembly of NPs with a chiral shape or a chiral organization.

1.5 Synthesis, Purification and Size Separation

1.5.1 Synthesis

The literature dealing with NPs synthesis is uncountable and a wide variety of techniques have been reported using precursors from liquid, solid and gas phases. Metallic NPs can be prepared by the top-down (physical) approach for example by mechanical

subdivision of metallic aggregates or by lithography techniques. NPs can also be prepared by the opposite approach called bottom-up (chemical). The top-down approach easily allows controlling the organization of NPs in 1, 2 and 3 dimensions. However, the bottom-up approach is considerably cheaper and allows the preparation of very small particles.

The chemical approach is based on the nucleation and growth of metallic atoms in liquid media or in gas phase. The literature describes five general methods for the chemical preparation of transition metal NPs. 1) Chemical reduction of metal salts, 2) thermal, photochemical or sonochemical decomposition, 3) electrochemical reduction, 4) metal vapor synthesis and 5) ligand reduction and displacement from organometallic complexes.

Among the huge number of methods listed in literature, only a few have been used for the preparation of optically active metallic NPs. A few examples of micro- and nano- particle arrays (not necessarily of chiral NPs) with chiral shapes[27] or chiral organizations[28, 29] have been studied theoretically[28] or prepared using top-down methods such as electron–beam lithography and lift-off techniques.

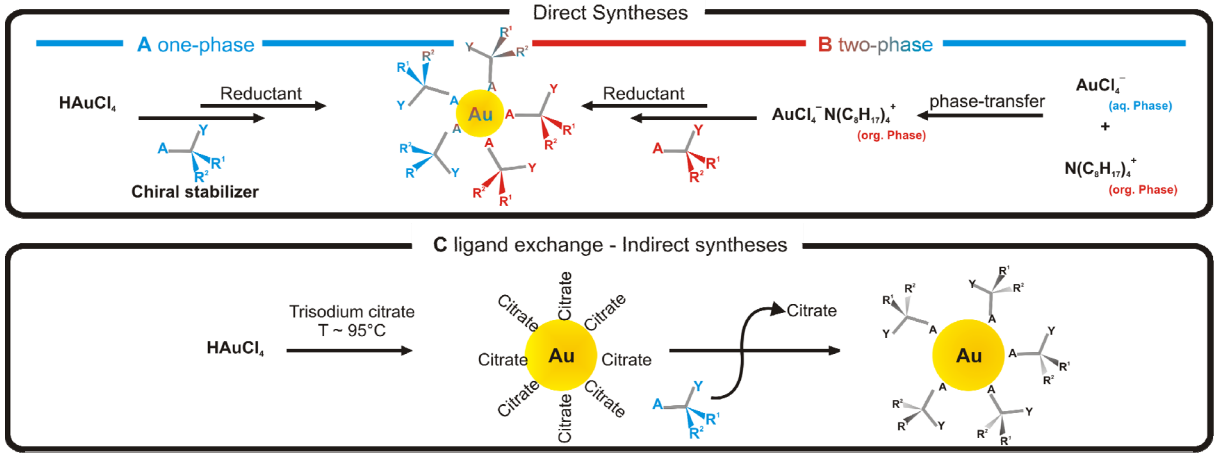

Figure 1.4 : Different methods exploited for the syntheses of optically active NPs with chiral ligands.

Most optically active metallic NPs have been prepared by the bottom-up approach and more specifically by the chemical reduction of metal ions or of precursor complexes in solution, which is illustrated in **Figure 1.4**.[30] The reduction of the metal salts is often performed in the presence of chiral stabilizers such as thiols, phosphines and amines (DNA and alkaloid) in a one-pot procedure (direct syntheses). (A) NPs are prepared in a single phase when the metallic salt and the ligand are both soluble in the same solvent such as water, alcohols, acetic acid, tetrahydrofuran (THF) or a mixture of these (see Section 3.3.2). (B) If their solubilities are not compatible, the Brust-Schiffrin synthesis[31] provides a ready access in a biphasic reaction taking advantage of phase transfer compounds, generally tetraoctylammonium bromide (TOAB) to shuttle ionic reagents to an organic phase where particles nucleation, growth and passivation occur (see section 4.3.2). (C) When the functional groups are not compatible with the reducing agent, the optical activity can be induced via a post synthetic modification of the ligand shell like a ligand exchange reaction (indirect syntheses). This two-step method presents some advantage in both purification and separation. Indeed some NPs are very well characterized and both their separation and purification processes are well established. The gold NPs prepared by the citrate method of Turkevich *et al.*[32] and those developed by Schmid[33], which are protected by triphenylphosphine (TPP), are surely the more frequently used NPs for the ligand exchange reaction. This strategy avoids time consuming search of efficient parameters for purification and separation of each new type of NPs. However, the post-synthetic modifications such as ligand exchange in an excess of ligand often modify the size distribution of the NPs.[34-37] More details on ligand exchange reaction will be giving in Chapter 6.

1.5.2 Purification and Separation of Nanoparticles

The physical properties of NPs are strongly size and shape dependent as emphasized in the last section of this chapter. Fine tuning of properties for a specific purpose often requires a perfect control of these two parameters as well as a high control of functionalization and purity. Procedures for the preparation of NPs are in constant progress but till now only few methods yield monodisperse particles with high purity. However this fine tuning can be reached after appropriate purification and separation processes. Current methods for purification of NPs samples, that is removal of free ligand and reducing agent, involve centrifugation, precipitation, washing, dialysis, chromatography or extraction to remove impurities. Size selection can be based on fractional crystallization, size exclusion chromatography (SEC), electrophoresis and membrane based methods such as ultrafiltration or diafiltration. These techniques are particularly appropriate for the size separation of water-soluble NPs but are generally time consuming and only viable for production on a small scale. The size separation of NPs soluble in organic media is suffering from the lack of methods compatible with organic solvents. The fundamental studies of the size dependant chiroptical properties have been mainly performed with water-soluble NPs separated according to their size and charge by high density polyacrylamide gel electrophoresis (PAGE).[17, 38-41] The only size selection of chiral NPs soluble in organic media has been realized using SEC (see **Figure 1.3** and Section 4.3.3).[42]

1.5.3 Polyacrylamide Gel Electrophoresis

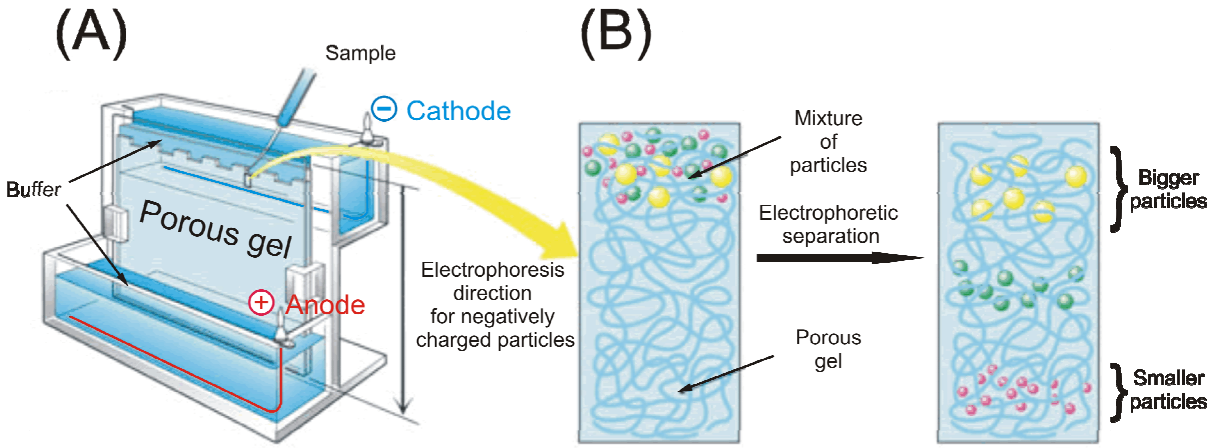

Figure 1.5 : (A) Scheme of a vertical electrophoreses. (B) Position of the particles before (left) and after electrophoretic separation (right).

Electrophoresis is the migration of charged molecules in buffered solution in response to an electric field created between a cathode and an anode (see **Figure 1.5** A). Their rate of migration depends on the strength of the field; on the net charge, size and shape of the molecules and also on the ionic strength, viscosity and temperature of the medium in which the molecules are moving. As an analytical tool, electrophoresis is simple, rapid and highly sensitive. It is used analytically to study the properties of a single charged species, and as a separation technique.

Generally the sample is run in a support matrix such as paper, cellulose acetate, starch gel, agarose or polyacrylamide gel. The matrix inhibits convective mixing caused by heating and provides a record of the electrophoretic run: at the end of the run, the matrix can be stained and used for scanning, autoradiography or storage. Due to their color gold nanoparticles are directly visible by eye.

In addition, the most commonly used support matrices agarose and polyacrylamide provide a means of separating molecules by size (see **Figure 1.5 B**), because of their porous structure. A porous gel may act as a sieve by retarding, or in some cases completely obstructing, the movement of large macromolecules while allowing smaller molecules to migrate freely. Because dilute agarose gels are generally more rigid and easy to handle than polyacrylamide of the same concentration, agarose is used to separate larger macromolecules such as nucleic acids, large proteins and protein complexes.

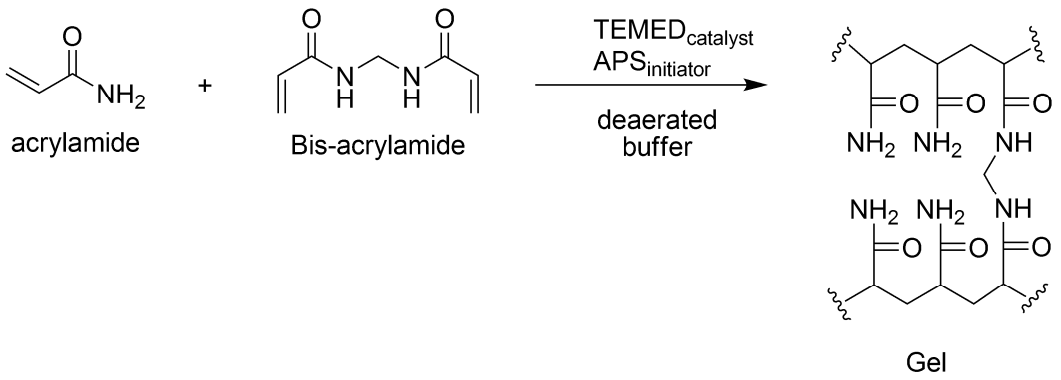

Figure 1.6 : Formation of polyacrylamide gel.

Polyacrylamide, which is easy to handle and to make at higher concentrations, is used to separate most proteins and small oligonucleotides that require a small gel pore size for retardation. It should be noted that acrylamide monomer is a potent cumulative neurotoxin which should be manipulated with care. We used the latter media for the separation of the water soluble and charged nanoparticles that were studied in this thesis because their averaged diameter is relatively small, 1 to 2 nanometers. The best separations were achieved with high-density polyacrylamide gels at T = 20-27% and C = 7%, where T is the mass-volume

percentage of monomer including crosslinker, N, N'-methylene-bis-acrylamide (Bis), and C is the proportion of crosslinker as a percentage of total monomer (see **Equation 1-1**).[38]

$$T = \frac{m(acrylamide) + m(Bis - acrylamide)}{Total\ Volume} \times 100 \qquad (though\ strictly\ \ g/ml)$$

$$C = \frac{m(Bis - acrylamide)}{m(acrylamide) + m(Bis - acrylamide)} \times 100$$

Equation 1-1 : Concentrations of the monomers.

The pore size of the polyacrylamide gel can be changed by adjusting either the total monomer concentration (T) or by adjusting the crosslinking monomer concentration (C). As shown in **Figure 1.6**, acrylamide gels are formed by the free radical polymerization of acrylamide and Bis-acrylamide in a deaerated buffer. This reaction is catalyzed by N,N,N',N'-tetramethylethylenediamine (TEMED) and initiated by ammonium persulfate (APS). This separation method is very efficient but very time-consuming and thus impractical on large scale.

1.6 Chiroptical Properties of Nanoparticles

Due to their organic shell, monolayer-protected NPs can be dissolved in various solvents and are thus amenable to chiroptical techniques such as ECD and VCD. The former has demonstrated its aptitude for the study of protein secondary and tertiary structures whereas the latter has been used for the determination of conformation and absolute

configuration of organic molecules in solution.[43, 44] Recently, these complementary techniques have been applied to NPs covered with different chiral organic ligands. VCD in the infrared region selectively probes molecular vibrations located in the organic shell, whereas ECD in the UV-visible is sensitive towards electronic transitions which may be located in the inorganic core.

1.6.1 Vibrational Circular Dichroism

Infrared absorption (IR) and Raman spectroscopies are the two principal tools available for the study of molecular vibrations. Both techniques have also been used to study vibrational optical activity (VOA) of chiral molecules.

The IR form known as VCD is a spectroscopic technique which specifically measures the differential absorption of left and right circularly polarized infrared light by chiral molecules. Similar to ECD, VCD provides important information on the configuration and on the conformation of chiral molecules in solution and in the solid state. Although the signal is generally a few orders of magnitude smaller than that obtained from ECD, VCD has the advantage that spectra are easier to simulate by electronic structure determination.

Since the first VCD measurement was reported in 1973,[45] instrumentation was quickly developed. Improvements were made especially by using the photoelastic modulator (PEM) and the Fourier transform IR (FTIR) approaches developed respectively by Stephen's and Nafie's groups. [46, 47]

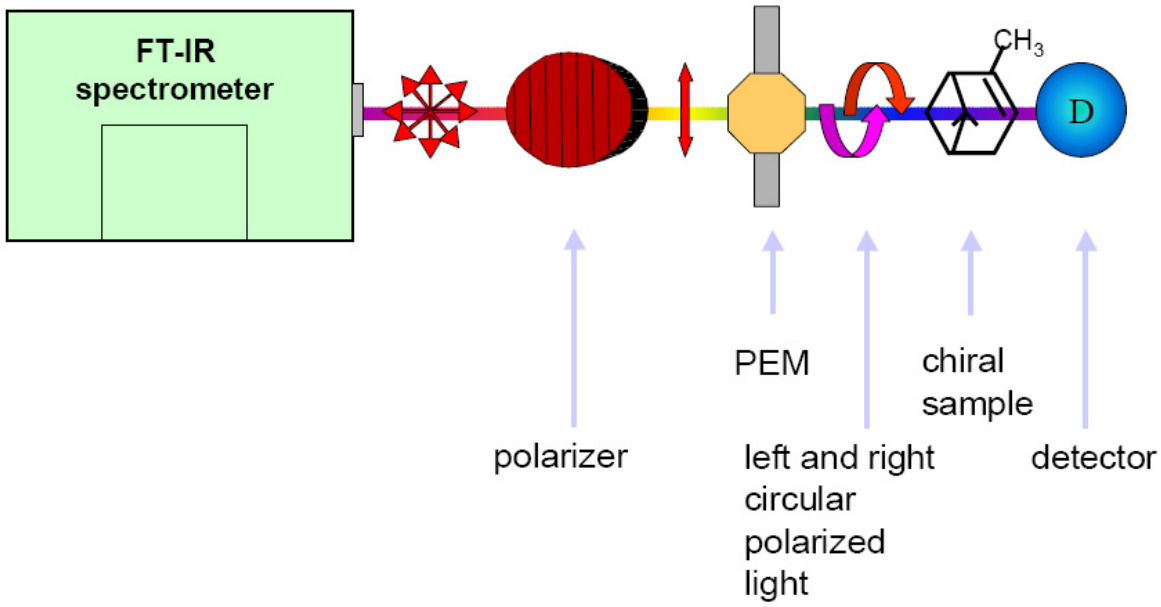

Figure 1.7 : Diagram of typical FTIR-VCD optical bench.

Since VCD signals are typically 4-6 orders of magnitude smaller than the normal absorption signals, the use of a PEM allows one to obtain the differential signals directly and rapidly. The FTIR-VCD spectrometer has several advantages over the classical dispersive IR spectrometer especially when a wide spectral range (for example 1000 cm^{-1}) is studied or high resolution is needed.

In the FTIR-VCD spectrometer, the IR beam from the light source first passes through an interferometer and then goes to a VCD optical bench described in Figure 1.7**.** The FTIR's Michelson interferometer modulates each optical wavelength at different Fourier frequency below several kilohertz (Fourier modulation). The VCD optical bench is composed of a linear polarizer, a PEM, a sample holder and a detector. The Fourier modulated IR beam is polarized linearly before to be modulated between left and right circular polarization state by the PEM. This modulation is about 10 times faster than the highest Fourier frequency. Finally, the beam

goes through the chiral sample before to reach the detector. The resulting signal is processed separately to obtain the average ($(A_L+A_R)/2$) and the differential spectra (A_L-A_R). The average signal is computed according to the conventional methods used in the standard FTIR system.

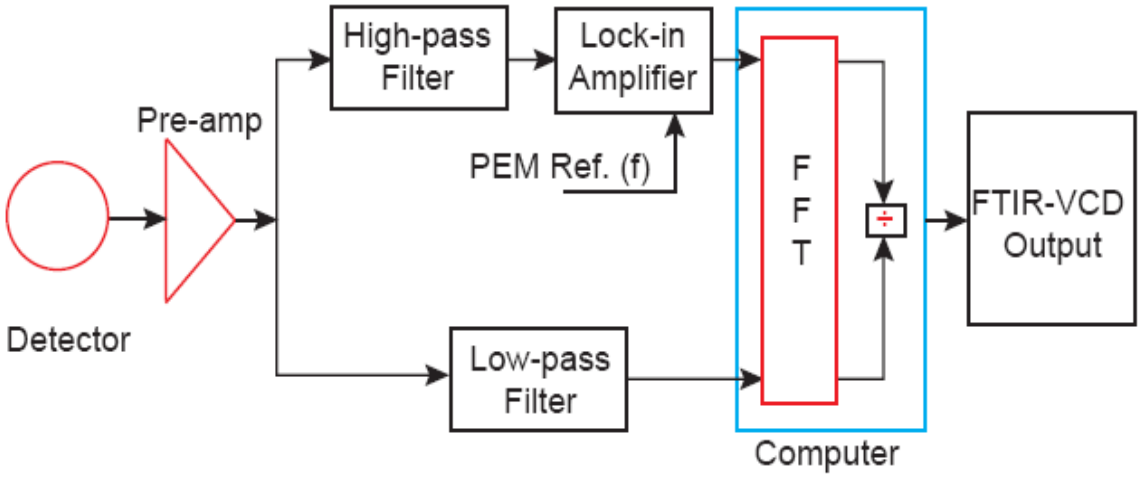

Figure 1.8 : Electronic block diagram for typical FTIR-VCD spectrometer.

To obtain the differential signal, the pre-amplified detector signal is first passed through a high pass filter in order to attenuate the Fourier modulated signals, and is then output to a lock-in amplifier referenced to the PEM frequency. The time constant of the lock-in amplifier should be set short enough to pass the Fourier frequencies efficiently for the rapid scan FTIR-VCD experiments. The demodulated signal from the lock-in amplifier is then sent to the FTIR standard electronics for fast Fourier transform (FFT). A typical electronic block diagram for the processing of FTIR-VCD is shown in **Figure 1.8**. After phase correction, the final VCD spectrum is obtain from the ratio of the differential spectrum to the average spectrum and the calibration of the VCD intensity. The original and successful solution for phase correction in a VCD spectrum is to use a transferred phase obtained at the same

condition as for the VCD spectrum. It is normally obtained from a slightly stressed birefringent IR window which produces large single signed VCD signals. In order to obtain the raw VCD data, it is necessary to have the ratio of the polarization modulated signal to the normal IR signal. An intensity calibration device constructed from a quarter wavelength plate followed by a polarizer is used to obtain the VCD with the correct intensity.

VCD spectroscopy was applied in this thesis to gold NPs of about 2 nm core diameter in order to study the conformation of adsorbed chiral cysteine derivatives.[17, 48] In order to extract structural information the measured spectrum has to be compared with the calculated ones for different conformers. **Figure 1.9** shows IR and VCD spectra of gold NPs covered by the two enantiomers of N-isobutyryl-cysteine (NIC). Whereas the IR spectra are identical for the two enantiomers, the VCD spectra show a mirror image relationship. Density functional theory (DFT) calculations show that the structure of the underlying gold cluster does not have a large effect on the simulated VCD spectra, whereas the conformation of the adsorbed thiol has a large influence. The calculated VCD spectrum of one stable conformer of NIC adsorbed on a small gold cluster matches well with the experimental data. This conformation is characterized by an interaction of the carboxylate with the gold cluster (see **Figure 1.9**). Thus the carboxylate group seems to be a second anchoring point beside the strong Au-S bond. Full details are describes in Chapters 2 and 3. This two-point interaction may influence the optical activity of the NPs as discussed in section 1.6.3.

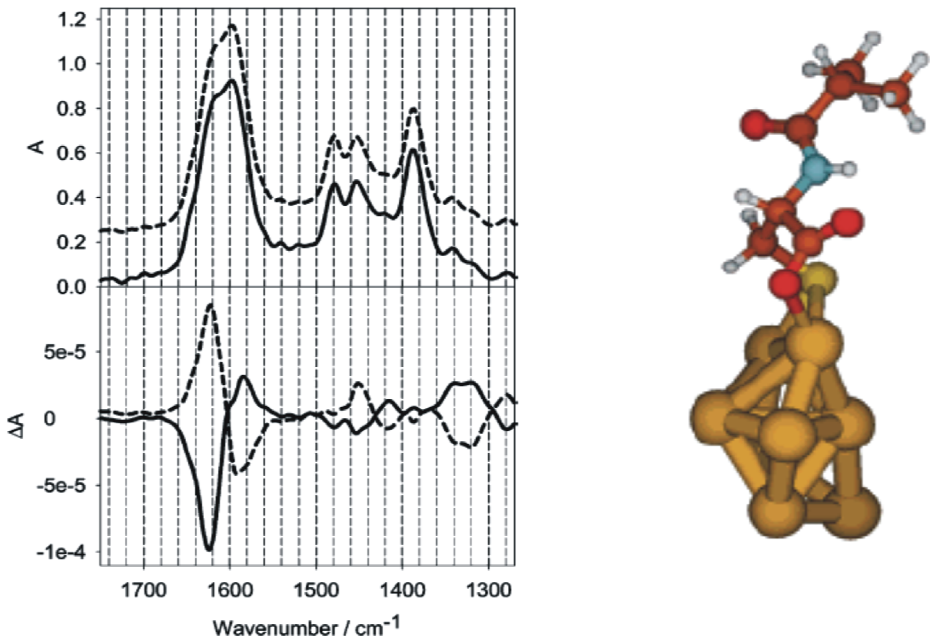

Figure 1.9 : Infrared (top) and VCD (bottom) spectra of NILC protected gold NPs. The calculated VCD spectrum of the conformer on the right on a Au_8 cluster fits best the experimental spectrum. Reproduced with permission from ref. [17]. Copyright (2006) American Chemical Society.

1.6.2 Electronic Circular Dichroism

It is tempting to assume that the structure of NPs correspond to a fragment of the highly symmetric bulk crystal lattice. However, in 1996 calculations performed by Wetzel and DePristo, and experimental observation of Riley *et al.* indicated that naked Ni_{39} clusters prefer a lower (D_5) symmetry chiral structure.[49, 50] At the same time, Whetten and co-workers experimentally observed optical activity in the MBETs for a Au_{28} cluster covered with *L*-glutathione (GSH), a chiral tripeptide.[38] They furthermore isolated similar well defined clusters with different mass by PAGE. The three smaller isolated clusters with a core mass between 4 and 8 kDa showed a strong optical activity whereas neither the crude mixture nor the higher molecular weight components possess such a strong optical activity. The

optical activity in the near-infrared (NIR), visible and near-ultraviolet is clearly size dependant and its amplitude is comparable to the signals observed for intrinsically chiral conjugated systems like chiral fullerenes or larger helicenes.

Recently, optical activity in metal-based electronic transitions (MBETs) has been reported for gold, silver and palladium nanoclusters having a more or less well defined size and an organic shell composed of different chiral molecules.[17, 30, 39, 40, 51-53] **Figure 1.10** summarizes the chemical structures of the different molecules that have been shown to induce optical activity in NPs as well as the size and the maximum of amplitude of the anisotropy factor ($\Delta\varepsilon/\varepsilon$) measured for gold or silver NPs.

Name	Structure	METAL $\Delta\varepsilon/\varepsilon$ max. SIZE
N-acetyl-*L*-cysteine (NALC)	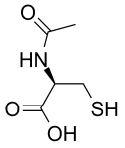	
N-isobutyryl-*L*-cysteine (NILC)	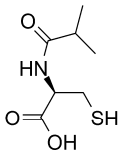	Au 0.5×10^{-3} (1 to 2 nm)
L-cysteine	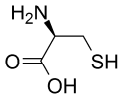	
L-cysteine methyl ester	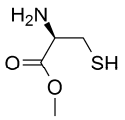	Au 0 (20 to 25 nm)
L-penicillamine (*L*-pen)	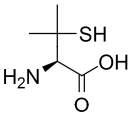	Au 3×10^{-4} to 1×10^{-4} (0.57 to 1.75 nm) Ag 1×10^{-3} to 1×10^{-5} (1 to 1.9 nm)
L-glutathione (GSH)	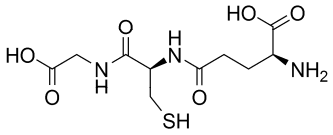	Au 2×10^{-4} to 1×10^{-3} (0.7 to 1 nm)
(*R*)-BINAS	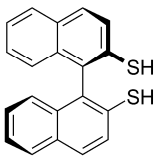	Au 4×10^{-3} (1 to 2 nm)
(*R*)-BINAP	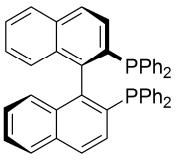	Au 1.4×10^{-3} (1 to 2 nm)

Figure 1.10 : Chemical structures of chiral molecules inducing optical activity to metallic NPs. Size of the particule, type of metal and anisotropy factor of the particles.

Pairs of clusters with similar inorganic core, size or size distribution and the same number and type of ligands but with opposite absolute configuration exhibit mirror image

ECD spectra as common chiral molecules do (see Chapter 3). No optical activity is observed for the clusters prepared with a racemic mixture of ligand. However, in the case of silver particles covered by penicillamine it was reported that the UV-vis spectra of the separated NPs are slightly different from the homochiral ones.[39] These silver NPs are not as stable as gold NPs. In all cases where optical activity in size-selected NPs was observed, the ECD signals change with the size of the NPs. In some cases the anisotropy factor gradually increases with a decrease in the mean cluster diameter.[17, 39, 40] Thus it seems that the subnanometer and the nanometer classes of nanoclusters are the best candidates for displaying optical activity. This may be related to the fact that in this range scale, most of the metals atoms reside at the surface of the core and thus interact directly with the chiral ligands. Another explanation for the tendency of decreasing optical activity with increasing particle size is simply the increased configurational space for larger particles (larger number of gold atoms and ligands) and thus the increased probability of multiple energy minima on the potential energy surface. An increasing number of conformers leads to a decreased observable optical activity as positive and negative bands of different conformers average out.

In contrast, optical activity was also reported by Park and coworkers for considerably larger penicillamine or cysteine capped silver particles (23.5 nm)[52] and also for silver nanocrystals grown on a double stranded DNA scaffold.[53] However, these particles were not size separated, and it can not be excluded that the observed optical activity is due to a fraction of small particles. Recently, this hypotheses was verified by Kimura and coworkers who have separated silver NPs according to their size and observed optical activity only for NPs in the nanometer range.[40]

When comparing the characteristics of all the ligands able to impart optical activity in the MBETs, it becomes evident that most of them and especially cysteine derivatives are able to form hydrogen bond mediated self-assembly. This property was proposed to be a crucial parameter for inducing optical activity.[52, 54] However, the atropisomeric bidentate ligands BINAS and BINAP do not display such behavior despite the fact that they are particularly well suited to impart optical activity (see Chapter 4).[30, 51] On the other hand, a common feature is that all the ligands can interact with the cluster surface by at least two functional groups as emphasized in Section 1.6.1. Furthermore, it was demonstrated that by blocking the acid group (anchoring point) in cysteine derivatives the optical activity was lost.[52] In addition, Hegmann and co-workers studied the optical activity of small gold NPs covered by the chiral naproxen and observed that this molecule, which only possesses one interaction point, does not induce optical activity in MBETs.[55]

In all of the cases described above, the optical activity in the NIR, visible and UV can be attributed neither to the metallic precursors nor to the organic species and its origin remains unclear due to the lack of structural information and to the very few examples of well defined nanoclusters.

1.6.3 Origin of Optical Activity in Metal-Based Transitions

The observed optical activity in MBETs of small metal particles protected with chiral thiols can be attributed to two opposite and one intermediate model (see **Figure 1.11**). In the first one, the optical activity arises from an intrinsically chiral inorganic core (A). In the presence of chiral ligands one of the two possible enantiomers of the core is favored. Such

behavior is found, as discussed in section 1.7, for coordination clusters with a chiral framework. In the second one, the inorganic core can be achiral and the optical activity is induced by a chiral environment due to the chiral organic shell through a vicinal effect or through a chiral electrostatic field (B). Both models have support from theoretical calculations.[56-58] Garzón *et al.* have predicted that small metal particles such as Au_{28} or Au_{55} prefer low symmetry chiral over high-symmetry nonchiral structures.[56, 57] Goldsmith and co-workers have demonstrated that optical activity could arise from achiral metal core perturbated by a dissymmetric field originating from the chiral organic shell.[58] Trends in the electronic transition frequencies and amplitudes with cluster size observed experimentally are qualitatively in agreement with both models. It is likely that the two mechanisms concurrently impart optical activity to the core and the key question whether the core is chiral or not remained unanswered at that point.

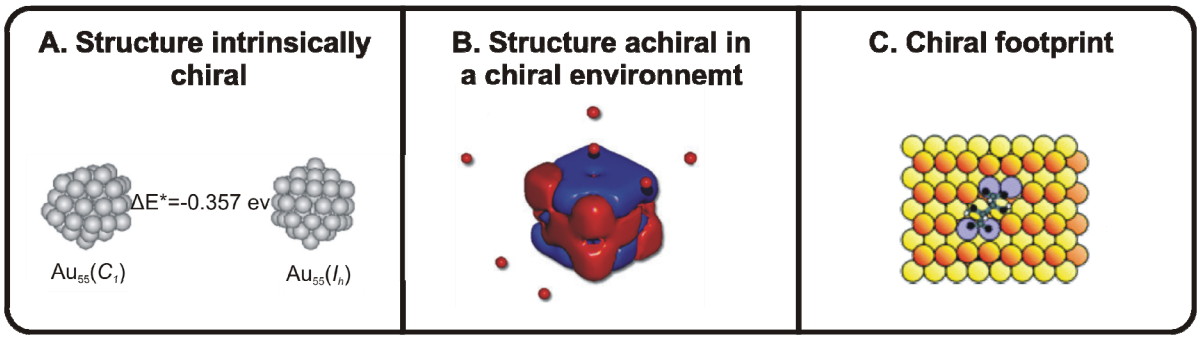

Figure 1.11 : Possible origins of optical activity. A) The calculated chiral structure (C_1) of bare Au_{55} is more stable than the highly symmetric structure (I_h). Reprinted from ref. [56] with kind permission of The European Physical Journal (EPJ). B) Chiral distribution of electron density in Au_{28} gold clusters induced by a chiral point-charge system. Red points correspond to negative point-charges and red and blue surfaces in the core represent, respectively, regions of high and low electron density. Reproduced from ref. [58] by permission of the PCCP Owner Societies. C) Chiral footprint of bitartrate on Ni(100) surface. Reproduced with permission from ref. [59]. Copyright (2002) American Chemical Society.

In the intermediate model, the grand core can be achiral but the relaxation of the surface atoms involved in the adsorption of the chiral ligand creates a chiral "footprint" similarly as observed for tartaric acid adsorption on Ni surfaces (C) (see Chapter 3).[59] This is favored for ligands that posses at least two anchoring points on the surface. Such double interactions have indeed been documented on surfaces [60-63] and seem to be a common characteristic of the ligand able to induce optical activity in MBETs as discussed in Section 1.6.2. DFT calculations have shown that the ligands are not only playing the role of passivating molecules, but they also distort the metal cluster structure.[56]

Very recently, the first total structure determination of a small gold-thiolate nanocluster composed of 102 gold atoms and 44 *p*-mercaptobenzoic acids (*p*-MBA) has been published.[64] As shown in **Figure 1.12**, the particles are chiral and formed as a racemic mixture in the crystal (A). However, the central gold atoms are packed in a Marks decahedron (MD) which is highly symmetric as the fcc structure of bulk gold (B). The chirality arises from the number and geometry of equatorial atoms on the surface. The deviations in local symmetry may reflect the interaction of the equatorial atoms with the *p*-MBA monolayer. Furthermore, most sulfur atoms bonded to two gold atoms in two different shells are stereogenic centers (C).

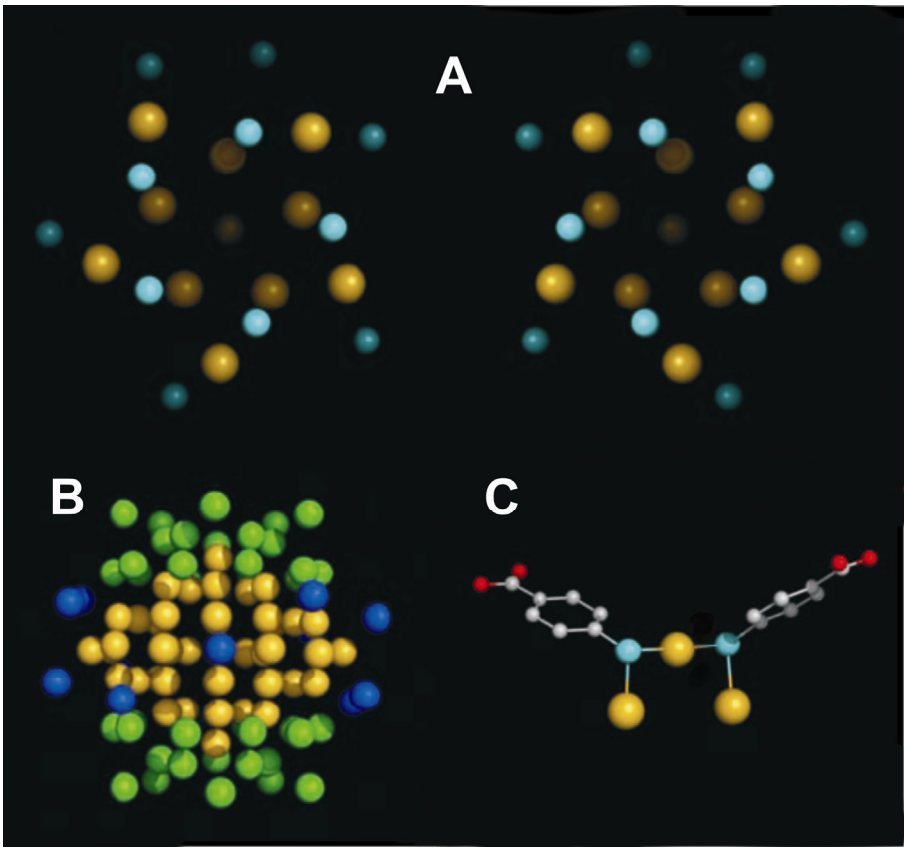

Figure 1.12 : X–ray crystal structure determination of the Au_{102}(*p*-MBA)$_{44}$ NPs. A) View down the cluster axis of the two enantiomers (gold atoms in yellow and sulfur atoms in cyan). B) Packing of gold atoms in the core. MD (2,1,2) in yellow, two 20-atom "caps" at the poles in green, and the 13-atom equatorial band in blue. C) Sulfur-gold interactions in the surface of the NPs. Example of two *p*-MBAs interacting with three gold atoms in a bridge conformation. Gold atoms are yellow, sulfur atoms are cyan, oxygen atoms are red, and carbon atoms are gray. Reprinted from Jadzinsky, Pablo D. *et al.*, ref. [64], with permission from AAAS.

Evidently, we can not assume that the structure of the center part of NPs considerably smaller than 102 gold atoms resembles the bulk metal structure. Indeed, Häkkinen and co-workers using DFT calculations predicted that the structure of a $Au_{38}(SCH_3)_{24}$ cluster consists of ringlike $(AuSCH_3)_4$ units protecting a central Au_{14} core.[65] The three models described above can still act concomitantly but their individual contribution remained undetermined.

Distortion of surface atoms involved in the adsorption of capping agent, is now proved to be a major element in chirality of NPs. Bidentate chiral ligands have demonstrated their ability to induce optical activity in MBETs probably by controlling enantioselectively the geometry of the surface atoms and the absolute configuration of the thiolate-stereogenic centers.

1.7 Optically Active Coordination Clusters

As NPs and organometallic complexes, coordination clusters have stimulated great interest in the field of catalysis and especially for asymmetric catalysis.[66, 67] In addition to the classical asymmetric induction originating from the chirality of the organic ligands, clusters are expected to be able to induce chirality through their chiral metallic framework.

The development of intrinsically chiral organometallic clusters is closely related to methods for their rational synthesis with a desirable molecular geometry. The work of Beurich[68] on metal exchange reaction as well as the multi-step addition and substitution reactions by systematic incorporation of organometallic units have laid the basis on cluster design.[69-73] Actually various types of chiral clusters such as hetero- or homo-metallic tetrahedrane-type clusters[74, 75] or pentanuclear wing-type butterfly heterotrimetallic clusters[76] are accessible by systematic synthetic procedures. Such pathway inevitably leads to a racemic mixture of the chiral metallic framework. The mixture can be enriched in one of its enantiomeric forms when a chiral ligand is used.[77] Tunik *et al.* have reported that the reaction of the ligand (*S*)-BINAP[78] with $H_4Ru_4(CO)_{12}$ or (*S*,*S*)-BOTPHOS[79] with $CpRhRu_3(H)_3(CO)_{10}$ produces clusters with up to 100% stereoselectivity. However, this type of quantitative stereoselectivity is still uncommon and furthermore the separation into

enantiomers remains one of the major challenges in order to use this material as asymmetric catalyst. The traditional method consists in the derivatization of the racemic mixture with a chiral auxiliary before separation of the diastereoisomers by chromatography or fractional crystallization. This method allows the efficient separation of enantiomers of clusters which are optically active even after removal of the auxiliary.[80, 81] However, this pathway is often time-consuming or inefficient and removal of the chiral auxiliary can lead to damaging or racemizing the cluster.[77, 82] High pressure liquid chromatography is an efficient alternative mild method that does not require derivatization when a chiral stationary phase is used. Nevertheless very few clusters have been separated by this method.[83] The optical activity of enantiopure chiral clusters is very strong and depends on the composition of the metallic framework as much as on the type of the capping ligand. The presence of a chiral auxiliary modulates the ECD curves but does not change the general appearance of the signal.[74]

Clusters have become especially important in a wide variety of heterogeneous catalytic reactions such as for example, oxidation, isomerization of alkenes, carbonylation and reduction of multiple bonds.[84] This list is not exhaustive and industrial reactions, such as oxidation of butane to maleic anhydride, can enlarge this panel.[85] However, despite this rich catalytic activity of organometallic clusters, the envisioned breakthrough in the field of asymmetric catalysis using clusters with framework chirality is still unsuccessful. This situation is probably due to on the one hand the very small number of enantiopure clusters known today, but also on the other hand due to the racemization of the metallic framework under the catalytic conditions such as CO pressure, UV irradiation or heating.[74] Furthermore, the question whether organometallic complexes and clusters act as catalyst or

whether they are precursor for the formation of NPs which are the real catalyst remains open for many reactions. Recently, Mario Barberes and coworkers have published the catalytic cyclopropanation of styrene with ethyl diazoacetate using a chiral heterodimetallic cubane-type cluster with 25% enantiomeric excess (ee) but this small ee can not be attributed only to the chiral metallic framework since the ligands are also chiral.[86] The concept of asymmetric catalysis using metallic framework still remains to be demonstrated.

1.8 Nanoparticles of Chiral Organic Compounds

In recent years ONPs of various compounds have been in the focus of interest of researchers due to their potential use in the fields of optoelectronics, nonlinear optics, photonics, sensing,[87] recognition,[88] and DNA delivery.[89] ONPs have been extensively described in the book of Masuhara.[90] ONPs bridge the gap between isolated molecules and the bulk crystal. As for their inorganic analogues, the properties of ONPs strongly depend on their size, their shape and also to their assembly. However, in the case of ONPs, the electronic and optical properties are fundamentally different from those of metal and semiconductor NPs. This has to do with the much weaker interaction between the constituents in ONPs, which are typically of the van der Waals type. In the case of ONPs the size dependant properties arise from aggregation, increased intermolecular interaction (many body interaction) and surface effects.[91, 92] For example emission spectra are tunable by alteration of the size of the ONPs. Besides that additional great diversity of properties can be obtained through variation of organic molecular structures. Park and coworkers have shown that ONPs of 1-cyano-trans-1,2-bis-(4'-methylbiphenyl)ethylene (CN-MBE) exhibit an

enhanced emission when compared to the weak fluorescence of the monomers in solution. The fluorescence switches off in the presence of organic vapor, which is interesting for sensing applications.[87] This unusual enhancement of emission in CN-MBE NPs is attributed to the synergetic effect of intramolecular planarization and *J*-type aggregate formation that restrict excimer formation to NPs.

The optical activity of chiral ONPs is also size dependent. Recently, different ONPs from chiral auxiliary such as (*R*)-(+)-1,1'-bi-2-naphthol dimethyl ether (BNDE), (*R*)-di-2-naphthylprolinol (DNP) and (*R*)-(–)-2,2'-bis-(*p*-toluenesulfonyloxy)-1,1'- binaphthalene (*R*-BTBN) have been prepared and studied by Yao and coworkers.[93-95] Their studies show that the optical activity of the chiral ONPs follows the same trend as the absorption. The exciton chirality peaks evolves to the low-energy side with increase in particles size. Surprisingly, the ECD spectra of the ONPs of BNDE and DNP are completely opposite to ECD spectra of the dilute monomers. For the *R*-BTBN NPs, the intensity ratio of the first to the third Cotton effects increases as the size of the ONPs increases to 60 nm. This trend is explained by the more effective excimer formation between the two chromophores in adjacent molecules due to the change of torsion angle as the ONPs grow in size. These works successfully demonstrate the manipulation of exciton chirality by simply changing the size of the ONPs. This degree of chirality control might be of practical value, for example, for the use of the particles as active components in optically switchable devices and in asymmetric syntheses via photochemistry in the solid-state with the ionic chiral auxiliary approach.[96] Cho *et al.* have demonstrated the ability of chiral hexablock copolymeric NPs for the chiral recognition of bilirubin.[88]

ONPs are generally prepared using simple methods such as reprecipitation,[97] evaporation or formation of microemulsion.[98] In reprecipitation, the most commonly used process, a molecularly disperse solution of the organic compounds in a water-miscible solvent is mixed vigorously with an aqueous phase, which induces the nucleation and growth of ONPs. The size is controlled by the growth parameters such as the monomer and the solvents concentrations. The stability of ONPs prepared by the reprecipitation method can be increased by the formation of a protective layer using a surfactant or a water soluble polymer as for example gelatin or poly(vinyl alcohol) (PVA). The size of ONPs can be tailored by adding the stabilizer at different aging times.[99]

1.9 Applications

NPs are of considerable interest because of to their wide variety of potential application in various fields such as biosensing,[100] optics,[101] electronics, photonics,[26] catalysis,[102] nanotechnology[15] and drug or DNA delivery.[89, 103] Chiral NPs are particularly interesting for asymmetry amplification at different length scales that means as chiral catalysts for chemical synthesis and chiral selective membranes or chiral dopant in LCs. Further applications may be envisaged for the detection of chirality or may be related to the optical activity.

1.9.1 Asymmetric Catalysis

Metallic NPs are potentially able to be active in catalysis. NPs can also be used as catalyst support. In this case the properties of homogenous and heterogenous catalysis are

combined. For example the catalytic properties of complexes supported on NPs can be influence by the neighboring chiral ligands.[104] An advantage of such a catalyst is the rapid separation from products and subtracts by using precipitation, membrane based techniques, SEC, or even magnetic fields. Recently, Hu and coworkers reported the immobilization of preformed Ru catalysts on magnetite NPs. These systems catalyzed the asymmetric hydrogenation of aromatic ketones with an ee up to 98%. The latter chiral catalyst, which can be removed magnetically, was easily recycled up to 14 times without loss of activity and enantioselectivity.[105]

The intrinsic catalytic behavior of NPs has been widely examined. Many NPs proved to be efficient and selective catalysts not only for reactions that are also known to be catalyzed by molecular complexes, such as olefin hydrogenation or C-C coupling,[12] but moreover for reactions which are not or are poorly catalyzed by molecular species, such as aromatic hydrogenation.[106] Unambiguous distinction between colloidal and molecular catalysis is, however often very difficult to make.[107, 108] As shown in the section 1.6, metallic NPs may be intrinsically chiral and, as discussed for organometallic clusters, optically active NPs can potentially combine the chirality of their core and of their organic shell in order to induce enantioselectivity to prochiral substrates. Despite the impressive progress in catalysis; however, only a few NPs systems have been shown to be efficient in asymmetric catalysis till today.[51, 102, 109-116]

The first example of an asymmetric reaction shown in **Figure 1.13** was reported in 1994 by Lemaire and coworkers who used rhodium NPs stabilized by a chiral amine ((*R*)-dioctylcyclohexyl-1-ethylamine) for the hydrogenation of *o*-cresol trimethylsilyl ether (top) or 2-methylanisole (bottom) with poor but significant ee values.[117]

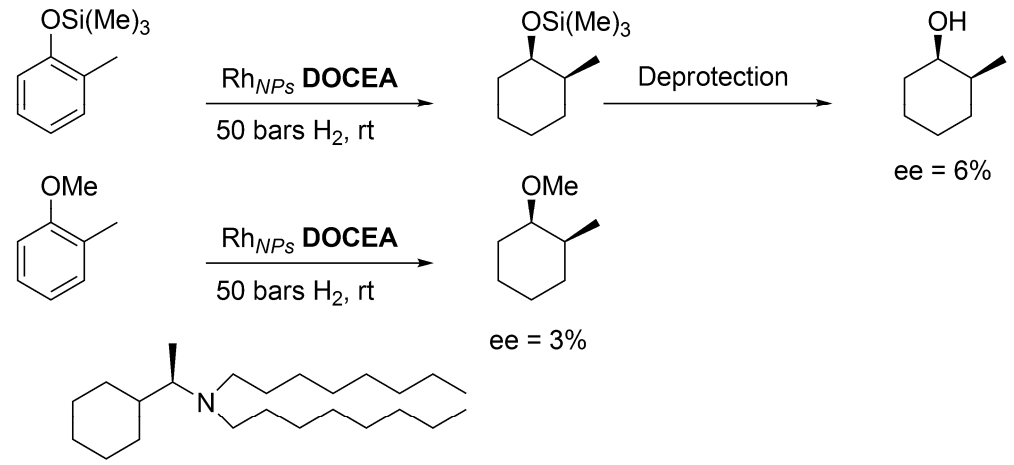

(*R*)-dioctylcyclohexyl-1-ethylamine (DOCEA)

Figure 1.13 : Enantioselective reduction of *o*-cresol trimethylsilyl ether and 2-methylanisol.

As shown in **Figure 1.14**, the most relevant systems involve Pt and Pd NPs stabilized by cinchonidine (CD), in the hydrogenation of pyruvate derivatives. When Bönneman introduced this concept in 1996, he reported the hydrogenation of ethyl pyruvate into (*R*)-ethyl lactate with 75-80% ee using platinium particles stabilized with dihydrocinchonidine salt (DH-CIN) in the liquid phase or immobilized on charcoal or silica.[109, 111]

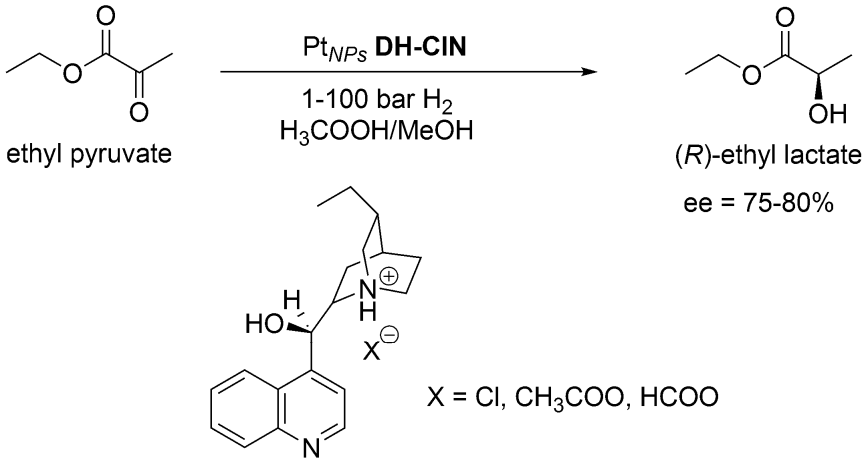

Figure 1.14 : Enantioselective reduction of ethyl pyruvate.

The preparation of the catalyst was more recently revisited and Pt NPs stabilized with PVP and modified with CD have allowed improving the ee up to 95-98%.[112-114] The sense of enantioselectivity can be reversed with respect to the CD Pt NPs system either by changing the chiral modifier to cinchonine (CN) or by changing Pt for Pd.[118] The latter switch is not explained but it reveals the significant role of the metal in the enantioselectivity. Interestingly, also the size of the NPs seems to influence enantioselectivity.

In 2003, Tamara *et al.* reported that Pd NPs (2 nm) optically active in MBETs and stabilized by BINAP, catalyze the hydrosilylation of styrene with trichlorosilane with an ee of 95% (see **Figure 1.15**). Interestingly, palladium complexes coordinated with BINAP are not active for this reaction.[51]

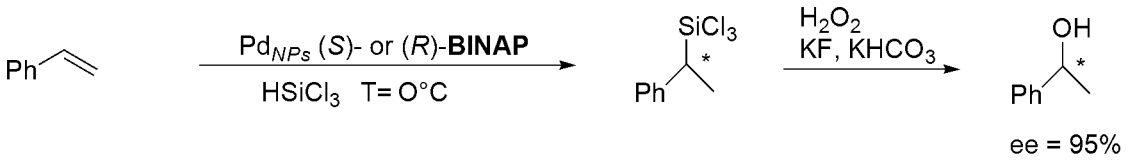

Figure 1.15 : Stereoselective hydrosilylation of styrene with trichlorosilane in the presence of chiral Pd catalyst.

Chaudret and coworkers performed the enantioselective allylic alkylation of rac-3-acetoxy-1,3-diphenyl-1-propene with dimethyl malonate catalyzed by palladium NPs (4 nm) in the presence of a chiral xylofuranoside diphosphite. This reaction, shown in **Figure 1.16**, gives rise to 97% ee for the alkylation product and a kinetic resolution of the substrate recovered with 90% ee.[102]

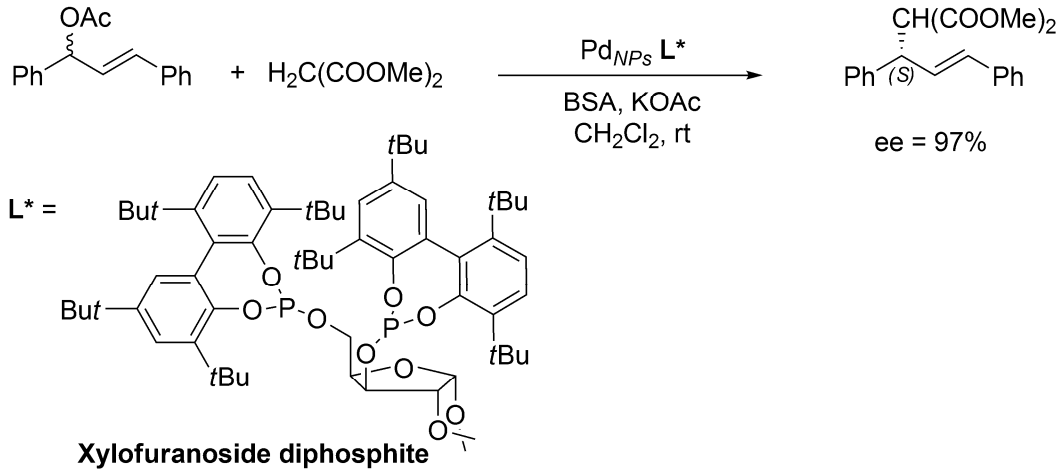

Figure 1.16 : Enantioselective allylic alkylation catalyzed by palladium NPs.

1.9.2 Nanoparticles in Liquid Crystal Media

A challenge in nanotechnology remains the control of the organization of NPs in order to integrate them in high-tech devices such as waveguides, band gap materials, light scattering

devices, flat panels and perfect lenses by avoiding the use of the top-down approach. Liquid crystalline (LC) materials appear as perfect candidates for the control of the crucial parameters size, shape and self-assembly of nanoscale materials in a one pot process. The use of LCs in syntheses and self-assembly has recently been reviewed by Hegmann and coworkers.[119] Organization of nanomaterials in LCs can furthermore respond to external stimuli such as an electric (magnetic) field or temperature. This opens the possibility to use such composites as electrical actuators.

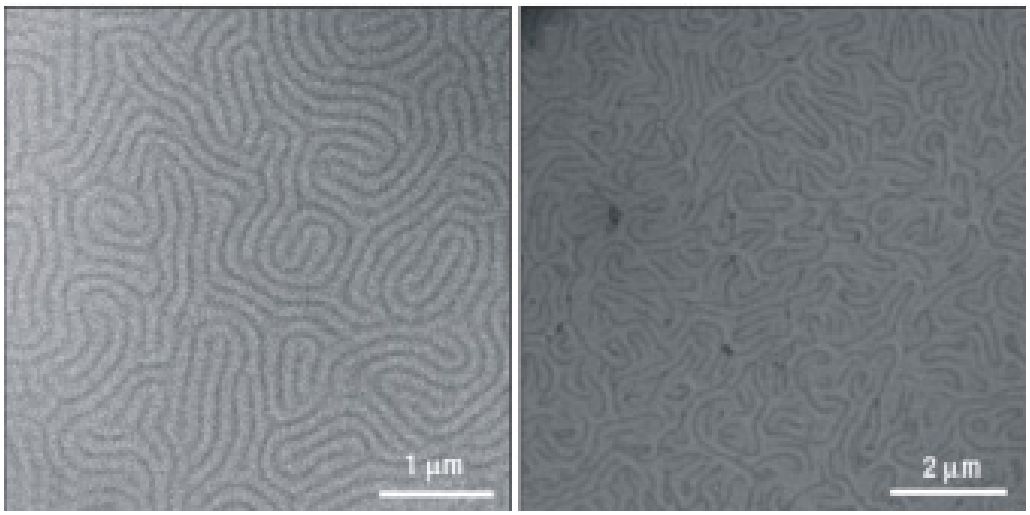

Figure 1.17 : TEM micrographs of the fingerprint cholesteric texture for the pure (left) and doped with achiral NPs (right) chiral liquid crystalline material. Reprinted with permission from Macmillan Publishers Ltd: Nature Materials, ref. [120], copyright (2002).

Figure 1.17 shows that the achiral NPs dispersed with a zwitterionic surfactant when in a cholesteric LC can order in accordance to the chiral helical structure of the chiral phase. The platinium NPs form periodic ribbons, which mimic the well-known cholesteric texture. De Guerville *et al.* also demonstrated that the NPs do not only decorate the pristine structure but create a novel structure characterized by a larger periodicity.[120, 121] They also

observed that this periodicity, that is the distance between the ribbons, can be tuned by varying the molar fraction of chiral mesogens present in the pure cholesteric host.

Recently, Hegmann has demonstrated that gold NPs protected by a chiral ligand, a Naproxen functionalized thiol, can be used to induce chirality to a non chiral nematic LC phase.[55] He also envisioned that the formed stripe texture might be tunable according to the size of the NPs or their functionality. This opens a pathway for improving LC mixtures for a variety of applications.

1.9.3 Chiral Discrimination

Self-assembled monolayers of chiral thiols on metal surfaces have proved their potential for enantiodiscrimination.[63] On account of their higher surface area compared with monolayers, chiral NPs should be even more interesting for discrimination. Kong and coworkers have already shown that gold NPs are efficient sensors with capability of probing chiral amino acids at the sub-picomolar level. The signal was monitored by differential potential voltammetry using a glassy carbon electrode modified with bovine serum albumine, which is a chiral modifier and amplified by silver atoms anchored on the gold NPs.[122]

1.10 Outlook

Nanoscience is still in the discovery phase, and this is particularly true for chiral NPs. Only very few examples of well-defined optically active NPs have been synthesized and only on a small scale (milligrams). However, examples of applications described in the last section show the very large potential of chiral NPs for example in enantioselective catalysis, in LC

displays and in chiral recognition. Progresses in enantioselective synthesis and in resolution of chiral NPs are expected in the near future. Integration of NPs in larger systems may allow the preparation of nanoscale optical components[29] and planar polarization-sensitive devices.[27] The merging of optical activity with SPs may pave the way for new types of "chirophotonic devices". NPs are already starting materials or catalysts for the preparation of larger anisotropic nanomaterials such as NRDs. Perhaps chiral NPs will allow the preparation of larger chiral nanomaterials. Finally, chiral NPs are also of fundamental interest as nanometer size analogues of extended chiral metal surfaces and serve as models for the better understanding of interactions between surfaces and organic molecules.

1.11 References

[1] M. O. Lorenzo, S. Haq, T. Bertrams, P. Murray, R. Raval, C. J. Baddeley, *J. Phys. Chem. B* **1999**, *103*, 10661.

[2] C. F. McFadden, P. S. Cremer, A. J. Gellman, *Langmuir* **1996**, *12*, 2483.

[3] C. F. McFadden, P. S. Cremer, A. J. Gellman, *J. Am. Chem. Soc.* **1996**, *12*, 2483.

[4] J. D. Horvath, A. J. Gellman, *J. Am. Chem. Soc.* **2001**, *123*, 7953.

[5] G. A. Attard, *J. Phys. Chem. B* **2001**, *105*, 3158.

[6] S. M. Barlow, R. Raval, *Surf Sci* **2005**, *590*, 243.

[7] M. Parschau, S. Romer, K. H. Ernst, *J. Am. Chem. Soc.* **2004**, *126*, 15398.

[8] R. Fasel, M. Parschau, K.-H. Ernst, *Nature* **2006**, *439*, 449.

[9] Y. Izumi, *Adv. catal.* **1983**, *32*, 215.

[10] Y. Orito, S. Imai, S. Niwa, *J. Chem. Soc. Japan* **1979**, 1118.

[11] M. Haruta, *Catal. Today* **1997**, *36*, 153.

[12] A. Roucoux, J. Schulz, H. Patin, *Chem. Rev.* **2002**, *102*, 3757.

[13] G. Schmid, *Nanoparticles From Theory to Application* Wiley-vch, Weinheim, **2004**.

[14] J. A. Dahl, B. L. S. Maddux, J. E. Hutchison, *Chem. Rev.* **2007**, *107*, 2228.

[15] M. C. Daniel, D. Astruc, *Chem. Rev.* **2004**, *104*, 293.

[16] K. L. Kelly, E. Coronado, L. L. Zhao, G. C. Schatz, *J. Phys. Chem. B* **2003**, *107*, 668.

[17] C. Gautier, T. Bürgi, *J. Am. Chem. Soc.* **2006**, *128*, 11079.

[18] S. Park, M. Pelton, M. Liu, P. Guyot-Sionnest, N. F. Scherer, *J. Phys. Chem. C* **2007**, *111*, 116.

[19] K. K. Caswell, J. N. Wilson, U. H. F. Bunz, C. J. Murphy, *J. Am. Chem. Soc.* **2003**, *125*, 13914.

[20] X. Hu, W. Cheng, T. Wang, E. Wang, S. Dong, *Nanotechnology* **2005**, *16*, 2164.

[21] J. Y. Chang, H. Wu, H. Chen, Y. C. Ling, W. Tan, *Chem. Commun.* **2005**, 1092.

[22] Y. Oshima, H. Koizumi, K. Mouri, H. Hirayama, K. Takayanagi, Y. Kondo, *Phys. Rev. B* **2002**, *65*, 121401.

[23] Y. Oshima, A. Onga, K. Takayanagi, *Phys. Rev. Lett.* **2003**, *91*, 205503.

[24] J. B. Pendry, *Phys. Rev. Lett.* **2000**, *85*, 3966.

[25] R. Elghanian, J. J. Storhoff, R. C. Mucic, R. L. Letsinger, C. A. Mirkin, *Science* **1997**, *277*, 1078.

[26] W. L. Barnes, A. Dereux, T. W. Ebbesen, *Nature* **2003**, *424*, 824.

[27] V. Tuomas, J. Konstantins, T. Jari, V. Pasi, S. Yuri, *Appl. Phys. Lett.* **2003**, *83*, 234.

[28] S. Yuri, Z. Nikolay, O. Michail, *Appl. Phys. Lett.* **2001**, *78*, 498.

[29] B. Canfield, S. Kujala, K. Laiho, K. Jefimovs, J. Turunen, M. Kauranen, *Vol. 5927* (Ed.: I. S. Mark), SPIE, **2005**, p. 59270C.

[30] Y. Yanagimoto, Y. Negishi, H. Fujihara, T. Tsukuda, *J. Phys. Chem. B* **2006**, *110*, 11611.

[31] M. Brust, M. Walker, D. Bethell, D. J. Schiffrin, R. Whyman, *J. Chem. Soc., Chem. Commun.* **1994**, 801.

[32] J. Turkevich, P. Stevenson, J. Hillier, *Discuss. Faraday Soc.* **1951**, *11*, 55.

[33] G. Schmid, *Inorg. Synth.* **1990**, *27*, 214.

[34] Y. Song, T. Huang, R. W. Murray, *J. Am. Chem. Soc.* **2003**, *125*, 11694.

[35] Y. Shichibu, Y. Negishi, T. Tsukuda, T. Teranishi, *J. Am. Chem. Soc.* **2005**, *127*, 13464.

[36] R. Balasubramanian, R. Guo, A. J. Mills, R. W. Murray, *J. Am. Chem. Soc.* **2005**, *127*, 8126.

[37] Y. Shichibu, Y. Negishi, H. Tsunoyama, M. Kanehara, T. Teranishi, T. Tsukuda, *Small* **2007**, *3*, 835.

[38] T. G. Schaaff, G. Knight, M. N. Shafigullin, R. F. Borkman, R. L. Whetten, *J. Phys. Chem. B* **1998**, *102*, 10643.

[39] H. Yao, K. Miki, N. Nishida, A. Sasaki, K. Kimura, *J. Am. Chem. Soc.* **2005**, *127*, 15536.

[40] N. Nishida, H. Yao, T. Ueda, A. Sasaki, K. Kimura, *Chem. Mater.* **2007**, *19*, 2831.

[41] H. Yao, T. Fukui, K. Kimura, *J. Phys. Chem. C* **2007**, *111*, 14968.

[42] C. Gautier, R. Taras, S. Gladiali, T. Bürgi, *Chirality* **2007**, *20*, 486.

[43] L. A. Nafie, *Annu. Rev. Phys. Chem.* **1997**, *48*, 357.

[44] T. B. Freedman, X. Cao, R. K. Dukor, L. A. Nafie, *Chirality* **2003**, *15*, 743.

[45] C. H. Edward, G. Holzwarth*, Vol. 59*, AIP, **1973**, pp. 4678.

[46] L. A. Nafie, T. A. Keiderling, P. J. Stephens, *J. Am. Chem. Soc.* **1976**, *98*, 2715.

[47] L. A. Nafie, M. Diem, *Appl. Spectr.* **1979**, *33*.

[48] C. Gautier, T. Bürgi, *Chem. Commun.* **2005**, *43*, 5393.

[49] T. L. Wetzel, A. E. DePristo, *J. Chem. Phys.* **1996**, *105*, 572.

[50] E. K. Parks, K. P. Kerns, S. J. Riley, *J. Chem. Phys.* **1998**, *109*, 10207.

[51] M. Tamura, H. Fujihara, *J. Am. Chem. Soc.* **2003**, *125*, 15742.

[52] T. Li, H. G. Park, H. S. Lee, S. H. Choi, *Nanotechnology* **2004**, *15*, S660.

[53] G. Shemer, O. Krichevski, G. Markovich, T. Molotsky, I. Lubitz, A. B. Kotlyar, *J. Am. Chem. Soc.* **2006**, *128*, 11006.

[54] N. Bovet, N. McMillan, N. Gadegaard, M. Kadodwala, *J. Phys. Chem. B* **2007**.

[55] H. Qi, T. Hegmann, *J. Mater. Chem.* **2006**, *16*, 4197.

[56] I. L. Garzón, M. R. Beltran, G. Gonzalez, I. Gutierrez-Gonzalez, K. Michaelian, J. A. Reyes-Nava, J. I. Rodriguez-Hernandez, *Eur. Phys. J. D* **2003**, *24*, 105.

[57] I. L. Garzón, J. A. Reyes-Nava, J. I. Rodríguez-Hernández, I. Sigal, M. R. Beltrán, K. Michaelian, *Phys. Rev. B* **2002**, *66*, 073403.

[58] M. R. Goldsmith, C. B. George, G. Zuber, R. Naaman, D. H. Waldeck, P. Wipf, D. N. Beratan, *Phys. Chem. Chem. Phys.* **2006**, *8*, 63.

[59] V. Humblot, S. Haq, C. Muryn, W. A. Hofer, R. Raval, *J. Am. Chem. Soc.* **2002**, *124*, 503.

[60] M. Bieri, T. Bürgi, *J. Phys. Chem. B* **2005**, *109*, 22476.

[61] M. Bieri, T. Bürgi, *Langmuir* **2005**, *21*, 1354.

[62] M. Bieri, T. Bürgi, *Phys. Chem. Chem. Phys.* **2006**, *8*, 513.

[63] M. Bieri, C. Gautier, T. Bürgi, *Chem. Phys. Phys. Chem.* **2007**, *9*, 671.

[64] P. D. Jadzinsky, G. Calero, C. J. Ackerson, D. A. Bushnell, R. D. Kornberg, *Science* **2007**, *318*, 430.

[65] H. Häkkinen, M. Walter, H. Gronbeck, *J. Phys. Chem. B* **2006**, *110*, 9927.

[66] P. Bladon, P. L. Pauson, H. Brunner, R. Eder, *J. Organomet. Chem.* **1988**, *355*, 449.

[67] R. D. Adams, *Catalysis by Di- and Polynuclear Metal Cluster Complexes*, John Wiley and Sons, New York, **1998**.

[68] H. Beurich, H. Vahrenkamp, *Angew. Chem. Int. Ed.* **1978**, *17*, 863.

[69] D. Mani, H. Vahrenkamp, *Chem. Ber.* **1986**, *119*, 3639.

[70] M. Müller, H. Vahrenkamp, *Chem. Ber.* **1983**, *116*, 2311.

[71] M. Müller, H. Vahrenkamp, *Chem. Ber.* **1983**, *116*, 2322.

[72] P. Gusbeth, H. Vahrenkamp, *Chem. Ber.* **1985**, *118*, 1746.

[73] F. Gordon, A. Stone, *Angew. Chem. Int. Ed.* **1984**, *23*, 89.

[74] H. Vahrenkamp, *J. Organomet. Chem.* **1989**, *370*, 65.

[75] L. Vieille-Petit, G. Suss-Fink, B. Therrien, T. R. Ward, H. Stoeckli-Evans, G. Labat, L. Karmazin-Brelot, A. Neels, T. Bürgi, R. G. Finke, C. M. Hagen, *Organometallics* **2005**, *24*, 6104.

[76] S. P. Gubin, T. V. Galuzina, I. F. Golovaneva, A. P. Klyagina, L. A. Polyakova, O. A. Belyakova, Y. V. Zubavichus, Y. L. Slovokhotov, *J. Organomet. Chem.* **1997**, *549*, 55.

[77] H. V. Eckehart Roland, *Chem. Ber.* **1984**, *117*, 1039.

[78] S. P. Tunik, T. S. Pilyugina, I. O. Koshevoy, S. I. Selivanov, M. Haukka, T. A. Pakkanen, *Organometallics* **2004**, *23*, 568.

[79] I. O. Koshevoy, S. P. Tunik, A. J. Poe, A. Lough, J. Pursiainen, P. Pirila, *Organometallics* **2004**, *23*, 2641.

[80] H. V. Felix Richter, *Chem. Ber.* **1982**, *115*, 3243.

[81] M. Müller, H. Vahrenkamp, *Chem. Ber.* **1983**, *116*, 2748.

[82] R. Blumhofer, H. Vahrenkamp, *Chem. Ber.* **1986**, *119*, 683.

[83] X. Wang, W. Z. Li, Q. Y. Zhao, Y. M. Li, L. R. Chen, *Anal. Sci.* **2005**, *21*, 125.

[84] I. I. Moiseev, M. N. Vargaftik, *New J. Chem.,* **1998**, *22*, 1217.

[85] G. Busca, G. Centi, *J. Am. Chem. Soc.* **1989**, *111*, 46.

[86] M. Feliz, E. Guillamón, R. Llusar, C. Vicent, S. E. Stiriba, J. Pérez-Prieto, M. Barberis, *Chem. Eur. J.* **2006**, *12*, 1486.

[87] B. K. An, S. K. Kwon, S. D. Jung, S. Y. Park, *J. Am. Chem. Soc.* **2002**, *124*, 14410.

[88] T. W. Chung, K. Y. Cho, J. W. Nah, T. Akaike, C. S. Cho, *Langmuir* **2002**, *18*, 6462.

[89] S. Kommareddy, M. Amiji, *Nanomedicine: NBM* **2007**, *3*, 32.

[90] H. Masuhara, H. Nakanishi, K. Sasaki, *Single Organic Nanoparticles*, Springer, Verlag, **2003**.

[91] H. Fu, B. H. Loo, D. Xiao, R. Xie, X. Ji, J. Yao, B. Zhang, L. Zhang, *Angew. Chem. Int. Ed.* **2002**, *41*, 962.

[92] H. B. Fu, J. N. Yao, *J. Am. Chem. Soc.* **2001**, *123*, 1434.

[93] D. Xiao, W. Yang, J. Yao, L. Xi, X. Yang, Z. Shuai, *J. Am. Chem. Soc.* **2004**, *126*, 15439.

[94] L. Xi, H. Fu, W. Yang, J. Yao, *Chem. Commun.* **2005**, 492.

[95] Y. Zhang, A. Peng, J. Wang, W. Yang, J. Yao, *J. Photochem. Photobiol., A* **2006**, *181*, 94.

[96] J. R. Scheffer, W. Xia, in *Organic Solid State Reactions*, Springer, Berlin / Heidelberg, **2005**, pp. 233.

[97] N. D. Denkov, O. D. Velev, P. A. Kralchevsky, I. B. Ivanov, H. Yoshimura, K. Nagayama, *Nature* **1993**, *361*, 26.

[98] F. Debuigne, L. Jeunieau, M. Wiame, J. B.Nagy, *Langmuir* **2000**, *16*, 7605.

[99] R. Xie, D. Xiao, H. Fu, X. Ji, W. Yang, J. Yao, *New J. Chem.* **2001**, *25*, 1362.

[100] N. L. Rosi, C. A. Mirkin, *Chem. Rev.* **2005**, *105*, 1547.

[101] S. Sun, C. B. Murray, D. Weller, L. Folks, A. Moser, *Science* **2000**, *287*, 1989.

[102] S. Jansat, M. Gomez, K. Philippot, G. Muller, E. Guiu, C. Claver, S. Castillon, B. Chaudret, *J. Am. Chem. Soc.* **2004**, *126*, 1592.

[103] R. Hong, G. Han, J. M. Fernandez, B. j. Kim, N. S. Forbes, V. M. Rotello, *J. Am. Chem. Soc.* **2006**, *128*, 1078.

[104] T. Belser, M. Stohr, A. Pfaltz, *J. Am. Chem. Soc.* **2005**, *127*, 8720.

[105] A. Hu, G. T. Yee, W. Lin, *J. Am. Chem. Soc.* **2005**, *127*, 12486.

[106] J. A. Widegren, R. G. Finke, *J. Mol. Catal. A: Chem.* **2003**, *191*, 187.

[107] I. W. Davies, L. Matty, D. L. Hughes, P. J. Reider, *J. Am. Chem. Soc.* **2001**, *123*, 10139.

[108] J. A. Widegren, R. G. Finke, *J. Mol. Catal. A: Chem.* **2003**, *198*, 317.

[109] H. Bönnemann, G. A. Braun, *Angew. Chem. Int. Ed.* **1996**, *35*, 1992.

[110] M. Studer, H. U. Blaser, C. Exner, *Adv. Synth. Catal.* **2003**, *345*, 45.

[111] H. Bönnemann, G. A. Braun, *Chem. Eur. J.* **1997**, *3*, 1200.

[112] X. Zuo, H. Liu, D. Guo, X. Yang, *Tetrahedron* **1999**, *55*, 7787.

[113] J. U. Köhler, J. S. Bradley, *Catal. Lett.* **1997**, *45*, 203.

[114] J. U. Köhler, J. S. Bradley, *Langmuir* **1998**, *14*, 2730.

[115] V. Mevellec, C. Mattioda, J. Schulz, J. P. Rolland, A. Roucoux, *J. Catal.* **2004**, *225*, 1.

[116] S. Jansat, D. Picurelli, K. Pelzer, K. Philippot, M. Gomez, G. Muller, P. Lecante, B. Chaudret, *New J. Chem.* **2006**, *30*, 115.

[117] K. Nasar, F. Fache, M. Lemaire, J. C. Beziat, M. Besson, P. Gallezot, *J. Mol. Catal.* **1994**, *87*, 107.

[118] P. J. Collier, J. A. Iggo, R. Whyman, *J. Mol. Catal. A: Chem.* **1999**, *146*, 149.

[119] T. Hegmann, H. Qi, V. M. Marx, *J. Inorg. Organomet. Polym. Mat.* **2006**, 483.

[120] M. Mitov, C. Portet, C. Bourgerette, E. Snoeck, M. Verelst, *Nat. Mater.* **2002**, *1*, 229.

[121] M. Mitov, C. Bourgerette, F. de Guerville, *J. Phys.: Condens. Matter* **2004**, *16*, S1981.

[122] Y. Wang, X. Yin, M. Shi, W. Li, L. Zhang, J. Kong, *Talanta* **2006**, *69*, 1240.

2

Vibrational Circular Dichroism of NAC

Gold NPs

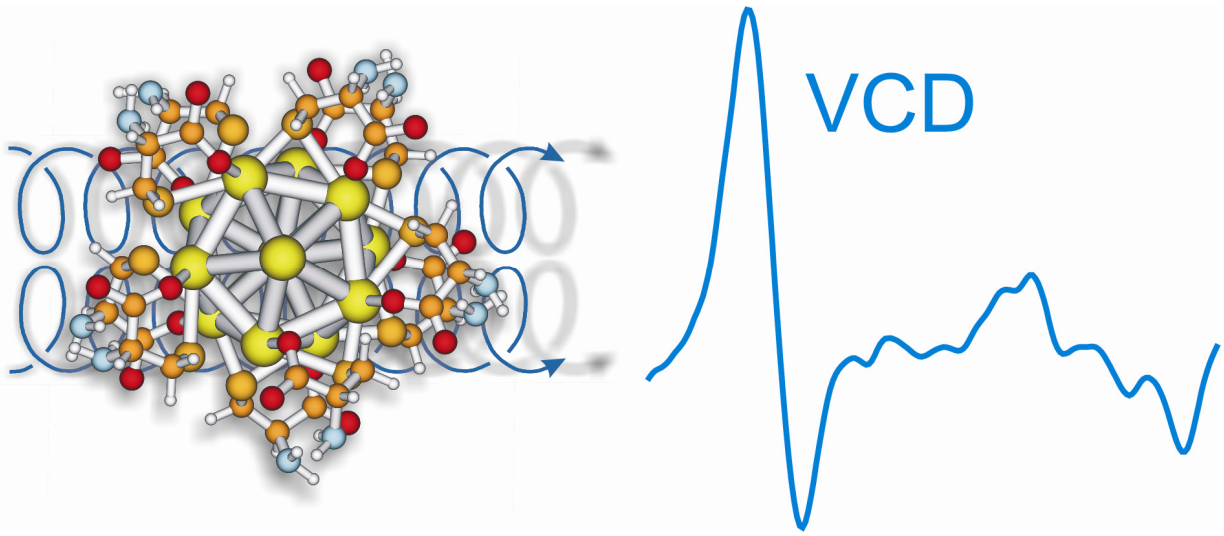

2.1 Introduction

Monolayer protected metal nanoparticles are of considerable interest due to their potential application in various fields such as bio-sensing, catalysis, electronics and nanotechnology.[1] Whereas the physical properties of monolayer protected nanoparticles (MPNs) are largely associated with the metal core, their chemical behaviour such as solubility, molecular recognition and organization is determined by the protection layer. The engineering of the latter is currently making tremendous progress.[2] The conformation of the molecules adsorbed on the metal particles directly affects the chemical properties. Structure determination would therefore greatly help the rational design of functionalized particles.

Vibrational circular dichroism (VCD) spectroscopy, *i.e.* the differential absorption of left and right circular polarized infrared light, yields detailed information on the conformation of a chiral molecule in solution.[3] VCD is more sensitive towards conformation than infrared (IR) spectroscopy and its power for structure determination of dissolved molecules, by the comparison between experimental and theoretical spectra, has impressively been demonstrated in the past.[4-7]

In this chapter we show that very small (< 2 nm) gold nanoparticles chirally modified with N-acetyl-*L*-cysteine (**Chart 2.1**) exhibit VCD activity associated with the molecules in the protection layer. Comparison with calculated VCD spectra of N-acetyl-*L*-cysteine adsorbed on small gold clusters allows getting rather detailed structural information. Whereas optical activity in the UV-vis of MPNs was reported before,[8] to the best of our knowledge this is the first report on VCD activity associated MPNs.

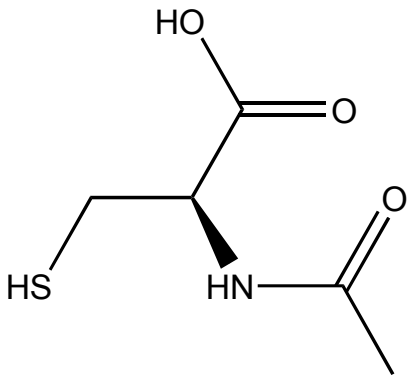

Chart 2.1 : Structure of N-acetyl-*L*-cysteine

2.2 Preparation of Gold NPs Protected with NAC

The MPNs were prepared following a previous report.[9] 400 mg of tetrachloroauric acid (1.01 mmol) and 663 mg N-acetyl-*L*-cysteine (4.06 mol) were dissolved in 200 ml of 6:1 methanol:acetic acid, giving a red solution, which rapidly turned into a cloudy white suspension. This indicates the formation of the a Au(I)N-acetyl-*L*-cysteine polymer.[10] After 15 minutes, the polymer was reduced by slow addition of a freshly prepared aqueous $NaBH_4$ solution (70 ml, 2.13 mol/l) under vigorous stirring. After 90 min of additional stirring, the resulting solution was filtered using 0.2 μm PTFE membranes (Millipore) to remove precipitates and subsequently evaporated under vacuum to near dryness. The nanoparticles were purified in two steps. The first one consisted in a series of precipitations with ethanol and filtration using 0.2 μm PTFE membranes. The removal of the remaining unreacted thiol or disulfide was finally completed by dialysis (Spectra/Por CE, molecular weight cut-off MWCO = 3'500 Da). Particles were dissolved in 30 ml water and loaded into a membrane, which was then placed in a 2 L beaker of water and slowly stirred. The water was changed

every 10 hours over the course of 96 hours. The black solution was evaporated under vacuum at T ≤ 40° C to give a black powder.

2.3 Transmission Electron Microscopy and UV-vis Spectroscopy

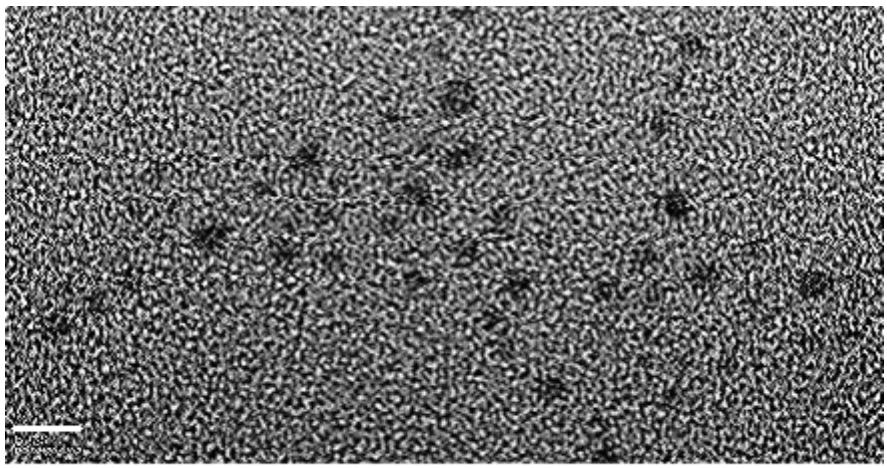

Figure 2.1 : Transmission electron microscopy of N-acetyl-*L*-cysteine MPNs.

Transmission electron microscopy (TEM) revealed gold particles with a maximum of the core size distribution below 2 nm (see **Figure 2.1**). This is in good agreement with the UV-vis spectrum of the sample (see **Figure 2.2**), which showed almost no surface plasmon resonance, thus revealing that the gold particles have core diameters of 2 nm or less.[11] Experimental details are described in Appendix A.2 on page 176.

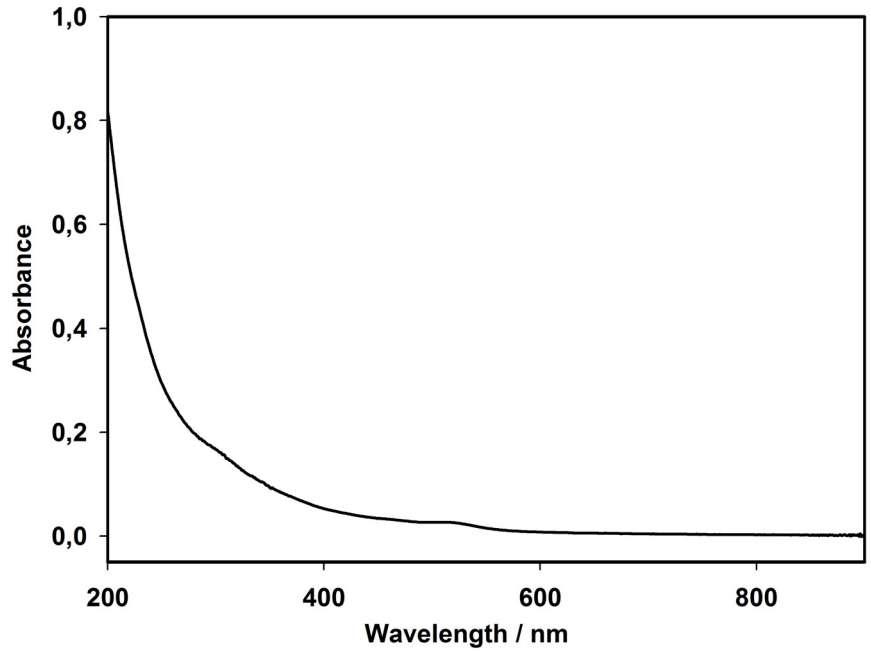

Figure 2.2 : UV-visible spectrum of N-acetyl-*L*-cysteine MPNs in water (c = 0.0235 mg.ml^{-1}).

The ^{1}H and ^{13}C NMR spectra of the sample (see **Figure 2.3**) are consistent with N-acetyl-*L*-cysteine adsorbed on the gold particles. Compared to the free molecule the resonances are significantly broadened. The absence of sharp resonances showed that the sample contained no free N-acetyl-*L*-cysteine molecules.

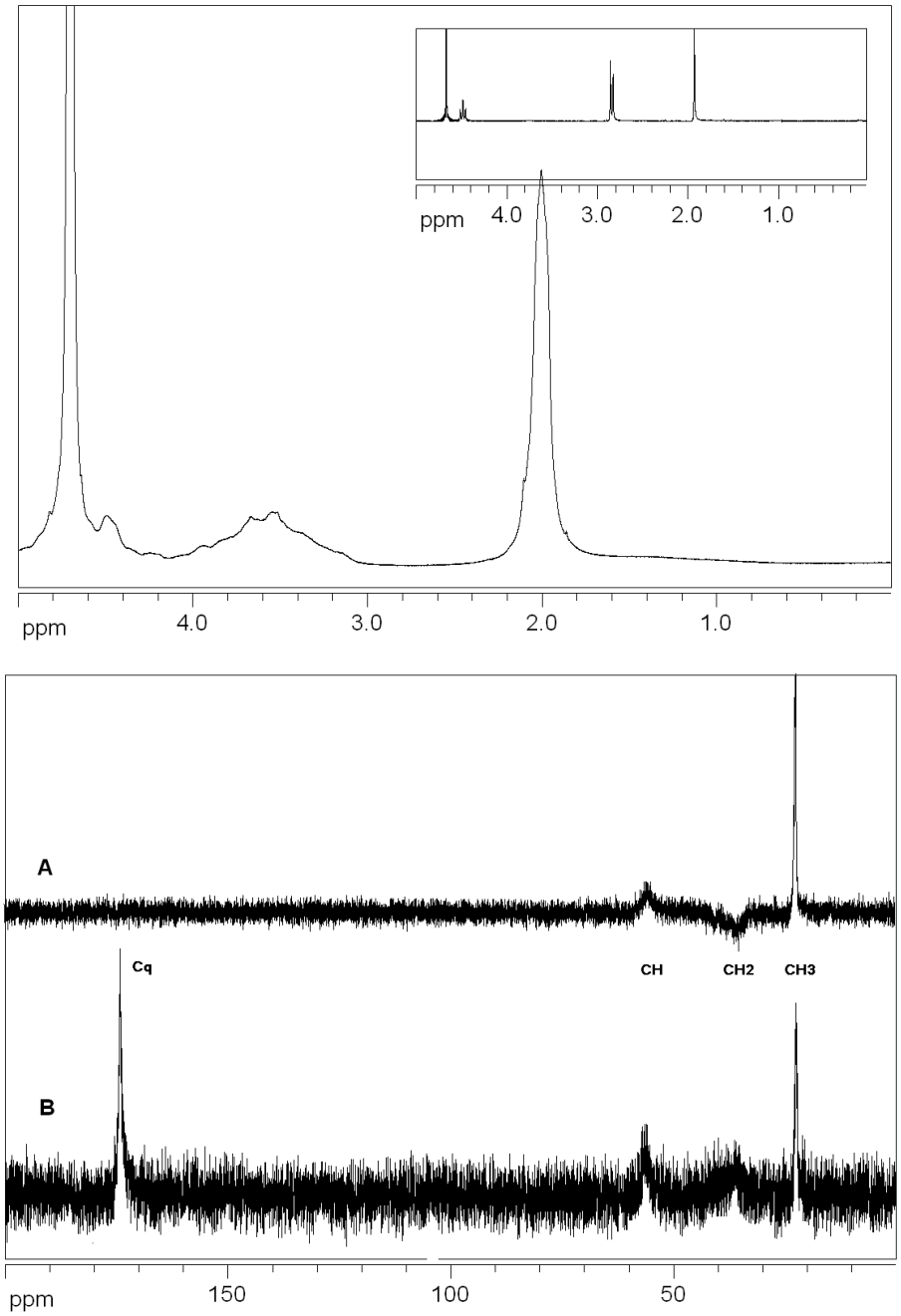

Figure 2.3 : Top: 400 MHz ^{1}H spectrum of N-acetyl-*L*-cysteine MPNs in D_2O at 298 K. The inset shows the free ligand for comparison. The resonance at 4.8 ppm is due to water. Bottom: 100 MHz NMR of N-acetyl-*L*-cysteine MPNs in D_2O (A) Distortion less enhancement by polarization transfer 135° (DEPT), (B) ^{13}C NMR.

2.4 IR and VCD Spectra

Figure 2.4 shows the experimental infrared and VCD spectra of the N-acetyl-*L*-cysteine protected gold nanoparticles. In D_2O a part of the acid groups are not deprotonaed. NaOD was therefore added in order to achieve complete deprotonation. Based on titration experiments the carboxylate vibrations $\upsilon_s(COO^-)$ and $\upsilon_{as}(COO^-)$ can easily be assigned to bands at 1387 and 1595 cm^{-1}. The former signal contains also the symmetric CH_3 deformation mode $\upsilon_s(CH_3)$, since a weak band below 1400 cm^{-1} is also observed in the fully protonated state. The amide I vibration is located at 1627 cm^{-1}. The rather broad feature around 1480 cm^{-1} is assigned to the amide II mode of the deuterated (N-D) molecules.[12] The band around 1425 cm^{-1} can be assigned to the $_{as}(CH_3)$ mode. The CH_2 scissoring mode also contributes to this band. This assignment is supported by the calculations (see below) and follows the assignment given by Pradier and coworkers for cysteine adsorbed on Cu(110).[13] Finally, the weaker band at around 1330 cm^{-1} is due to a CH bending mode. Experimental details are described in Appendix A.3 on page 176.

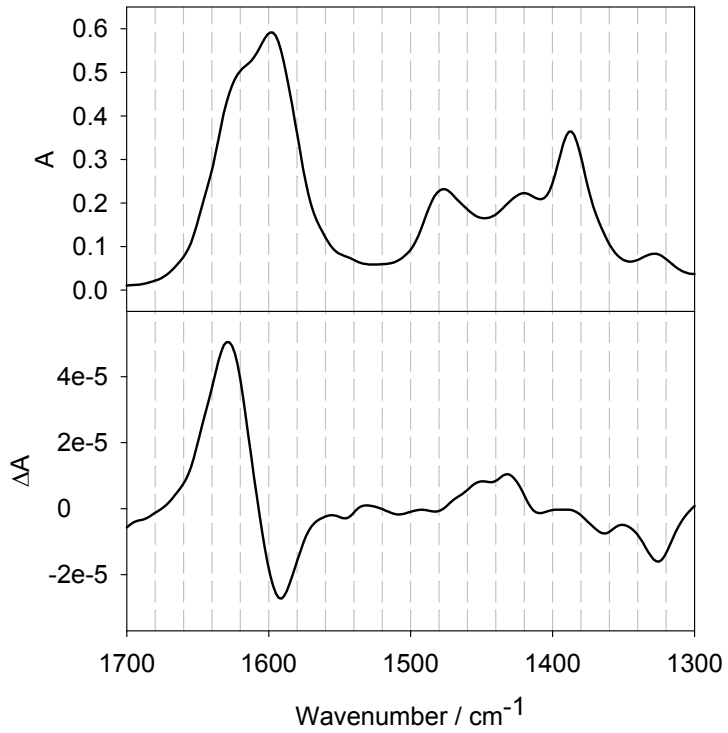

Figure 2.4 : Infrared (top) and VCD (bottom) spectra of N-acetyl-*L*-cysteine protected gold nanoparticles in D_2O. NaOD was added to deprotonate all acid groups. The solution was made from 8 mg sample in 70 µl solvent.

2.5 Conformation of NAC Adsorbed on Gold NPs

In order to extract structural information, the experimental VCD spectra have to be compared to calculated ones for the relevant conformers. The N-acetyl-*L*-cysteine protected nanoparticles investigated here contain 20-200 gold atoms (1-2 nm core diameters) and up to several tenths of adsorbed N-acetyl-*L*-cysteine molecules. The entire particle is too large to be calculated at the required accuracy and therefore models have to be used. Such an approximation is justified since molecular vibrations are a local property. For example, the vibrational spectrum of molecules adsorbed on a metal surface can very well be reproduced

by calculations that consider only one single molecule adsorbed on a small cluster of a few atoms.[14, 15]

N-acetyl-*L*-cysteine has several pertinent conformational degrees of freedom, namely the rotations around the three bonds comprising the chiral carbon atom (one C-N and two C-C bonds, **Chart 2.1**). Potential energy minima are largely determined by the hydrogen bond between the amide N-H and the carboxylate group. The part comprising the amide and methyl group on the other hand is rather rigid. Computational details are described in Appendix A.4 on page 177.

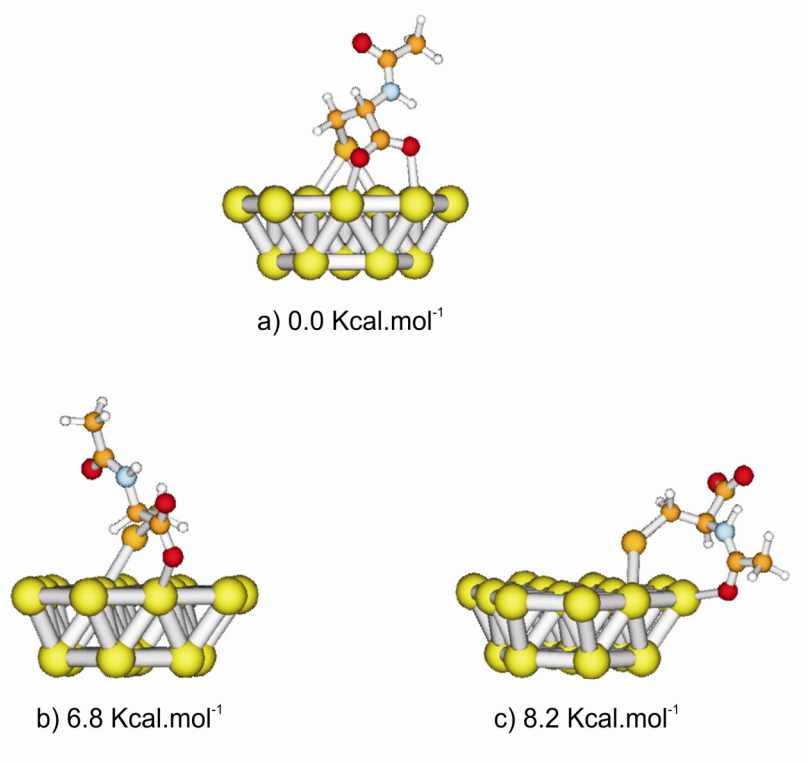

Figure 2.5 : Calculated conformers of deprotonated N-acetyl-*L*-cysteine on a Au_{19} cluster. The structures were optimized using ADF.[16] The numbers indicate the relative stability with respect to the most stable conformation a). For the calculations the structure of the Au_{19} cluster was fixed. For computational details see the experimental part.

To explore the potential energy surface for N-acetyl-*L*-cysteine adsorption on gold, cluster calculations were first performed using ADF.[16] It should be noted here that upon adsorption a thiolate is formed and therefore the corresponding thiolate of N-acetyl-*L*-cysteine was considered in the calculations. As a model served a Au_{19} cluster. The positions of the gold atoms were fixed at their bulk interatomic distance. The adsorption is primarily determined by the strong Au-S bond. We found that an additional interaction via the carboxylate leads to considerable stabilization. Some stable adsorption geometries are given in **Figure 2.5**. It should be mentioned here that the relative stability of the different conformers is likely affected by intermolecular interactions between adjacent molecules, which are neglected in the calculations. However, the relative stability of a conformer is not used as the primary argument for structure determination. It is rather the comparison between calculated and experimental VCD spectra that yields this information and the vibrational properties are much less affected by weak intermolecular interactions.

The size of the cluster was then further reduced in order to calculate VCD spectra of adsorbed N-acetyl-*L*-cysteine using Gaussian03.[17] We first considered the four gold atoms of the larger Au_{19} cluster that directly interact with the molecule. The structure of the adsorbed N-acetyl-*L*-cysteine was then re-optimized, keeping the positions of the gold atoms in the Au_4 cluster fixed. Structure a') in **Figure 2.6** is the result of such a calculation. **Figure 2.8** shows the calculated VCD spectrum (trace a')) for this structure. The corresponding IR spectrum is given in **Figure 2.7**.

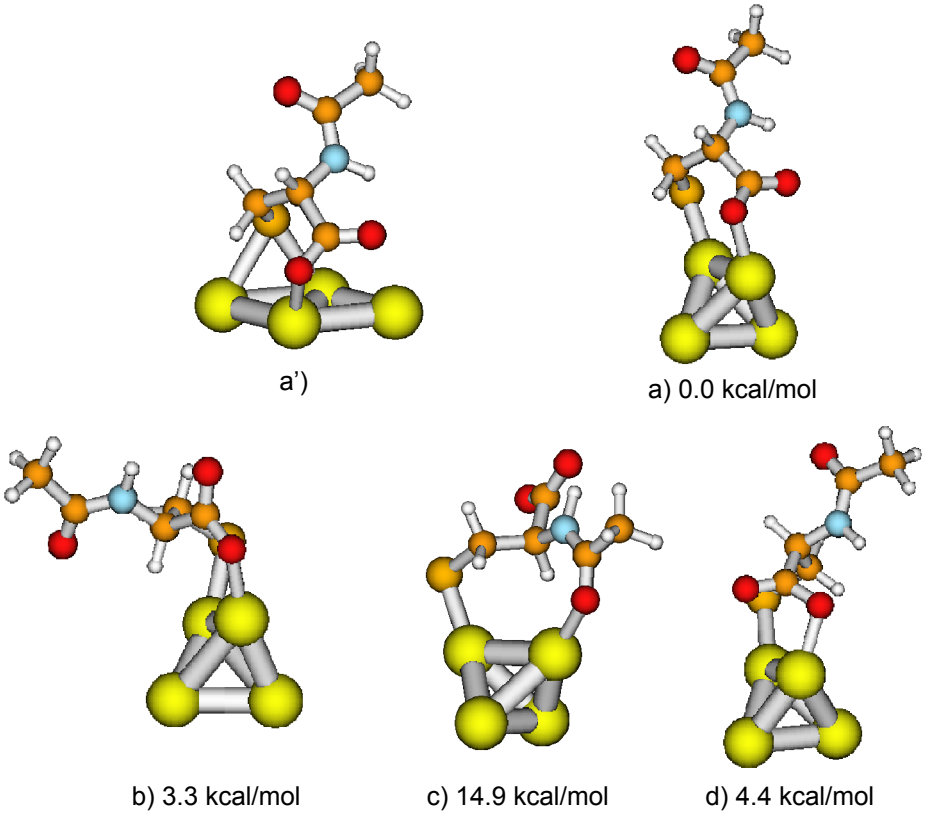

Figure 2.6 : Calculated conformers of deprotonated N-acetyl-*L*-cysteine on a Au_4 cluster. The structures were optimized using Gaussian03.[17] For structure a') the Au_4 cluster was fixed. For the other structures all degrees of freedom were relaxed during optimization. The numbers indicate the relative stability with respect to the most stable conformation a).

For the calculations of structure a') in **Figure 2.6** the positions of the gold atoms were fixed as described above. Complete relaxation of all degrees of freedom, including the Au atoms, lead to structure a), where the four gold atoms adopt a tetrahedron. The conformation of the adsorbed N-acetyl-*L*-cysteine on the other hand hardly changed with respect to structure a'). The VCD spectra of structures a') and a) are very similar, indicating that the nature of the gold cluster has only minor influence on the vibrations located within the molecule. The intensity of $\nu_s(COO^-)$ and the C-H bending mode decreased (bands with labels

2 and 1 in **Figure 2.8**) and the $\nu_{as}(COO^-)$ mode shifted in frequency when going from the planar to the tetrahedral Au_4 cluster.

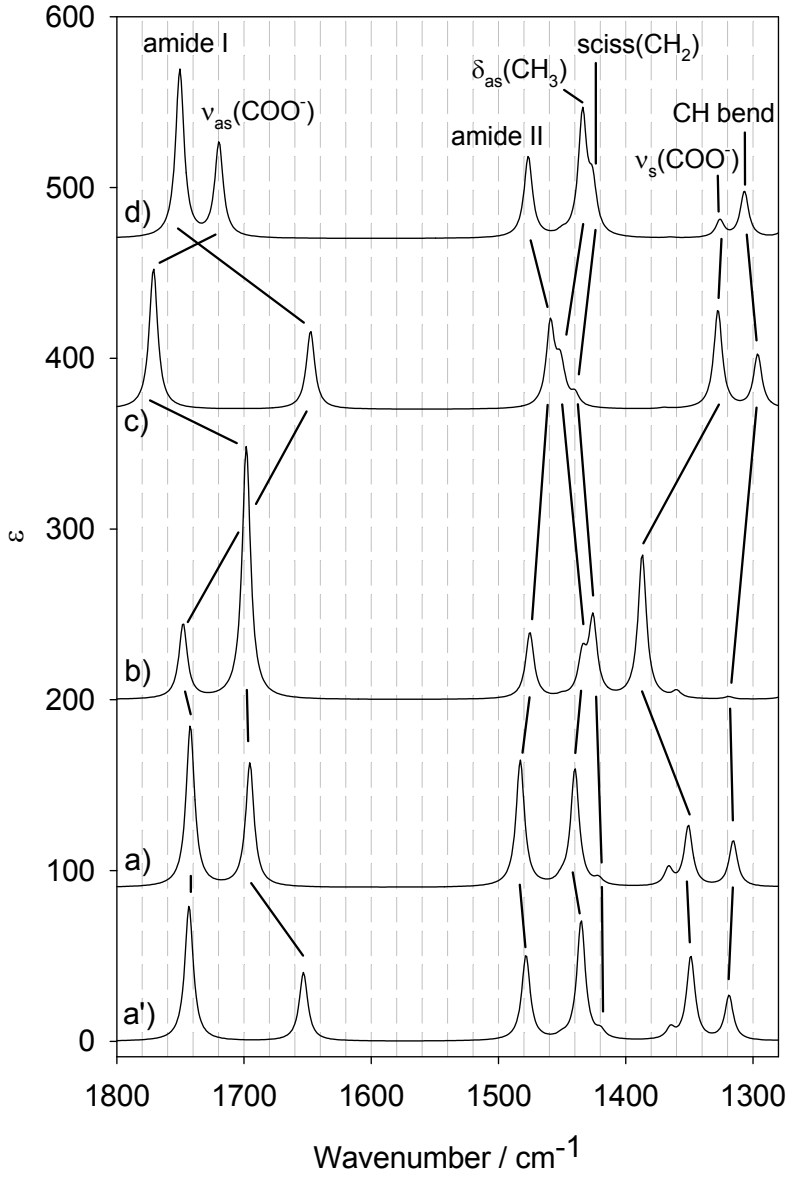

Figure 2.7 : Calculated infrared spectra for the structures shown in **Figure 2.6**. Solid lines connect vibrational bands with similar character.

Figure 2.6 shows other conformers that were calculated. All of these were found to be less stable than conformer a). Conformers b) and d) also interact via the carboxylate group with the Au_4 cluster, whereas conformer c) interacts via the amide group. The difference between the most stable conformer a) and conformer d) is at the level of the CH_2 and COO^- groups. **Figure 2.8** shows that the VCD spectra strongly depend on the conformation of the adsorbed N-acetyl-*L*-cysteine. This is most evident from the signals associated with the amide I and $\nu_{as}(COO^-)$ vibrations. Both bands are negative for conformations b) and c), whereas both are positive for conformation d). Only conformer a) (and a')) have the correct the sign for both bands. However, also the rest of the spectrum gives the best fit between calculated and experimental spectra for conformation a) (a')), particularly bands 4 and 5 and also the C-H bending mode (band 1), which is clearly negative in the experimental spectrum.

The results presented above show that chiral molecules adsorbed on small gold particles exhibit VCD activity. The experimental and calculated spectra for the most stable conformer of the adsorbed molecule are in reasonable agreement, indicating that the applied computational strategy, despite the inherent approximations, is reliable. The calculations indicate that the VCD spectrum is more sensitive to the conformation of the molecule than towards the structure of the metal particle onto which the molecule is attached. Still, the (unknown) local structure of the adsorption site represents an uncertainty for the calculation of VCD spectra of adsorbed molecules, which may explain some differences between experimental and calculated spectra.

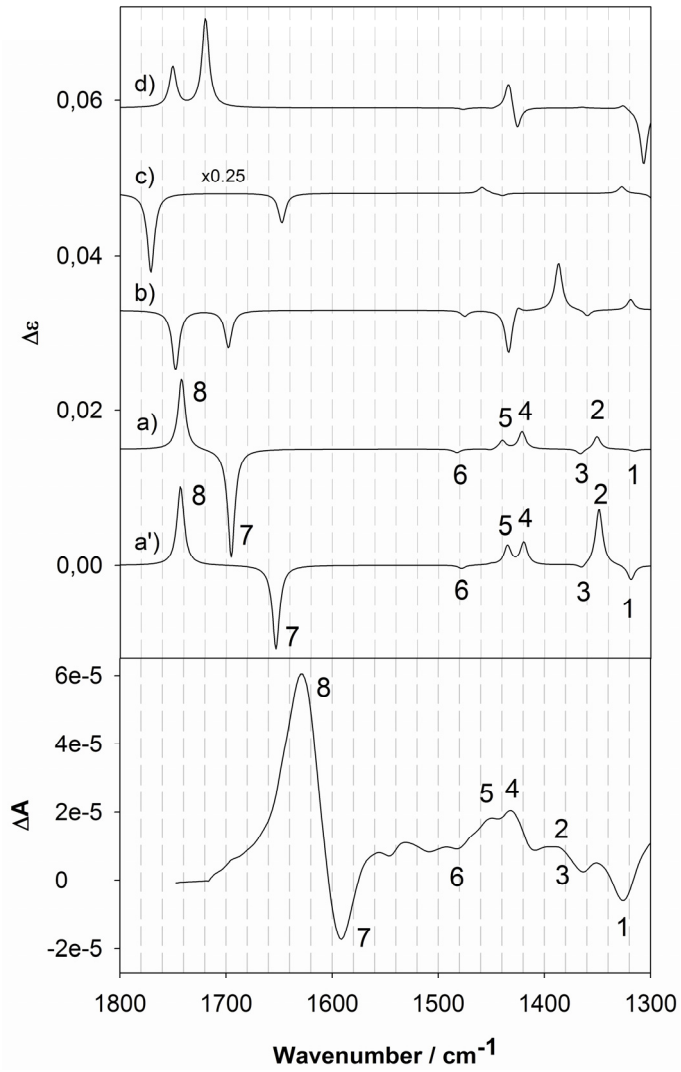

Figure 2.8 : VCD spectra for the structures shown in **Figure 2.6** (top) compared to the experimental specrum (bottom). Labels indicate corresponding bands.

The proposed structure (**Figure 2.6** a), a')) strongly resembles the one determined for cysteine adsorbed on Cu surfaces by reflection absorption infrared spectroscopy,[18] in particular the part comprising the adsorbed thiol and carboxylate groups. In cysteine the amine group points away from the surface as does the amide group in N-acetyl-*L*-cysteine. It should also be pointed out that in this adsorption geometry the molecule occupies only little space, which allows high coverage on the metal particle surface. The latter property

contributes to the high stability of the particles by preventing the metal cores from agglomeration.

2.6 Conclusions

MPNs can be viewed as the nanometer-size analogues of self-assembled monolayers (SAMs) on extended metal surfaces.[19] An increasingly important class of metal surfaces are those modified with a chiral molecule,[20-23] which have for example been used for heterogeneous enantioselective catalysis[24] and chiral discrimination.[25, 26] The discrimination between and separation of enantiomers or the selective production of one enantiomer is of great importance, as chirality is a fundamental aspect of molecular biology. The structure of the adsorbed molecules plays a fundamental role in these processes. Our results indicate that VCD spectroscopy may greatly help elucidating the structure of chiral molecules adsorbed on metal particles.

2.7 References

[1] M.-C. Daniel, D. Astruc, *Chem. Rev.* **2004**, *104*, 293.

[2] E. Katz, I. Willner, *Angew. Chem., Int. Ed.* **2004**, *43*, 6042.

[3] L. A. Nafie, *Annu. Rev. Phys. Chem.* **1997**, *48*, 357.

[4] P. L. Polavarapu, J. He, *Anal. Chem.* **2004**, *76*, 61.

[5] T. B. Freedman, X. Cao, R. K. Dukor, L. A. Nafie, *Chirality* **2003**, *15*, 743.

[6] P. J. Stephens, F. J. Devline, A. Aamouche, *ACS Symp. Ser.* **2002**, *810*, 18.

[7] T. Bürgi, U. Urakawa, B. Behzadi, K.-H. Ernst, A. Baiker, *New. J. Chem.* **2004**, *28*, 332.

[8] T. G. Schaaff, R. L. Whetten, *J. Phys. Chem. B* **2000**, *104*, 2630.

[9] A. C. Templeton, S. Chen, S. M. Gross, R. W. Murray, *Langmuir* **1999**, *15*, 66.

[10] F. C. I. Shaw, N. A. Schaeffer, R. C. Elder, M. K. Eidsness, J. M. Trooster, G. H. M. Calis, *J. Am. Chem. Soc.* **1984**, *102*, 3511.

[11] M. M. Alvarez, J. T. Khoury, T. G. Schaaff, M. N. Shafigullin, I. Vezmar, R. L. Whetten, *J. Phys. Chem. B* **1997**, *101*, 3706.

[12] J. F. Pearson, M. A. Slifkin, *Spectrochim. Acta* **1972**, *28A*, 2408.

[13] E. Mateo Marti, C. Methivier, C. M. Pradier, *Langmuir* **2004**, *20*, 10223.

[14] T. Bürgi, M. Bieri, *J. Phys. Chem. B* **2004**, *108*, 13364.

[15] M. Neurock, *Topics in Catalysis* **1999**, *9*, 135.

[16] E. J. Baerends *et al.* 2004.01 ed., SCM, Amsterdam, **2004**.

[17] M. J. Frisch *et al.* Rev. C.01 ed., Gaussian, Inc., Wallingford CT, **2003**.

[18] M. E. Marti, C. Methivier, C. M. Pradier, *Langmuir* **2004**, *20*, 10223.

[19] A. Ulman, *Chem. Rev.* **1996**, *96*, 1533.

[20] M. O. Lorenzo, C. J. Baddeley, C. Muryn, R. Raval, *Nature* **2000**, *404*, 376.

[21] A. Kühnle, T. R. Linderoth, B. Hammer, F. Besenbacher, *Nature* **2002**, *415*, 891.

[22] R. Fasel, J. Wider, C. Quitmann, K. H. Ernst, T. Greber, *Angew. Chem, Int. Ed.* **2004**, *43*, 2853.

[23] J. V. Barth, J. Weckesser, G. Trimarchi, M. Vladimirova, A. De Vita, C. Z. Cai, H. Brune, P. Gunter, K. Kern, *J. Am. Chem. Soc.* **2002**, *124*, 7991.

[24] T. Bürgi, A. Baiker, *Acc. Chem. Res.* **2004**, *37*, 909.

[25] T. Nakanishi, N. Yamakawa, T. Asahi, T. Osaka, B. Ohtani, K. Uosaki, *J. Am. Chem. Soc.* **2002**, *124*, 740.

[26] R. McKendry, M.-E. Theoclitou, T. Rayment, C. Abell, *Nature* **1998**, *391*, 566.

3

Size Separation and Chiroptical Properties of NILC gold NPs

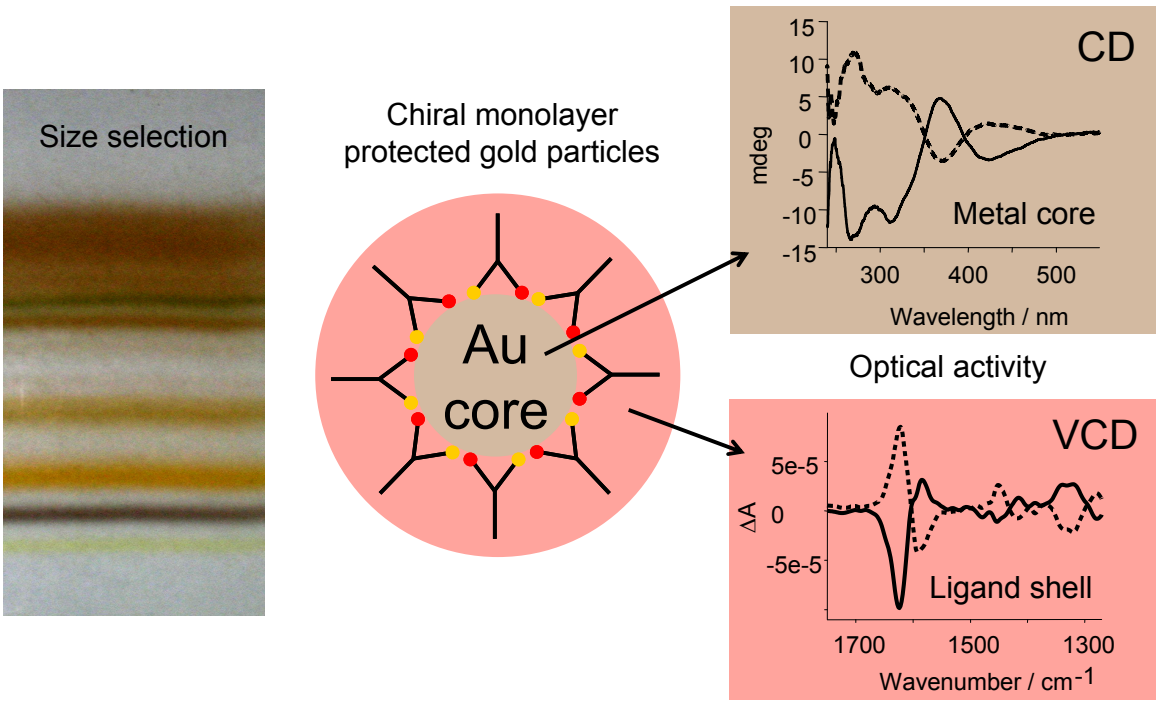

3.1 Abstract

We have prepared gold nanoparticles covered with N-isobutyryl-*L*-cysteine and N-isobutyryl-*D*-cysteine, respectively. These particles with a mean particle size smaller than 2 nm are highly soluble in water and are amenable to chiroptical techniques like vibrational circular dichroism (VCD) and electronic circular dichroism (ECD) spectroscopy. Density functional theory shows that the VCD spectra are sensitive towards the conformation of the adsorbed thiol. Based on the comparison between the experimental VCD spectrum and the calculated VCD spectra for different conformers a preferential conformation of the thiol adsorbed on the gold particles can be proposed. In this conformation the carboxylate group interacts with the gold particle in addition to the sulfur. The particles could furthermore be separated according to their charge and size into well-defined compounds. The optical absorption spectra revealed a well-quantized electronic structure and a systematic red-shift of the absorption onset with increasing gold core size, which was manifested in a color change with particle size. Some compounds showed basically identical absorption spectra as analogous gold particles protected with *L*-glutathione. This shows that these particles have identical core size (10 – 12, 15 and 18 gold atoms, respectively) and indicates that the number and arrangement of the adsorbed thiol is the same, independent of the two thiols, which have largely different size. Some separated compounds show strong optical activity with opposite sign when covered with the *D*- and *L*-enantiomer, respectively, of N-isobutyryl-cysteine. The origin of the optical activity in the metal-based transitions is discussed. The observations are consistent with a mechanism based on a chiral footprint on the metal core imparted by the adsorbed thiol.

3.2 Introduction

Chemists tend to associate chirality with organic molecules, inorganic salts and biological materials but not necessarily with metals. The crystal structures of metals are highly symmetric and not chiral. Metal surfaces on the other hand can be chiral and are considered for example as heterogeneous enantioselective catalysts.[1, 2] Some high Miller index surfaces of metals such as for example Ag(643) are intrinsically or naturally chiral.[3] Such surfaces have been demonstrated to interact differently with the enantiomers of a chiral compound.[3-7] Another type of chirality is obtained through adsorption and long-range ordering of molecules on non-chiral metal surfaces,[8, 9] if the pattern formed by the adsorbate destroys the symmetry of the underlying metal surface. The adsorbate itself does not have to be chiral in this case resulting in a racemic mixture of domains on the surface with opposite chirality.[10] Finally, the adsorption of a chiral molecule[11-14] creates a locally chiral environment near the metal surface. This may lead to a "chiral footprint" on the non-chiral surface,[15] *i.e.* the slight distortion of the metal surface atoms involved in the adsorbate complex toward a chiral arrangement. Adsorbed molecules may also transfer chirality onto the electronic structure of the non-chiral metal.[16]

Monolayer protected metal nanoparticles (MPNs) or clusters are of considerable interest due to their potential application for bio-sensing,[17] catalysis,[18] electronics[19] and nanotechnology.[20] These organic-inorganic composite materials have a very large metal surface to volume ratio and in principle the same types of chirality as discussed above for extended metal surfaces could arise. Due to their solubility such particles are amenable to chiroptical techniques such as electronic circular dichroism (ECD) [21, 22] and vibrational

circular dichroism (VCD) spectroscopy,[23-26] which selectively probe their chiral properties. The former technique probes electronic transitions, which may be located in the metal core, whereas the latter is sensitive towards molecular vibrations. As demonstrated in Chapter 2, VCD can be used to obtain structural information on chiral molecules adsorbed on small metal nanoparticles.[27]

Schaaff and Whetten reported optical activity in gold nanoparticles protected with *L*-glutathione (*γ-glu-cys-gly*).[28] These particles, after preparation, were separated according to their size and charge into well-defined compounds in a gel electrophoresis. The separated compounds, corresponding to particles with core mass between 4 and 14 kDa (20-70 gold atoms), showed strong optical activity in metal based transitions. More recently Yao and coworkers reported optical activity in the visible and UV spectral range for gold nanoparticles of 0.6 – 1.8 nm diameter protected with penicillamine.[29] Three fractions of particles (containing about 6, 50 and 150 gold atoms, respectively) could be separated in a gel electrophoresis. These particles were optically active in the visible and UV spectral range, with the anisotropy factors decreasing with cluster size. In contrast, for the *L*-glutathione case the smallest particle did not show the highest anisotropy factors.[28] The origin of the observed optical activity and in particular the possibility that the metal core is intrinsically chiral was discussed, but this question remains open.[28, 29] Optical activity was also observed after coating large (23.5 nm) Ag colloids with cysteine, *L*-glutathione and penicillamine.[30] It was noted that no optical activity was observed when using gold colloids instead of silver and when using lysine, glutamine and cysteine methylester as ligands. Based on these observations it was concluded that association of nanoparticles mediated by hydrogen bonding between the adsorbed molecules is responsible for the optical activity. The

origin of optical activity in metal based electronic transitions is still unclear due to the very few examples of well-defined chiral particles described till today and the lack of structural information.

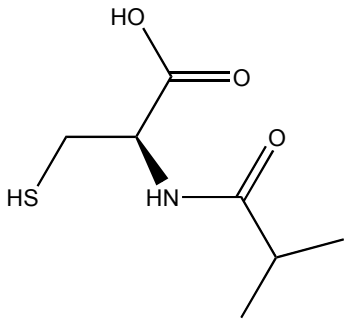

Chart 3.1 : Structure of N-isobutyryl-*L*-cysteine.

In this chapter, we present the preparation, the separation by gel electrophoresis and chiroptical properties in the UV-vis and infrared of N-isobutyryl-*L*-cysteine (**Chart 3.1**) and N-isobutyryl-*D*-cysteine protected gold particles. The vibrational circular dichroism spectra give direct information on the structure of the N-isobutyryl-cysteine molecules adsorbed on the metal particles. Up to eight different compounds could be separated in a gel electrophoresis. Some of the separated compounds showed UV-vis spectra very similar to those reported for *L*-glutathione-protected gold particles. Some separated compounds furthermore exhibited strong optical activity in metal based transitions the origin of which is discussed.

3.3 Experimental

3.3.1 Materials

D_2O (99.9%) was received from Cambridge Isotope Laboratories. Gold(III) chloride trihydrate ($HAuCl_4.3H_2O$, 99.99%), N-isobutyryl-*L*-cysteine (NILC, 99.5%), N-isobutyryl-*D*-cysteine (NIDC, 99.5%), sodium borohydride ($NaBH_4$, 98%), acrylamide (>99%), N,N'-methylenebisacrylamide (Bis, >99%), ammonium persulfate (APS, 98%), N,N,N',N'-tetramethylethylenediamine (TEMED, >99.5), tetraoctylammonium bromide (TOAB, >98%) were purchased from Aldrich, concentrated (10X) premixed tris(hydroxymethylaminomethane) (Tris)/glycine buffer (250 mM Tris, 1920 mM glycine), 0.5 M Tris-HCl Buffer pH 6.8 and 1.5 M Tris-HCl buffer pH 8.8 were purchased from BIO-RAD. Water was purified with a Milli-Q system ($\geq$18 MΩ.cm^{-1}). All other chemicals were analysis grade and used as received.

3.3.2 Synthesis of NIC MPNs

N-isobutyryl-*L*-cysteine and N-isobutyryl-*D*-cysteine MPNs were both prepared following a previous report.[27] Briefly, 400 mg of tetrachloroauric acid (1.0 mmol) and 777 mg of the corresponding enantiomer of N-isobutyryl-cysteine (4.0 mmol) were dissolved in 200 ml of a methanol : acid acetic solution 6:1 (v : v). The solution rapidly turned red before yielding a cloudy white suspension. This indicates the formation of a Au(I)-N-isobutyryl-cysteine polymer. After 30 minutes, the polymer was reduced by slow addition of a freshly prepared aqueous $NaBH_4$ solution (70 ml, 2.13 mol.l^{-1}) under vigorous stirring. The mixture was allowed to react for 90 minutes. The resulting dark solution was filtered using a

0.2 μm PTFE membrane to remove insoluble material and subsequently evaporated under vacuum at a temperature inferior to 40 °C to near dryness. The nanoparticles were precipitated several times with a large excess of ethanol and filtered using the same 0.2 μm PTFE membrane. The removal of remaining unreacted thiols or disulfides was finally completed by dialysis (Spectra/Por CE) in a bag with a molecular weight cut-off of 3500 Daltons. Particles were dissolved in 30 ml water and loaded into the membrane which was then placed in a 2 liter beaker of water and slowly stirred. The water was changed every 10 hours over the course of 96 hours. The black solution was evaporated under vacuum to yield 340 mg of a black powder.

3.3.3 Separation of MPNs by PAGE

PAGE was performed with a Biorad Protean II XI system with a gel of 3 mm thickness. The experimental conditions for PAGE are close to those employed in previous works.[28] The total content of the acrylamide monomers were 3% (acrylamide/Bis, 94 : 6) and 25% (acrylamide/Bis, 93 : 7) for the stacking gel and separation gel, respectively. The staking and the separating gels were buffered at pH = 6.8 and 8.8, respectively, with Tris-HCl solution. The eluting buffer consisted of a solution of glycine (192 mM) and Tris (25 mM) in 80%:20% (v/v) water:methanol. The purified MPNs were dissolved in a 5% glycerol solution in Milli-Q water to a concentration of 4 $mg.ml^{-1}$. This MPN solution was loaded on a 3 mm gel without lanes and eluted for 17 hours at a constant voltage of 150 V to achieve separation. Parts of the gel containing each separated fraction were cut out and placed in Milli-Q water

overnight. The gels lumps suspended in the solution were removed by filtration. MPNs were finally further purified by dialysis the same way as described above.

3.3.4 IR and VCD

Infrared (IR) and vibrational circular dichroism (VCD) spectra were recorded on a Bruker PMA 50 accessory coupled to a Tensor 27 Fourier transform infrared spectrometer. A photoelastic modulator (Hinds PEM 90) set at l/4 retardation was used to modulate the handedness of the circular polarized light. Demodulation was performed by a lock-in amplifier (SR830 DSP). An optical low-pass filter (< 1800 cm^{-1}) put before the photoelastic modulator was used to enhance the signal/noise ratio. All solutions of N-isobutyryl-*L/D*-cysteine MPNs were prepared in NaOH/D_2O solution. NaOH (6.5 mg in 0.8 ml D_2O) was added to completely deprotonate the carboxylic acid group. Solutions were prepared by dissolving 7 mg MPNs in 50 µl NaOH/D_2O solution. A VCD spectrum of a racemic mixture of N-isobutyryl-*L*-cysteine MPNs and N-isobutyryl-*D*-cysteine MPNs was measured and served as the reference. This reference VCD spectrum was subtracted from the VCD spectra of the MPN enantiomers. All spectra were recorded at room temperature with a resolution of 8 cm^{-1} in a cell equipped with CaF_2 windows and a 50 µm Teflon spacer. Both samples and reference were measured for four hours in time slices of one hour, corresponding to about 32'000 scans in total for samples and reference, respectively. The spectra are presented without smoothing or further data processing. More information about the experimental procedure can be found elsewhere.[31, 32]

3.3.5 Characterization by UV-vis, ECD and NMR

^{1}H NMR spectra of the as prepared particles were measured on a Brucker Avance 400 MHz spectrometer at room temperature. Solutions were prepared in D_2O at a concentration of approximately 50 mg.ml^{-1}. UV-vis and ECD spectra, respectively, of the separated particles were collected on a Cary 300 and a Jasco 710 spectrometer, respectively, using a quartz cell of 1 cm path lengths and solutions of approximately 0.3 mg.ml^{-1} in H_2O.

3.3.6 Transmission Electron Microscopy

TEM images were recorded with a Philips C200 electron microscope operated at 200 kV. MPNs were made hydrophilic in order to avoid aggregation of particles.[33] An aqueous solution (5 ml) containing 1 mg of MPNs was set to pH 11 by addition of an aqueous solution of NaOH. To this solution was added 0.6 mm toluene solution (5 ml) of TOAB. The vigorous stirring of the mixture for 30 min resulted in complete transfer of colored MPNs from the aqueous to the organic phase. The latter was separated and concentrated to 500 µl. TEM sample was prepared by casting of a drop of the solution onto a carbon-coated copper grid.

3.3.7 Density Functional Theory Calculations

The adsorption of deprotonated N-isobutyryl-*L*-cysteine on Au_8 clusters was studied using Gaussian03.[34] For the gold atoms an effective core potential was used. The calculations were performed using the b3pw91[35, 36] functional and a LanL2DZ basis set[37] for Au and 6-31G(d,p) basis set[38] for all other atoms. Vibrational frequencies were

scaled by a factor of 0.97. IR and VCD spectra were constructed from calculated dipole and rotational strengths assuming Lorentzian band shape with a half-width at half-maximum of 5 cm^{-1}.

3.4 Results and Discussion

3.4.1 TEM and NMR

Transmission electron microscopy of the MPNs before gel electrophoresis separation reveals particle sizes around 2 nm and smaller (see **Figure 3.1**). The ^1H NMR spectra (see Appendix B) of the unbound N-isobutyryl-cysteine display 4 signals corresponding to hydrogen which are not exchangeable with deuterium from D_2O. Their chemical shift are respectively 1.1 ppm (2 d, 6 H), 2.5 ppm (m, 1 H), 2.98 ppm (m, 2 H) and 4.59 ppm (m, 1 H) respectively for the two methyl groups, the methine group in the α position of the two methyl, the methylene and the asymmetric methine. ^1H NMR spectra of the NIC MPNs also show this 4 signals which are shielding and exhibit broadened resonances compare to the free ligand. This observation shows that the ligand is intact and demonstrates the absence of the free ligands in solution. Line broadening appears frequently in literature of MPNs NMR spectroscopy and are observed to be highest for hydrogen closest to the gold core. This statement is in good agreement with the ^1H NMR of gold NIC MPNs as the methylene group in the α position of the sulfur is the signal with the highest line broadening and shielding.

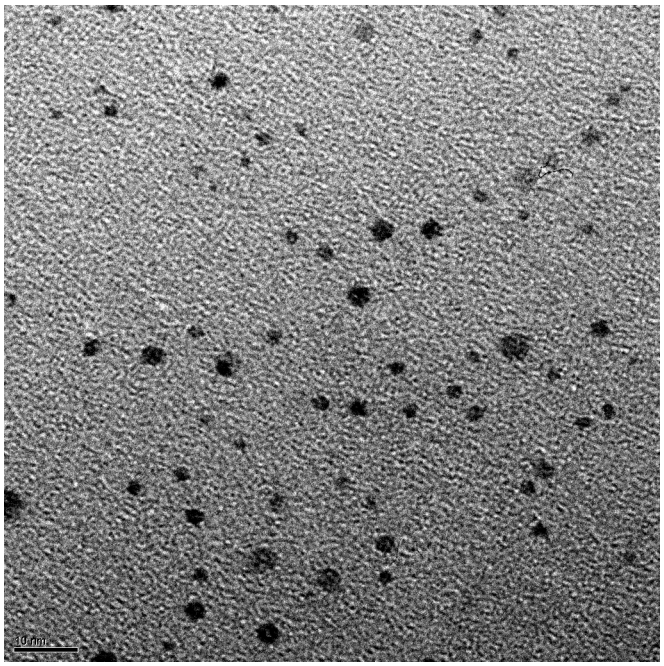

Figure 3.1 : TEM of N-isobutyryl-*L*-cysteine MPNs before gel electrophoresis separation. The bar corresponds to 10 nm.

3.4.2 IR and VCD Spectra of NILC and NIDC Adsorbed on Gold MPNs

The measured IR and VCD spectra of dissolved N-isobutyryl-*D*/*L*-cysteine MPNs are shown in **Figure 3.2**. Whereas the IR spectra of the two MPN enantiomers are identical the VCD spectra show mirror image relationship. The slight deviation from perfect mirror image relationship may be attributed primarily to noise. The largest deviation is observed for the $\nu_{as}(COO^-)$ band slightly below 1600 cm^{-1}. This band is the strongest in the spectrum. At this wavenumber the transmitted intensity is low and consequently the noise high. It should be noted that the measurements were performed on the as prepared samples, which are not mono-disperse. The appearance of relatively strong bands in the VCD spectra therefore indicates that the size of the particle has only a minor effect on the VCD and that the VCD is

a local property of the individual adsorbed molecules. In contrast, no significant optical activity was observed in the UV-vis for the as prepared particles.

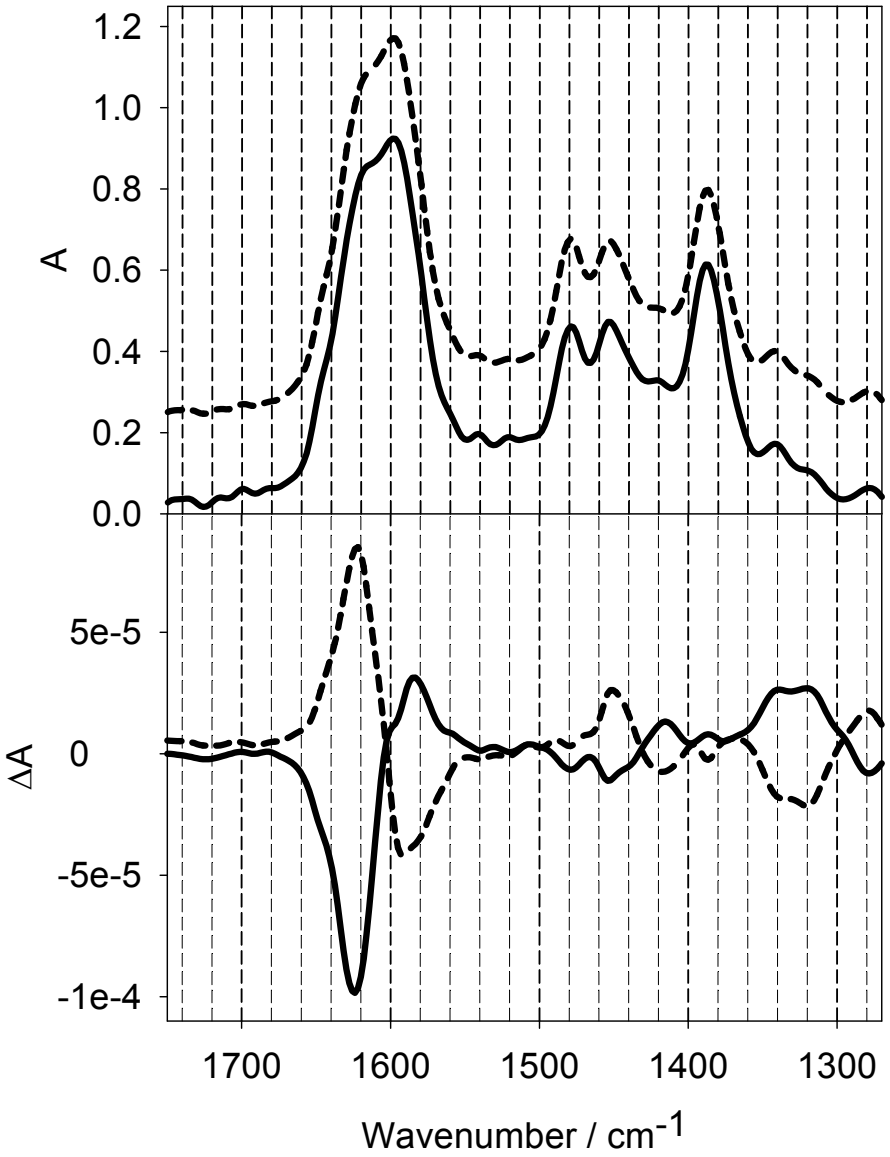

Figure 3.2 : Infrared (top) and VCD (bottom) spectra of N-isobutyryl-cysteine protected gold nanoparticles in $NaOH/D_2O$. Solutions were made from 7 mg sample in 50 μl solution. The dashed (solid) lines correspond to the spectra of the particles covered by the *L*-enantiomer (*D*-enantiomer). The IR spectrum of the particles covered with N-isobutyryl-*L*-cysteine was offset for clarity. See Section 3.3.4 for more details.

3.4.3 Calculated VCD Spectra of NILC MPNs

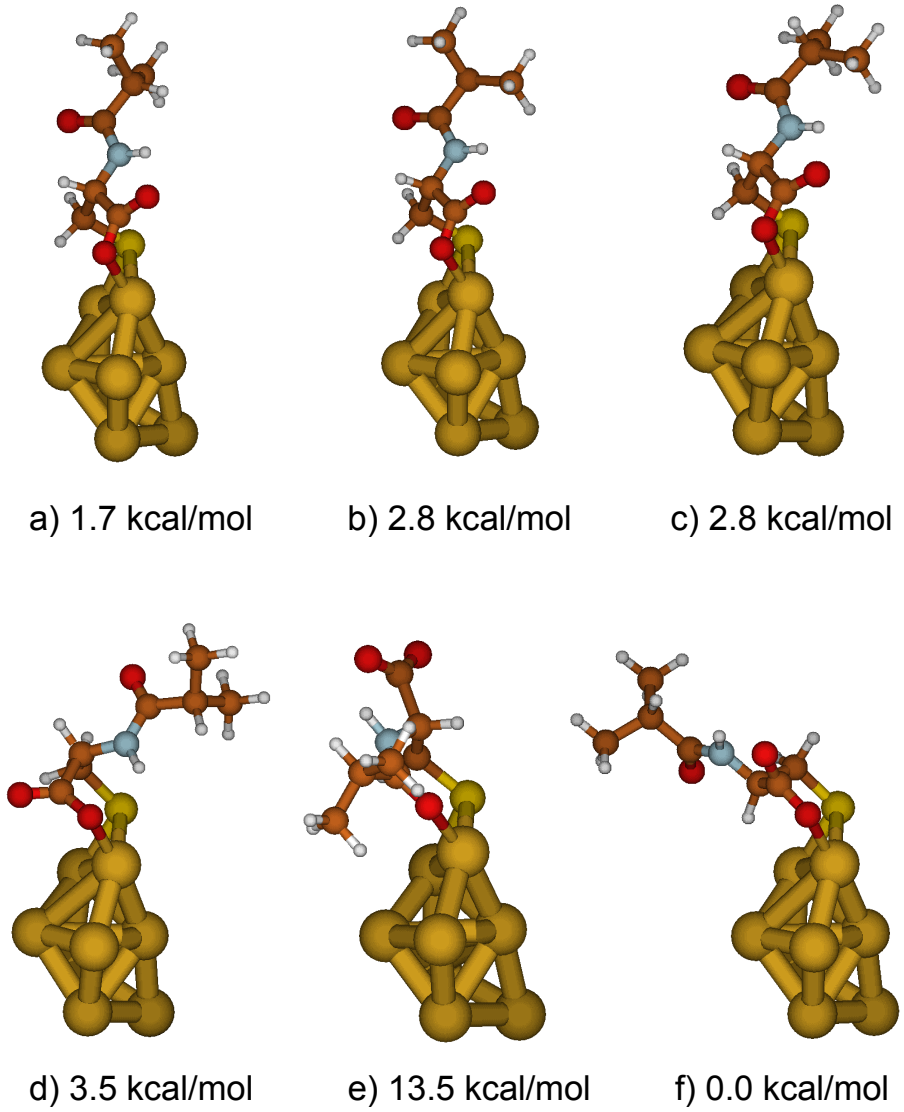

Figure 3.3 : Calculated conformers of deprotonated N-isobutyryl-*L*-cysteine on a Au_8 cluster. The numbers indicate the calculated relative stability with respect to the most stable conformer f). The calculations were performed at the B3PW91 level using a 6-31G(d,p) (LanL2DZ for Au) basis set.

VCD spectroscopy has been used in the past to determine the absolute configuration and to obtain structural information of small and medium-sized molecules in solution.[31, 32,

39-42] In order to extract this information, VCD spectra for different conformations have to be calculated and compared with experiment. For adsorbed molecules on the nanoparticles the metal surface has to be considered in the calculations. We have chosen a Au_8 cluster to study the conformation of adsorbed deprotonated N-isobutyryl-*L*-cysteine. The cluster resembles a low energy conformer found recently for Au_8 using second order perturbation theory (MP2) and coupled cluster methods (CCSD(T)).[43] Figure 3.3 shows some conformers of adsorbed deprotonated N-isobutyryl-*L*-cysteine that were found and **Figure 3.4** shows the corresponding calculated VCD spectra. The primary anchoring of the molecule to the cluster is through the sulfur atom in a bridge site, *i.e.* in between two Au atoms, in agreement with recent periodic density functional theory (DFT) calculations for cysteine[44] and methanethiol on Au(111).[45] The most important conformational degrees of freedom of the molecule are the rotations around the three single bonds involving the asymmetric C atom (two C-C bonds and one C-N bond, **Chart 3.1**). The amide part is rigid due to the strong preference of a trans arrangement of the C=O and N-H groups. Further conformational rigidity is provided by an intramolecular hydrogen bond between the N-H and the COO^- groups. The isopropyl group can adopt several positions with respect to the rest of the molecule (compare conformations a)-c) in Figure 3.3). Energetically the one conformation where the C-H and C=O bonds are in trans arrangement (*e.g.* conformation a)) is preferred over the other conformations (*e.g.* b) and c)). More importantly, we have noticed that the rotation of the isopropyl group has only a minor influence on the VCD spectra, as is obvious from **Figure 3.4**, spectra a-c. The reason for this finding emerging from the calculations is the weak VCD activity of the isopropyl group vibrations due to the local character of these modes (mainly CH_3).

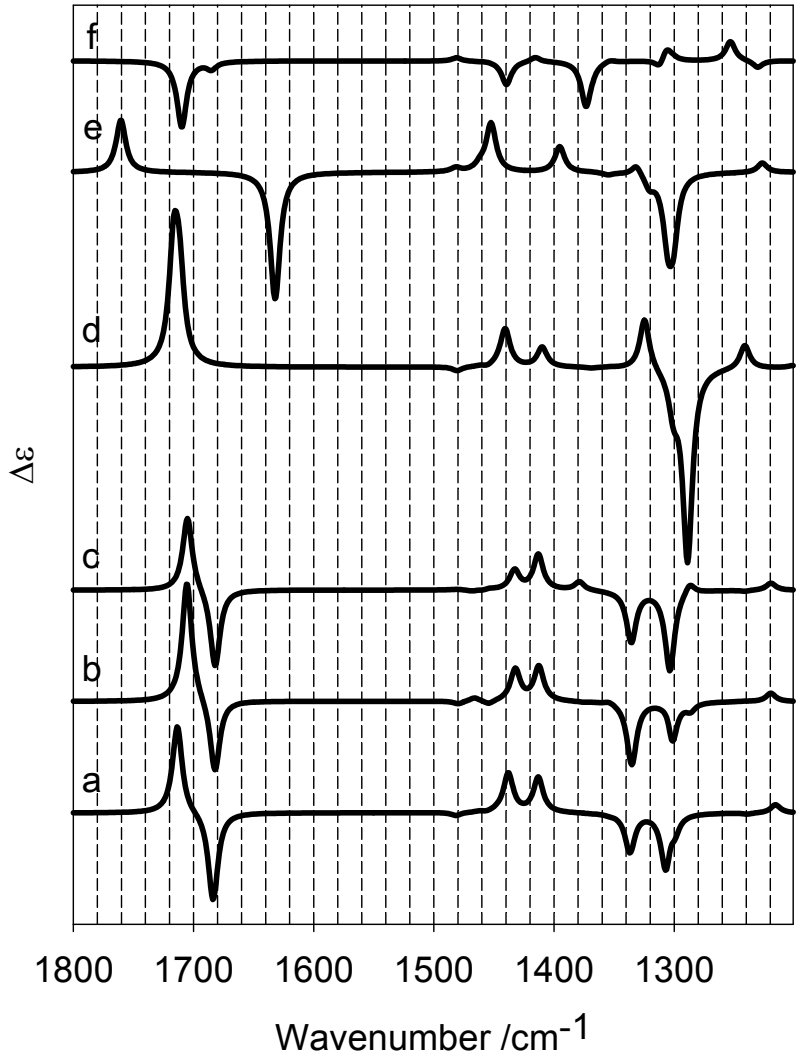

Figure 3.4 : Calculated VCD spectra for different conformers of N-isobutyryl-*L*-cysteine adsorbed on a Au_8 cluster. The letters correspond to the structures shown in **Figure 3.3**.

Conformer a) interacts with the Au_8 cluster via the sulfur atom and in addition with the carboxylate. The latter interaction leads to additional stability of the adsorbate complex. Note that in this conformation one oxygen atom of the COO^- group interacts with the surface whereas the other oxygen atom forms an intramolecular hydrogen bond with the N-H. In conformer d), one oxygen atom is responsible for both interactions (intramolecular hydrogen

bonding and binding to the gold surface), whereas the other oxygen is free. This conformation is slightly less stable than conformer a). In conformer e) the amide oxygen interacts with the surface, whereas the carboxylate does not, which leads to a considerable destabilization. In the most stable structure that was found, conformer f), the position of the asymmetric carbon atom within the seven-membered ring formed by the molecule and the Au_8 cluster (-Au-S-C-C-C-O-Au-) differs from its position in conformer a).

The VCD spectra for conformers a), d), e) and f) differ considerably. For the most stable conformer f) almost all prominent VCD bands are negative, in contrast to experiment. The VCD spectrum of conformer d) exhibits two overlapping positive bands for the amide I and $\nu_{as}(COO^-)$ vibrations (calculated slightly above 1700 cm^{-1}) in contrast to experiment. Conformers a) (and also the related conformers b) and c)) and e) exhibit the correct sign for the amide I (positive) and $\nu_{as}(COO^-)$ (negative) vibrations. Based on the calculated energy conformer e) is unlikely. The VCD spectrum of conformer a) (also b) and c)) fits qualitatively well with experiment, when considering the assignment of vibrational bands as shown in **Figure 3.5** and detailed below.

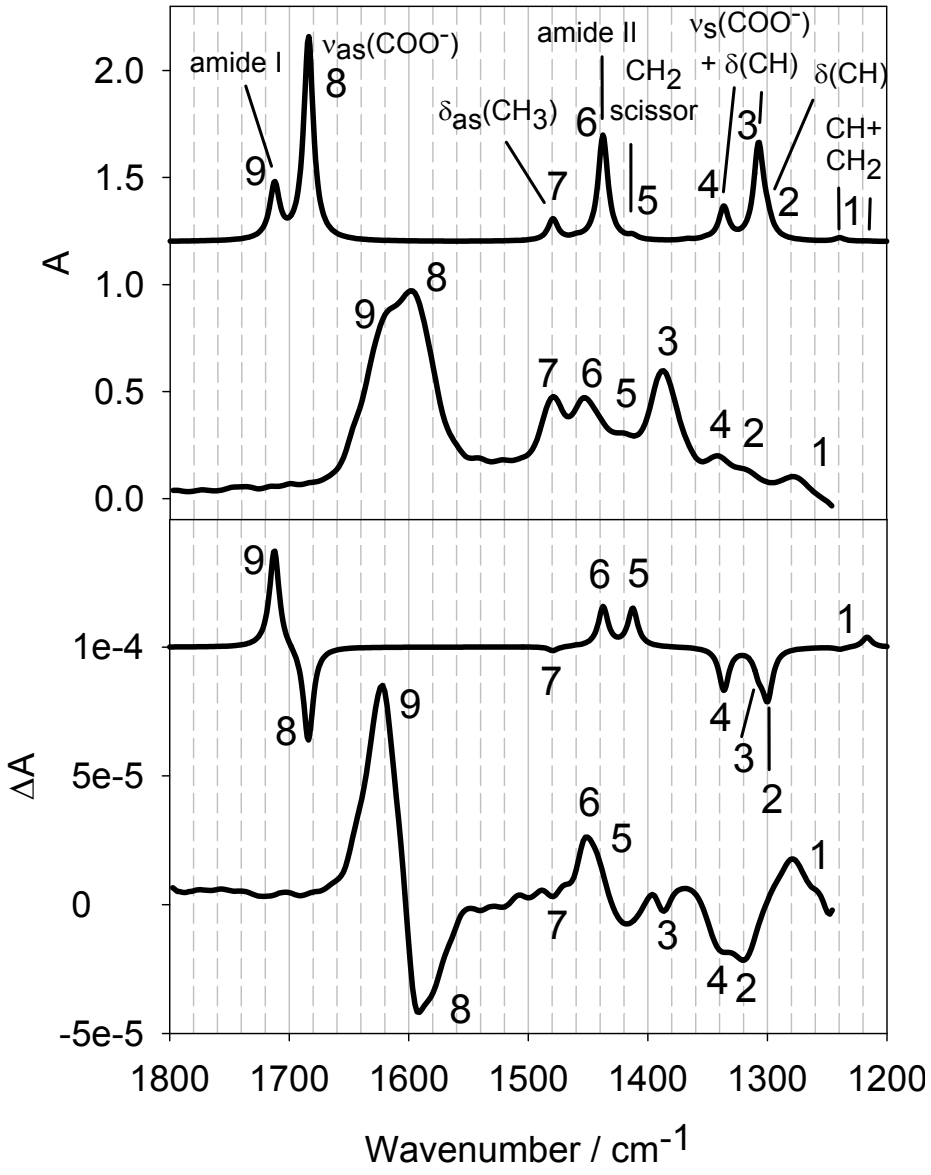

Figure 3.5 : Comparison between calculated (see **Figure 3.4**) and experimental IR and VCD spectra (see **Figure 3.2**) of N-isobutyryl-*L*-cysteine on gold. The calculated spectra are shown for conformer a) in **Figure 3.3**. Corresponding bands are numbered and the assignment is given in the upper part of the Figure.

The highest energy vibrations in the considered frequency range belong to the amide I (1620 cm^{-1}, mode nr. 9 in **Figure 3.5**) and $\nu_{as}(COO^-)$ (1595 cm^{-1}, 8) modes. Consistent with

the calculations for conformer a) the amide I vibration is less intense than the $\nu_{as}(COO^-)$ mode in the IR, whereas the former mode gains intensity (and even becomes more intense) relative to the latter in the VCD. Both modes are predicted at a too high frequency. This is primarily due to solvation effects, which strongly affects the frequency of these modes, and which are neglected in the calculations. The frequency of the $\nu_s(COO^-)$ mode observed at 1387 cm^{-1} (nr. 3) is also strongly influenced by solvation. Consistent with the calculation this mode is only weakly VCD active (negative). The assignment of the COO^- modes was confirmed by titration experiments. The $\delta_{as}(CH_3)$ modes above 1450 cm^{-1} (nr. 7) are almost silent in the VCD both in experiment and calculations. The amide II mode (1450 cm^{-1}, nr. 6) is significantly positive in the calculations, in agreement with experiment. The calculations predict the CH_2 scissor mode (nr. 5) to be only weakly IR active but significantly positive in the VCD. Possibly this band is overlapping with the positive amide II mode (nr. 6) in the experimental VCD spectrum. A weakly negative band is observed slightly below the amide II band. Modes 4 and 2 contain C-H bending character and have negative intensity both in the experiment and the calculation. Between 1200 and 1300 cm^{-1} the calculations predict a positive band with CH_2 (and some C-H) character in agreement with experiment. In summary, the VCD spectrum of conformer a) is in qualitative agreement with experiment, which suggests that conformer a) (and to lesser extent conformers b) and c)) is the predominant conformation of N-isobutyryl-*L*-cysteine adsorbed on the gold nanoparticles.

From a purely energetic point of view and based only on the calculations conformer f) should predominate. The VCD spectrum of the latter is however clearly not consistent with observation. It should also be noted that for N-acetyl-*L*-cysteine adsorbed on a Au_4 cluster the corresponding conformation a) was slightly more stable than the corresponding conformer

f),[27] which indicates that the relative energy of the different conformers may change slightly with structure and size of the gold cluster. Furthermore, the structural difference between the two ligands (N-acetyl-*L*-cysteine and N-isobutyryl-*L*-cysteine) is likely also influencing the relative stability of the corresponding conformers. In addition, lateral interaction between neighboring molecules, not considered in the calculation, may also influence the relative stability of the different conformers.

The conformation of N-isobutyryl-*L*-cysteine adsorbed on gold nanoparticles that we propose based on the VCD investigations resembles closely the one determined for N-acetyl-*L*-cysteine on gold surfaces based on attenuated total reflection infrared spectroscopy.[46] In the latter study the orientation of the molecule on the gold surface was determined from the orientation of the transition dipole moment for different vibrations. The proposed structure is also consistent with the structure of cysteine adsorbed on Cu surfaces as determined by reflection absorption spectroscopy.[47]

3.4.4 Separation of Particle Compounds

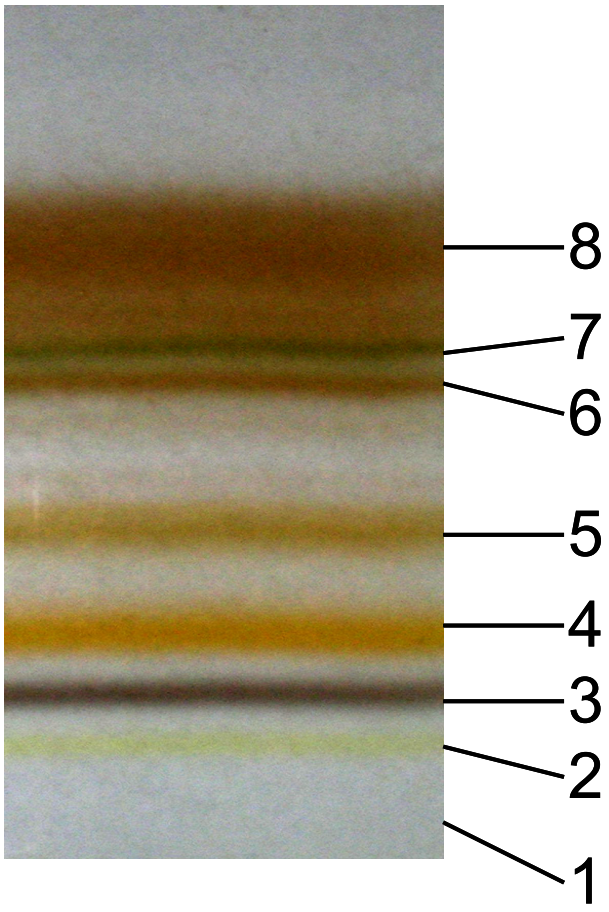

Figure 3.6 : Polyacrylamide gel electrophoresis separation of N-isobutyryl-*L*-cysteine protected gold particles. The separation was performed for 17 hours at 150 V. The separated compounds are numbered from **1-8** according to their decreasing electrophoretic mobility. Compound **1** is only visible under UV irradiation.

The N-isobutyryl-*L*-cysteine protected MPNs are charged and can therefore be separated according to their size and charge by PAGE. **Figure 3.6** shows a photograph of a gel after separation. Eight compounds could be separated and were numbered **1-8** according to increasing particle size. The UV-vis spectra of these compounds are given in **Figure 3.7**.

Percentage by weight of compounds **2-8** and TEM images of compounds **2** and **7** are given in the Appendix B. Analysis of the TEM graphs reveals that compound **2** (the smallest compound observable by TEM) is characterized by a particle size of about 0.7 nm, whereas compound **7** (the largest well-defined compound) is characterized by 1.3 nm particles. Compound **1** is invisible by the bare eye but becomes visible under UV irradiation. The color of the different compounds changes according to their size from yellow (**2**) over grayish (**3**) and orange (**4**) towards different tons of brown (**5-8**), which is a direct consequence of a quantum size effect. The separation is very good for compounds **1-5** whereas band **8** is quite diffuse, which may indicate that several compounds with different composition (number of gold atoms and thiol ligands) contribute to it. The appearance of discrete bands in the gel electrophoresis shows the presence of "magic number" compounds, *i.e.* the high relative abundance of compounds with certain composition. It should be noted that the migration in the electrophoresis depends both on the size and the charge of the particles, the latter being dependent on the surface composition, *i.e.* the number of adsorbed ligands. In fact, it has been shown that gold clusters differing by only one adsorbed thiol ligand can be separated in a gel electrophoresis.[48] However, in this case the UV-vis spectra of the two compounds showed the same absorption onset. In contrast, the UV-vis spectra of our separated compounds reveal a red-shift with decreasing migration in the electrophoresis, which shows that the size of the metal core of the separated compounds is different.

Comparable separation of gold particles covered with thiols has been achieved in the past only for the gold *L*-glutathione system.[28, 48-50] Schaaff and Whetten reported seven compounds,[28] whereas Tsukuda and coworkers reported up to nine separated compounds for the same system (and some less for homoglutathione).[48] Preparation and separation of

other water-soluble gold thiol MPNs has been reported but resulted in considerably less isolated compounds.[51] Very recently three different compounds were separated for gold particles coated with penicillamine.[29] 4-Mercaptobenzoic acid was reported to yield two separated bands by PAGE, whereas numerous other water soluble passivated gold particles did not show discrete bands.[51]

3.4.5 UV-vis Spectra

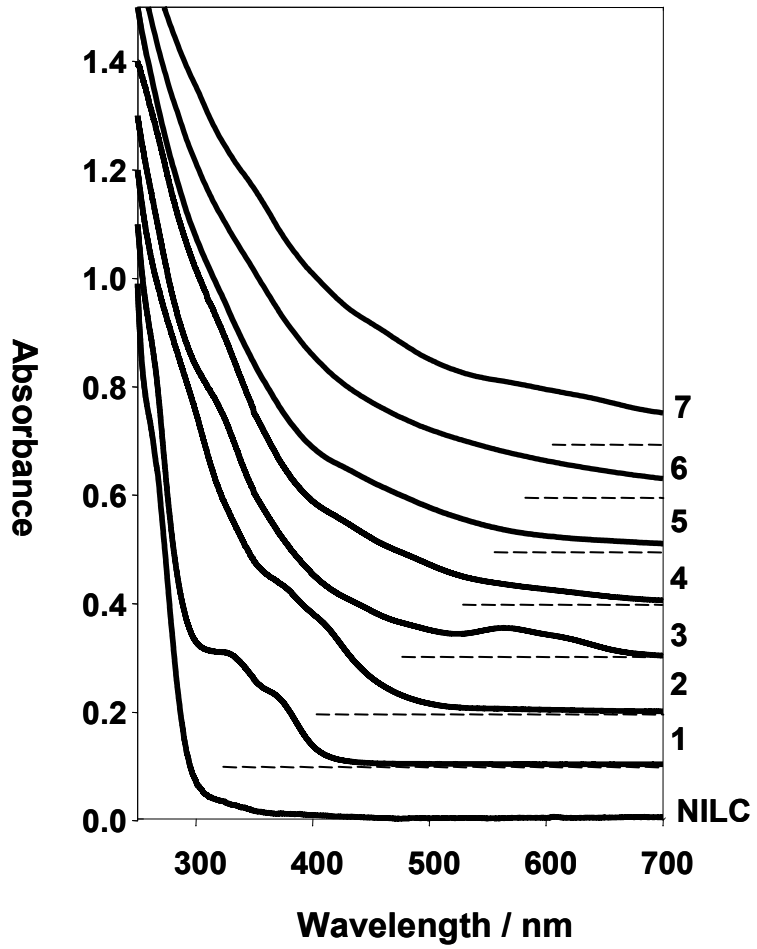

Figure 3.7 : UV-Vis spectra of the separated compounds **1-8** (see **Figure 3.6**). Spectra are offset for clarity and normalized to one absorbance unit at 250 nm. The bottom spectrum corresponds to N-isobutyryl-*L*-cysteine (First derivative spectra are given in Appendix B).

Figure 3.7 shows the UV-vis spectra of the compounds isolated from the gel and after purification by dialysis. The absorption spectra exhibit considerable structure, in particular for the smaller compounds (bands **1-3**), which is even more evident from the first derivative of the spectra (see Appendix B). The UV-vis spectra reveal that the compounds exhibit well quantized electronic structure. In addition, an absorption onset is observed, which shifts from

slightly above 400 nm for compound **1** to higher wavelengths as the size of the compound increases. For compounds **1-3** two distinct bands are observed after the absorption onset. Similar UV-vis spectra were reported for gold particles passivated by *L*-glutathione (*γ-glu-cys-gly*).[48]

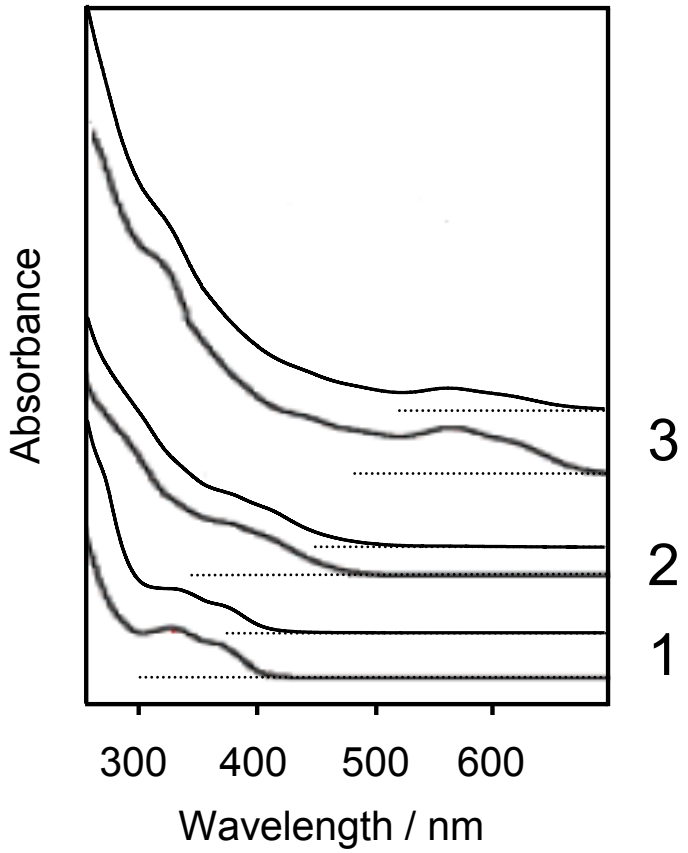

Figure 3.8 : Comparison between UV-vis spectra of separated gold N-isobutyryl-*L*-cysteine compounds **1-3** (see **Figure 3.6**) and corresponding *L*-glutathione compounds reported in ref [48] (with permission from the Am. Chem. Soc.).

Figure 3.8 shows a comparison between the first three compounds isolated for *L*-glutathione covered particles (from ref. [48]) and for N-isobutyryl-*L*-cysteine covered particles. The similarity is striking. From this comparison we conclude that the absorption

spectra are basically determined by the metal core of the particle, as the ligands (*L*-glutathione and N-isobutyryl-*L*-cysteine) are different. The comparison furthermore indicates that the corresponding particles have the same core size and similar core structure, since the electronic structure of such small metal particles is both sensitive to size and structure.[52]

Using electrospray ionization (ESI) mass spectrometry Tsukuda and coworkers analyzed the mass of separated gold – *L*-glutathione compounds.[48] From their results and the comparison in **Figure 3.8** it is concluded that the gold – N-isobutyryl-cysteine compounds **1**, **2** and **3** contain 10-12, 15 and 18 gold atoms, respectively. Tsukuda and coworkers concluded, based on X-ray photoelectron spectroscopy and photoemission spectroscopy, that even the smallest compound (10-12 gold atoms) is clearly distinguishable from a Au(I)-SR polymer.[48]

Based on DFT calculation on $[Au_{13}(SCH_3)_8]^{3+}$ the two characteristic bands above the absorption onset observed for small gold N-isobutyryl-cysteine (*L*-glutathione) compounds (see **Figure 3.7** and **Figure 3.8**) may be assigned to electronic transitions from the Au 6s to the Au 6s and Au 6s/6p orbitals corresponding to "intraband" transition in the bulk metal.[53] On the other hand the structure in the absorption spectra at around 300 nm and below may correspond to transitions from Au 5d to Au 6s/6p orbitals, corresponding to "interband" transitions in the bulk metal. According to these calculations some orbitals involved in the described electronic transitions contain appreciable sulfur 3p and 3s character. It is therefore expected that a different number of ligands or a different arrangement of the same number of ligands on the metal particle affect the electronic transitions and therefore the absorption spectrum. Indeed for the gold – *L*-glutathione particles ESI mass spectrometry indicated that two isolated compounds differed by only one ligand.[48] More precisely, compounds **4** and **5**

reported by Tsukuda and coworkers were assigned to Au_{22} particles containing 16 and 17 *L*-glutathione ligands, respectively. The corresponding UV-vis spectra showed appreciable differences. This observation is furthermore supported by electronic structure calculations on small gold clusters.[54] The latter calculations reveal that the adsorption of thiols modifies the frontier orbitals and leads to considerable deformation of the metal core.

The discussion in the previous paragraph and the striking similarity between the UV-vis spectra of the *L*-glutathione and N-isobutyryl-*L*-cysteine passivated gold particles (**Figure 3.8**) indicates that for compounds **1-3** the number and arrangement of thiols on the cluster is the same independent of the nature of the thiol. This is in accord with the general knowledge that the bonding of thiols on gold is determined by the strong affinity between sulfur and gold. However, this finding is somewhat surprising given the fact that the two thiols considered here (*L*-glutathione and N-acetyl-*L*-cysteine) have rather different size, which should translate into a different number of surface gold atoms occupied by one adsorbed molecule. This argument is certainly valid for flat surfaces, but the size of the thiol becomes less important for nanoparticles with their highly curved convex surfaces. It should be noted that the above discussion addresses the comparison between separated particles of the same very small size, which should not be confused with the mean particle size. The latter is normally shifted to smaller size when using larger thiols.[55]

It has been noted before for the gold *L*-glutathione system that the number n of gold atoms in the different compounds (“magic numbers”) does not correspond to the closing of geometrical (13, 20, 28, 38…) nor electronic shells (8, 18, 20…).[48] Another possibility that was considered is the completion of the ligand shell, which stabilizes certain sizes of the gold particles. The results discussed above indicate that this argument may not be valid, as the size

of the thiol ligand seems to have no influence on the number of thiols adsorbed on the corresponding gold compounds **1-3**. Furthermore, the size of the thiol ligand (steric demand) was argued to favor the selective production of very small particles and to render the latter more stable.[49] Our work shows that gold particles with the same size can be obtained using a considerably smaller ligand. In addition, the N-isobutyryl-cysteine protected gold particles were found to be at least as stable as similar *L*-glutathione gold particles prepared and stored under identical conditions. After storing the nanoparticles for several months at ambient conditions the electrophoresis hardly changed, whereas noticeable changes were observed for *L*-glutathione MPNs, as was already reported before.[48]

3.4.6 Optical Activity in the UV-Vis

Figure 3.9 shows a comparison between the UV-vis and CD spectra of compounds **2-4** covered with the two enantiomers of N-isobutyryl-cysteine. The corresponding spectra of N-isobutyryl-cysteine exhibit optical activity only below 300 nm (see Appendix B). The optical activity of the other compounds was weaker. The CD spectra of the particles covered with the two enantiomers show (nearly) mirror-image relationship, whereas the corresponding UV-vis spectra are basically identical. However, the mirror image relationship in the ECD spectra is not perfect particularly for compounds **3** and **4**.

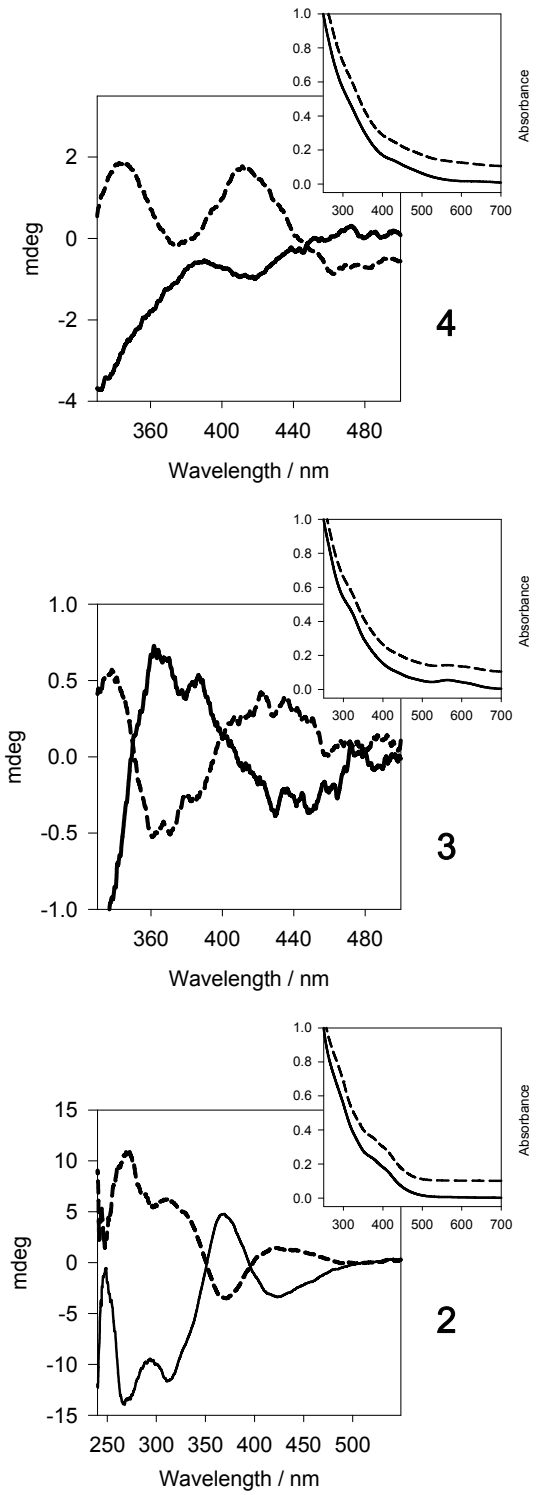

Figure 3.9 : ECD and UV-vis spectra of separated compounds **2-4** of gold particles covered with N-isobutyryl-*L*-cysteine (dashed) and N-isobutyryl-*D*-cysteine (solid line). The UV-vis spectra were scaled to 1 absorbance unit at 250 nm.

To the best of our knowledge the preparation, separation and ECD spectra of gold particles covered with enantiomers of thiols was reported only once before (for penicillamine-protected gold particles).[29] The ECD spectra of the particles covered with the enantiomers of penicillamine showed also (nearly) mirror image relationship. One possible explanation for the slight deviation from perfect mirror image relationship is that the isolated bands in the gel electrophoresis still contain two or more compounds with the same mobility and composition, but with slightly different structure. The varying relative amount of these sub-compounds obtained in different synthesis batches (different enantiomers) could cause the slight deviation from perfect mirror image relationship in the ECD spectra.

The strongest optical activity is observed for compound **2**. The anisotropy factors (see Appendix B) have the same order of magnitude as those reported for *L*-glutathione MPNs and penicillamine MPNs. For the penicillamine-protected gold particles the anisotropy factors decreased with increasing particle size.[29] Our findings do not contradict this tendency, although it seems less clear for the N-isobutyryl-*L*-cysteine case (only weak optical activity for compound **1**, relatively weak anisotropy factor for compound **3**). This tendency follows the surface to volume ratio of the particles and may thus point towards a surface effect as the origin for the optical activity (see discussion below).

It is important to note here that all the gold particles which were separated by a gel electrophoresis and for which optical activity has been reported in the UV-vis (*L*-glutathione,[28] penicillamine[29] and N-isobutyryl-*L*-cysteine) are relatively small. The metal core diameters of these particles are 1 nm or below, with the exception of one penicillamine gold particle showing only relatively weak optical activity, which had a particle diameter (according to SAXS) larger than 1 nm. In contrast, optical activity was also reported

for considerably larger silver particles (23.5 nm). However, these particles were not separated and it can not be excluded that the observed optical activity is due to a fraction of small particles formed during the addition of the thiol to the silver colloids.[30] Another explanation for the tendency of decreasing optical activity with increasing particle size is simply the increased configurational space for larger particles (larger number of gold atoms and ligands) and thus the increased probability of multiple energy minima on the potential energy surface. An increasing number of conformers leads to a decreased observable optical activity as positive and negative bands of different conformers average out.

Considering all the available ECD spectra of gold particles protected with chiral thiols (*L*-glutathione,[28] penicillamine[29] and N-isobutyryl-*L*-cysteine) another trend is remarkable. The ECD spectra tend to be preferentially either positive or negative. In the *L*-glutathione case the ECD is dominated by positive bands.[28] For the penicillamine-protected gold particles most of the bands in the ECD are positive in the for the *L*-enantiomer.[29] For the two larger compounds almost only positive bands were observed. For the N-isobutyryl-*L*-cysteine-protected gold particles investigated here this tendency is also observed, with more positive intensity in the ECD spectra for the *L*-enantiomer. The sign of the predominant intensity in the ECD spectra of the chiral particles (positive or negative) correlates with the absolute configuration of the thiol, penicillamine or cysteine (for N-acetyl-*L*-cysteine and *L*-glutathione). Due to the limited data available today, the described trend may be on the one hand only by chance but may on the other hand point towards the origin of the optical activity in these compounds.

3.4.7 Origin of Optical Activity in the UV-vis

The origin of the observed optical activity in the small gold particles protected with chiral thiols has been discussed before.[28, 29] The principal possibilities are the same as described for flat metal surfaces in the introduction. The key question remains whether the metal particle is intrinsically chiral or whether the optical activity is induced by the chiral environment.[56] The first possibility has support from theoretical calculations which indicate that small metal particles such as Au_{28} prefer low symmetry chiral over high symmetry non-chiral structures.[54, 57] Several mechanisms for the arising optical activity were proposed for non-chiral metal particles in a chiral environment. These include the chiral arrangement of the ligands and the influence of the asymmetric centers of the chiral ligands (through space or through bonds) on the electronic structure of the metal. Likely some of these effects are not easily separable for the gold compounds prepared in this study. For example, if the thiols indeed adsorb in a chiral arrangement, it is very likely that the gold particle itself is distorted towards a chiral structure because the adsorption of a thiol leads to a distortion of the surface gold atoms.[57] Even adsorption of single chiral molecules can lead to a chiral "footprint" on a non-chiral surface, *i.e.* the relaxation of the surfaces atoms involved in the adsorbate complex towards a chiral structure, as was shown for tartaric acid adsorption on Ni surfaces.[15] It is hard to imagine that the thiol gold interaction, *i.e.* a one point interaction, leads to a chiral "footprint". However, the VCD investigation indicates that the carboxyl group is also interacting with the gold particle, which may induce a chiral "footprint" on the surface of the particle and lead to the observed optical activity. A possible model of a chiral "footprint" induced by a double interaction is given in Appendix B. This possibility is consistent with the trend that the optical activity is decreasing with particle size. In addition,

all the thiols that were reported to induce optical activity in gold and silver particles, penicillamine[29, 30], *L*-glutathione,[28, 30] cysteine[30] and N-isobutyryl-cysteine contain an acid group, which can interact with the metal surface in addition to the thiol. Such double interactions have indeed been documented in the past.[27, 46, 47, 58, 59] Furthermore, it was reported for Ag particles that the adsorption of cysteine (penicillamine and *L*-glutathione) induced optical activity. However, when the acid group was blocked in cysteine methyl ester no optical activity was observed,[30] which further supports the idea that the acid group plays an important role for the induction of optical activity in the metal based transitions, through imparting a chiral "footpring" onto the metal particle surface. The idea that an adsorbed thiol can considerably distort the structure of the underlying small metal particle is not so astonishing. In fact, very recently several papers have appeared where the influence of thiol adsorption on the structure of small particles has been shown.[60, 61] The formation of a "chiral footprint" on a particle induced by a chiral thiol seems thus also plausible.

3.5 Conclusions

Small gold particles protected with N-isobutyryl-*D*-cysteine and N-isobutyryl-*L*-cysteine, respectively, were prepared and their optical activity in the infrared and UV-vis was investigated. The VCD spectra of the as prepared samples show mirror image relationship for particles covered with the two enantiomers. Density functional theory calculations reveal that the VCD spectra strongly depend on the conformation of the adsorbed N-isobutyryl-cysteine. The VCD spectra are consistent with a conformation where the carboxylate interacts with the

gold particle in addition to the thiol and the study furthermore demonstrates the power of VCD spectroscopy for structure determination of molecules adsorbed on nanoparticles.

The as prepared nanoparticles consist of few distinct compounds with well-defined composition, *i.e.* gold atoms and ligands, which can be separated according to their size and charge in a gel electrophoresis. The UV-vis spectra of the separated compounds reveal the well-quantized electronic structure of these particles and a systematic red-shift of the absorption onset with increasing particles size, which is also evident from the color of the individual compounds. The UV-vis spectra of some of the separated compounds are astonishingly similar to the UV-vis spectra of analogous particles covered with *L*-glutathione indicating the same composition, *i.e.* number of Au atoms and thiol ligands. Thus, for these small particles the composition is independent of the thiol, *i.e.* *L*-glutathione and N-isobutyryl-cysteine, respectively, despite the fact that the size of the two thiols is largely different. Some of the separated compounds reveal large optical activity. Based on the present findings and the information available on optically active gold nanoparticles the origin of the optical activity is discussed. Up to now, all the thiols leading to optically active nanoparticles contain at least one carboxylic acid group. The VCD investigation indicates that the carboxylic acid group interacts with the gold particle and it is proposed that this "two point interaction" leads to a "chiral footprint" on the particle surface, which is the origin of the observed optical activity.

3.6 References

[1] M. Studer, H. U. Blaser, C. Exner, *Adv. Synth. Catal.* **2003**, *345*, 45.

[2] T. Bürgi, A. Baiker, *Acc. Chem. Res.* **2004**, *37*, 909.

[3] C. F. McFadden, P. S. Cremer, A. J. Gellman, *Langmuir* **1996**, *12*, 2483.

[4] D. S. Sholl, *Langmuir* **1998**, *14*, 862.

[5] J. D. Horvath, A. J. Gellman, *J. Am. Chem. Soc.* **2002**, *124*, 2384.

[6] J. D. Horvath, A. Koritnik, P. Kamakoti, D. S. Sholl, A. J. Gellman, *J. Am. Chem. Soc.* **2004**, *126*, 14988.

[7] G. A. Attard, *J. Phys. Chem. B* **2001**, *105*, 3158.

[8] M. O. Lorenzo, C. J. Baddeley, C. Muryn, R. Raval, *Nature* **2000**, *404*, 376.

[9] M. O. Lorenzo, S. Haq, T. Bertrams, P. Murray, R. Raval, C. J. Baddeley, *J. Phys. Chem. B* **1999**, *103*, 10661.

[10] V. Humblot, R. Raval, *Appl. Surf. Sci.* **2005**, *241*, 150.

[11] D. Ferri, T. Bürgi, A. Baiker, *J. Chem. Soc. Chem. Commun.* **2001**, 1172.

[12] D. Ferri, T. Bürgi, *J. Am. Chem. Soc.* **2001**, *123*, 12074.

[13] M. Bieri, T. Bürgi, *J. Phys. Chem. B* **2005**, *109*, 10243.

[14] M. Bieri, T. Bürgi, *Chem. Phys. Chem.* **2006**, *7*, 514.

[15] V. Humblot, S. Haq, C. Muryn, W. A. Hofer, R. Raval, *J. Am. Chem. Soc.* **2002**, *124*, 503.

[16] W. A. Hofer, V. Humblot, R. Raval, *Surf. Sci.* **2004**, *554*, 141.

[17] R. Elghanian, J. J. Storhoff, R. C. Mucic, R. L. Letsinger, C. A. Mirkin, *Science* **1997**, *277*, 1078.

[18] S. Ghosh, K., S. Kundu, M. Mandal, T. Pal, *Langmuir* **2002**, *18*, 8756.

[19] S. H. Sun, C. B. Murray, D. Weller, L. Folks, A. Moser, *Science* **2000**, *287*, 1989.

[20] M.-C. Daniel, D. Astruc, *Chem. Rev.* **2004**, *104*, 293.

[21] J. A. Schellman, *Chem. Rev.* **1975**, *75*, 323.

[22] S. F. Mason, R. H. Seal, D. R. Roberts, *Tetrahedron* **1974**, *30*, 1671.

[23] L. A. Nafie, T. A. Keiderling, P. J. Stephens, *J. Am. Chem. Soc.* **1976**, *98*, 2715.

[24] P. J. Stephens, M. A. Lowe, *Annu. Rev. Phys. Chem.* **1985**, *36*, 213.

[25] L. A. Nafie, *Annu. Rev. Phys. Chem.* **1997**, *48*, 357.

[26] P. L. Polavarapu, L. A. Nafie, *J. Chem. Phys.* **1980**, *73*, 1567.

[27] C. Gautier, T. Bürgi, *Chem. Commun.* **2005**, 5393.

[28] T. G. Schaaff, R. L. Whetten, *J. Phys. Chem. B* **2000**, *104*, 2630.

[29] H. Yao, K. Miki, N. Nishida, A. Sasaki, K. Kimura, *J. Am. Chem. Soc.* **2005**, *127*, 15536.

[30] T. Li, H. G. Park, H.-S. Lee, S.-H. Choi, *Nanotechnology* **2004**, *15*, S660.

[31] T. Bürgi, A. Vargas, A. Baiker, *J. Chem. Soc. Perkin Trans. 2* **2002**, 1596.

[32] T. Bürgi, U. Urakawa, B. Behzadi, K.-H. Ernst, A. Baiker, *New. J. Chem.* **2004**, *28*, 332.

[33] Y. Negishi, T. Tsukuda, *J. Am. Chem. Soc.* **2003**, *125*, 4046.

[34] M. J. Frisch *et al.* Rev. C.01 ed., Gaussian, Inc., Wallingford CT, **2003**.

[35] A. D. Becke, *J. Chem. Phys.* **1993**, *98*, 5648.

[36] J. P. Perdew, J. A. Chevary, S. H. Vosko, K. A. Jackson, M. R. Pederson, D. J. Singh, C. Fiolhais, *Phys. Rev. B* **1992**, *46*, 6671.

[37] P. J. Hay, W. R. Wadt, *J. Chem. Phys.* **1985**, *82*, 270.

[38] R. Ditchfield, W. J. Hehre, J. A. Pople, *J. Chem. Phys.* **1971**, *54*, 724.

[39] P. L. Polavarapu, C. Zhao, A. Cholli, G. G. Vernice, *J. Phys. Chem. B* **1999**, *103*, 6127.

[40] A. Aamouche, F. J. Devlin, P. J. Stephens, *J. Am. Chem. Soc.* **2000**, *122*, 7358.

[41] T. B. Freedman, X. Cao, R. V. Oliveira, Q. Cass, L. A. Nafie, *Chirality* **2003**, *15*, 196.

[42] C. Herse, D. Bas, F. C. Krebs, T. Bürgi, J. Weber, T. Wesolowski, B. W. Laursen, J. Lacour, *Angew. Chem, Int. Ed.* **2003**, *42*, 3162.

[43] R. M. Olson, S. Varganov, M. S. Gordon, H. Metiu, S. Chretien, P. Piecuch, K. Kowalski, S. A. Kucharski, M. Musial, *J. Am. Chem. Soc.* **2005**, *127*, 1049.

[44] R. Di Felice, A. Selloni, E. Molinari, *J. Phys. Chem. B* **2003**, *107*, 1151.

[45] M. C. Vargas, P. Giannozzi, A. Selloni, G. Scoles, *J. Phys. Chem. B* **2001**, *105*, 9509

[46] M. Bieri, T. Bürgi, *J. Phys. Chem. B* **2005**, *109*, 22476.

[47] M. E. Marti, C. Methivier, C. M. Pradier, *Langmuir* **2004**, *20*, 10223.

[48] Y. Negishi, K. Nobusada, T. Tsukuda, *J. Am. Chem. Soc.* **2005**, *127*, 5261.

[49] T. G. Schaaff, G. Knight, M. N. Shafigullin, R. F. Borkman, R. L. Whetten, *J. Phys. Chem. B* **1998**, *102*, 10643.

[50] Y. Negishi, Y. Takasugi, S. Sato, H. Yao, K. Kimura, T. Tsukuda, *J. Am. Chem. Soc.* **2004**, *126*, 6518.

[51] C. J. Ackerson, P. D. Jadzinsky, R. D. Kornberg, *J. Am. Chem. Soc.* **2005**, *127*, 6550.

[52] X. Li, B. Kiran, J. Li, H.-J. Zhai, L.-S. Wang, *Angew. Chem, Int. Ed.* **2002**, *41*, 4786.

[53] K. Nobusada, *J. Phys. Chem. B* **2004**, *108*, 11904.

[54] I. L. Garzón, J. A. Reyes-Nava, J. I. Rodriguez-Hernandez, I. Sigal, M. R. Beltran, K. Michaelian, *Phys. Rev. B* **2002**, *66*, 73403.

[55] T. Yonezawa, K. Yasui, N. Kimizuka, *Langmuir* **2001**, *17*, 271.

[56] M.-R. Goldsmith, C. B. George, G. Zuber, R. Naaman, W. D. H., P. Wipf, D. N. Beratan, *Phys. Chem. Chem. Phys.* **2006**, *8*, 63.

[57] I. L. Garzón, M. R. Beltran, C. Gonzalez, I. Gutierrez-Gonzalez, K. Michaelian, J. A. Reyes-Nava, J. I. Rodriguez-Hernandez, *Eur. Phys. J. D* **2003**, *24*, 105.

[58] M. Bieri, T. Bürgi, *Langmuir* **2005**, *21*, 1354.

[59] M. Bieri, T. Bürgi, *Phys. Chem. Chem. Phys.* **2005**, *8*, 513.

[60] K. Nunokawa, S. Onaka, M. Ito, M. Horibe, T. Yonezawa, H. Nishihara, T. Ozeki, H. Chiba, S. Watase, M. Nakamoto, *J. Organomet. Chem.* **2006**, *691*, 638.

[61] Y. Negishi, Y. Takasugi, S. Sato, H. Yao, K. Kimura, T. Tsukuda, *J. Phys. Chem. B* **2006**, *110*, 12218.

4

BINAS-Stabilized Gold Clusters: Separation and Optical Activity in the UV-vis

4.1 Abstract

Gold particles passivated by 1,1'-binaphthyl-2,2'-dithiol (BINAS) were prepared. Using size exclusion chromatography it was possible for the first time to separate the sample into fractions with different size and colour. Transmission electron microscopy shows that the particles are very small, on the order of one nanometer or slightly above. The absorption spectra of the separated samples show rich structure. The particles show size-dependent optical activity in metal-based electronic transitions. The shape of the absorption and the circular dichroism spectra of one of the smallest fractions exhibits similarities with the spectra reported for Au_{11} covered by 2,2'-bis(diphenylphosphino)-1,1'-biphenyl although the spectra

are shifted to shorter wavelengths in the case of the dithiol. The anisotropy factors, $\Delta\varepsilon/\varepsilon$ of these particles are as large as 4 X 10^{-3}, which is larger than the values reported for gold particles stabilized by phosphines and water-soluble thiols. This indicates that BINAS is particularly well-suited to impart chirality onto gold particles.

4.2 Introduction

Monolayer protected nanoparticles (MPNs) are fascinating hybrid materials composed of a metallic core surrounded by an organic monolayer.[1] Their physical and chemical properties can easily be tuned for custom requirements by changing their size and by modifying in a judicious way the organic shell. Their potential applications were reported in various fields such as catalysis,[2] sensing,[3, 4] therapy,[5] electronics[6] and optics.[7] Among the huge number of different particles, the subnanometer range of inorganic-organic hybrid nanoparticles has gained great interest both in fundamental and applied research. This class of material exhibits strong size-dependant properties.[8, 9] From a fundamental point of view, these particles can be understood as the intermediate state of matter between a single metal atom and the bulk metal. As such they serve as models to understand fundamental physical properties like quantum confinement and structural evolution. Their solubility in various solvents makes them amenable to size separation and spectroscopic techniques which are of great help in elucidating the size dependence of their physical properties. MPNs can also be viewed as the nanometer size analogue of self-assembled monolayers (SAMs) on extended metal surfaces and are a powerful tool for a better understanding of the interaction between metal surfaces and organic molecules.

Recently the use of chiral passivating agents was considered. To probe the chiral nature of these particles, chiroptical techniques such as circular dichroism (ECD) and vibrational circular dichroism (VCD) are particularly helpful. Based on the comparison between the experimental and calculated VCD spectra, a preferential conformation of N-acetyl-cysteine [10] and N-isobutyryl-cysteine[11] absorbed on gold particles was proposed (see Chapters 2 and 3). Theses results were in good agreement with those obtained from measurements on a SAM of the thiol on extended gold surfaces.[12] Furthermore, the use of a chiral capping agent leads to optical activity located in metal-based electronic transitions.[11, 13-19] This shows that chirality can be bestowed to the metal. However, the question whether the metal core adopts an intrinsically chiral structure[20] or whether the chirality is only imposed onto the electronic structure of the metal core[21] remains still unanswered.

The optical activity located in metal-based transitions is promising for applications in the field of asymmetric reactions catalyzed by small metal nanoparticles. Fujihara *et al.* have reported the asymmetric hydrosilylation of styrene with trichlorosilane catalyzed by chiral palladium nanoparticles stabilized by optically active 2,2'-bis-(diphenylphosphino)-1-1'-binaphtyl (BINAP).[16]

Actually, Catalysis by gold is evolving every week. Gold is already effective as heterogeneous and homogeneous catalyst in hydrogenation, in selective oxidation, in nucleophilic addition to π systems and for many reactions for which a catalyst had not been previously identified.[22] Gold nanoparticles play an important role in gold catalysis thus chiral gold nanoparticles are expected to be of great interest in the field of enantioselectivity.

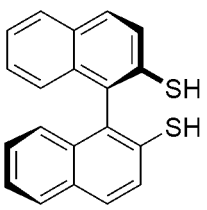

(*R*)-BINAS

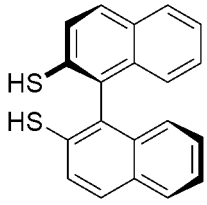

(*S*)-BINAS

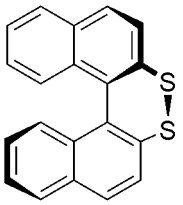

(*R*)-BINAS-cyclic disulphide

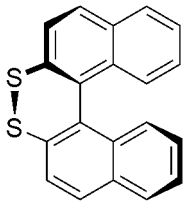

(*S*)-BINAS-cyclic disulphide

Chart 4.1 : Structure of (*R*)-BINAS, (*S*)-BINAS, (*R*)-BINAS-cyclic disulphide and (*S*)-BINAS-cyclic disulphide.

Here we report the preparation and chiroptical properties in the UV-vis of gold nanoparticles covered by the two enantiomeric forms of an atropisomeric dithiol: (*R*)-1,1'-binaphthyl-2,2'-dithiol [(*R*)-BINAS] and (*S*)-1,1'-binaphthyl-2,2'-dithiol [(*S*)-BINAS][23] (**Chart 4.1**). Size exclusion chromatography (SEC) allowed, for the first time, the separation of up to five different fractions with well-defined and distinctly different absorption spectra and color. The five separated fractions showed strong optical activity in metal-based electronic transitions. The origin of this optical activity is discussed.

4.3 Materials and Methods

4.3.1 Materials

The preparation of enantiomerically pure (*R*)- and (*S*)-BINAS was reported elsewhere.[23] Deuterated chloroform (99.8%) and was received from Cambridge Isotope

Laboratories. Gold(III) chloride trihydrate ($HAuCl_4.3H_2O$, 99.99%), sodium borohydride ($NaBH_4$, 98%) and tetraoctylammonium bromide (TOAB, >98%) were purchased from Aldrich, chloromethylated styrene-divinyl benzene (99:1) resin was obtained from Bio-Rad, Richmond, CA, USA (Bio-Beads SX1, 200–400 mesh). Water was purified with a Milli-Q system ($\geq$18 MΩ.cm^{-1}). Tetrahydrofuran (THF) and dichloromethane were distillated under nitrogen to remove dissolved oxygen. All other chemicals were analysis grade and used as received.

4.3.2 Synthesis of Gold BINAS MPNs

(*R*)-BINAS and (*S*)-BINAS MPNs were both prepared under anaerobic conditions following the two-phase method of Brust *et al.*[24] Briefly, to a vigorously stirred solution of tetrachloroauric acid (132 mg, 0.335 mmol) in 6 ml of deaerated Milli-Q (sonication under vacuum) was added 183 mg of TOAB (0.335 mmol) dissolved in 10 ml of distilled dichloromethane. The mixture was stirred for 30 minutes. The phase transfer of gold salts from water to dichloromethane results in a discoloration of the aqueous phase and an orange coloration of the organic phase. The two phases were allowed to settle. Then, the orange organic phase was withheld and added to 214 mg (0.67 mmol) of the corresponding enantiomer of BINAS dissolved in 100 ml of distilled dichloromethane. After 30 minutes, the solution was reduced by addition of a freshly prepared aqueous $NaBH_4$ solution (5 ml, 317 mg, 8.38 mmol) under vigorous stirring. The mixture was allowed to react for one night under an argon atmosphere. The resulting dark organic solution was extracted and washed three times with water. The solution was dried over Na_2SO_4 and filtered using a 0.2 μm PTFE

membrane to remove insoluble material. The filtrate was evaporated to near dryness at 40 °C and the nanoparticles were precipitated several times with a large excess of hexane and filtered using the same 0.2 μm PTFE membrane. Purification of BINAS gold nanoparticles was repeated until no free BINAS, disulfur and phase transfer catalyst were detected by ^{1}H NMR. We obtained finally 176 mg of gold nanoparticles protected with a monolayer of the corresponding enantiomer of BINAS.

4.3.3 Size Exclusion Chromatography

The THF used for elution and for packing the column was freshly distillated under nitrogen and protect from atmospheric contamination. Bio-Beads S-X1 beads were placed in THF (six times the resin weight). The resin was allowed to swell overnight and packed in a glass column (1.2 meter length and 2 cm in diameter). The column was washed with several bed volumes of solvent after packing and between separations. For size separation, the sample (90 mg) was dissolved in a minimum amount of distilled THF and loaded on the column. The elution was done with THF at a flow rate of *ca.* 0.5 $ml.min^{-1}$ and 5 ml fractions were collected. Each fraction was controlled by UV-vis spectrometry and classified according to its absorption profile.

4.3.4 UV-vis, ECD and NMR Spectroscopy

^{1}H NMR spectra of the as prepared particles were measured on a Brucker Avance 400 MHz spectrometer at room temperature. Solutions were prepared in $CDCl_3$ at a concentration of approximately 50 $mg.ml^{-1}$. UV-vis and ECD spectra, respectively, of the separated particles

were collected on a Cary 300 and a Jasco 710 spectrometer, respectively, using a quartz cell of 1 cm path length and solutions of *ca.* 0.3 $mg.ml^{-1}$ in THF.

4.3.5 Transmission Electron Microscopy

TEM images were recorded with a Philips C200 electron microscope operated at 200 kV. The nanoparticles were dissolved in dichloromethane (~ 0.5 $mg.ml^{-1}$). TEM sample was prepared by casting of a drop of the solution onto a carbon-coated copper grid.

4.4 Results and Discussion

4.4.1 Size Separation of Gold BINAS MPNs

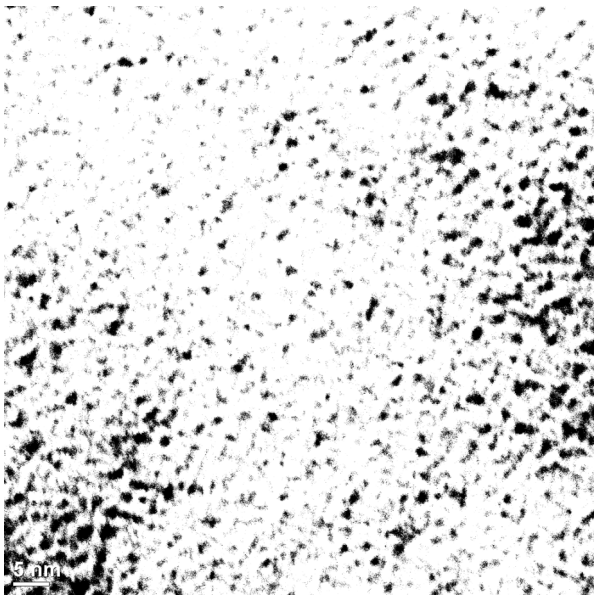

Figure 4.1 : TEM micrograph of gold BINAS MPNs fraction 1.

The as prepared product consists of gold BINAS MPNs with an average size smaller than 2 nm as shown by the TEM (**Figure 4.1**) and confirmed by the absence of a plasmon resonance band at around 520 nm in UV-vis (**Figure 4.2**). This type of small gold MPNs has a typical molecular weight range between *ca.* 4 and 20 kDa,[17, 25] which corresponds well with the operating range of commercially available gels like Bio-Beads S-X1.

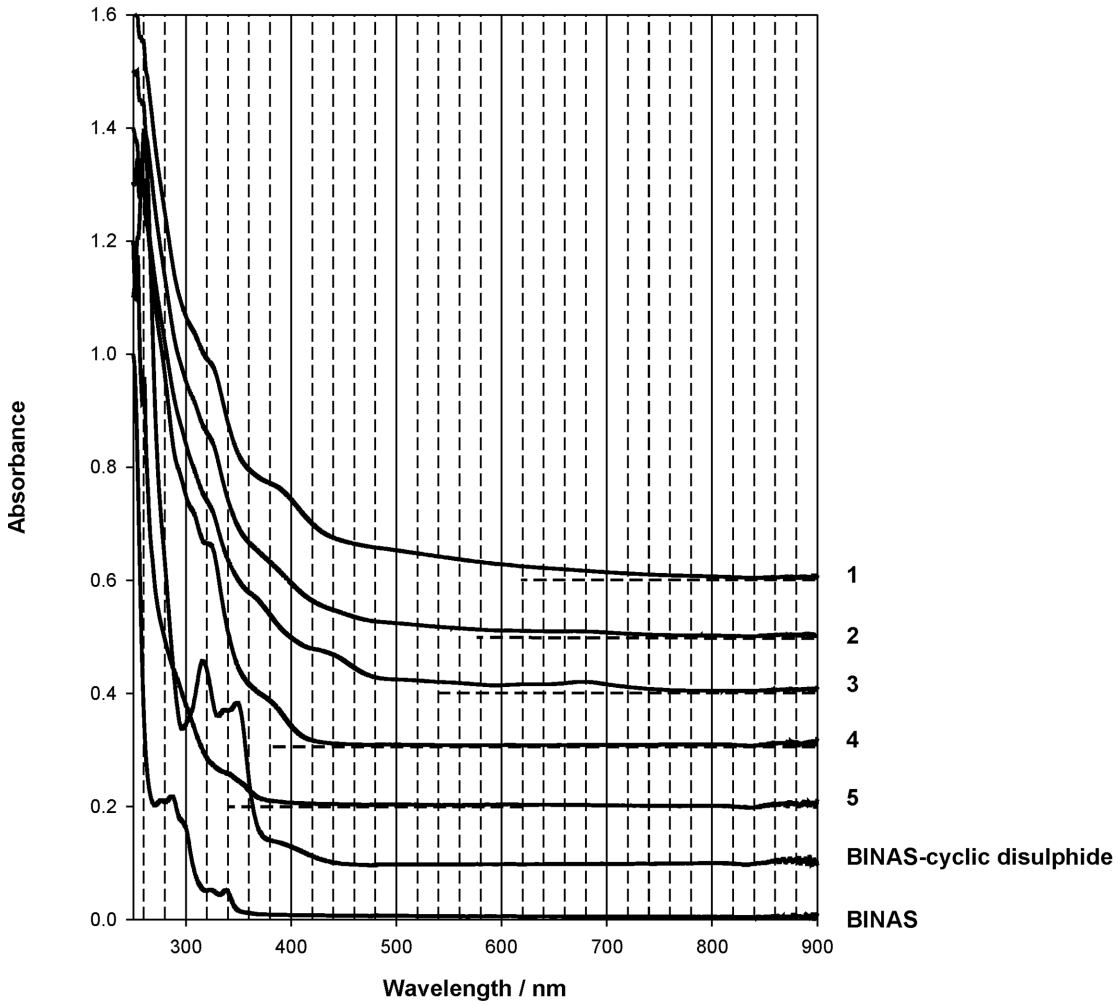

Figure 4.2 : UV-vis spectra of the separated fractions **1-5**. Spectra are offset for clarity and normalized to one absorbance unit at 250 nm. The bottom spectrum corresponds to BINAS and the second one to BINAS-cyclic disulphide.

Figure 4.3 shows a photograph of the SEC column during separation. Just after loading, the polydisperse sample gave rise to a *ca.* 2 cm long black band. During the separation this black band became increasingly broad showing that the average size of the nanoparticles is smaller than the exclusion limit of the beads that were used. Finally, five fractions with different color could be separated and were numbered **1-5** according to their elution order or their decreasing size.

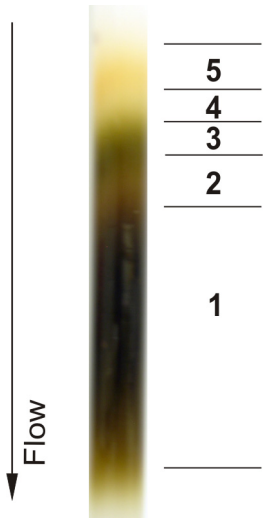

Figure 4.3 : Size exclusion chromatography separation of BINAS protected gold particles. The separated fractions are numbered from **1-5** according to their decreasing elution mobility. Horizontal lines show roughly the limit between adjacent fractions.

This shows that the size distribution is not homogenous and indicates the presence of magic number compounds, *i.e.* the high relative abundance of compounds with well-defined composition. The color-dependence on the size is a direct consequence of a quantum size effect. The latter is also responsible for the systematic red shift of the absorption onset for increasing particle size (from **5** to **1**). Fractions **1**, **3** and **5** are respectively brown, green and

yellow. Fraction **2** seems to be a mixture of the adjacent fractions **1** and **3** as judged from the UV-vis and ECD spectra (vide infra).

4.4.2 NMR of Gold BINAS Nanoparticles

The upper part of **Figure 4.4** shows the aromatic region of ^{1}H NMR spectra for polydisperse gold nanoparticles covered with BINAS, free BINAS and dinaphtho[2,1-c:1',2'-e][1,2]dithiin (BINAS-cyclic disulphide) (**Chart 4.1**). The lower part of the Figure compares the aliphatic part of both TOAB and the as prepared gold nanoparticles. In the aromatic region, the ^{1}H NMR spectrum of unbound BINAS displays six sets of signals with chemical shifts δ (ppm) = 7.89 (d, 2 H), 7.88 (d, 2 H), 7.55 (d, 2 H), 7.41 (m, 2 H), 7.28 (m, 2 H), 6.98 (d, 2 H) and BINAS-cyclic disulphide shows five sharp signals, δ (ppm) = 7.90 (d, 2 H), 7.84 (2d, 2 H), 7.79 (d, 2 H), 7.44 (ddd, 2 H), 7.22-7.14 (m, 4 H). BINAS-cyclic disulphide is a major by-product observed during the synthesis of BINAS-gold nanoparticles.

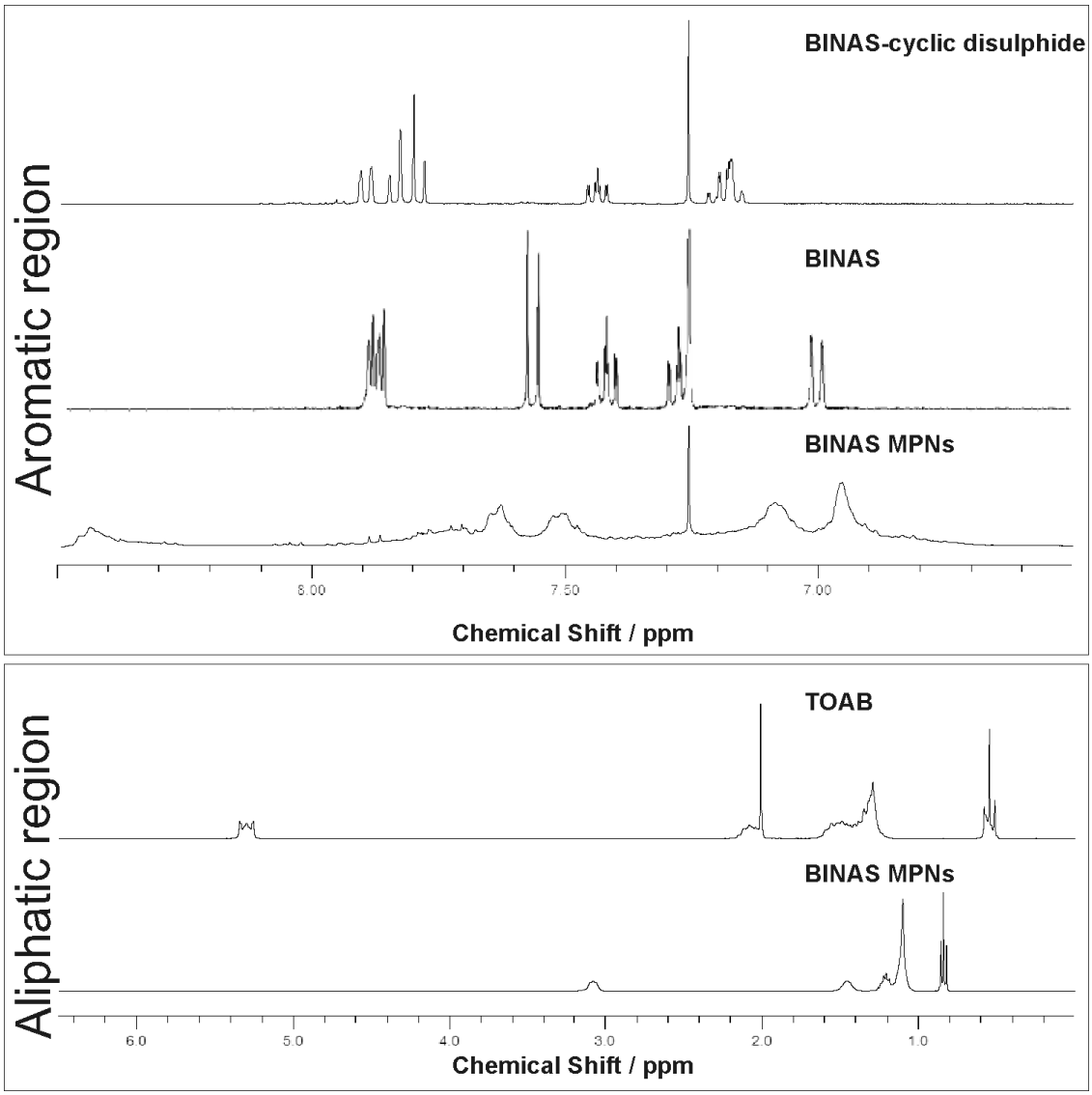

Figure 4.4 : ^{1}H NMR spectra (top) in the aromatic region of the polydisperse nanoparticles covered with BINAS, free BINAS and BINAS-cyclic disulphide and ^{1}H NMR spectra (bottom) in the aliphatic part of the polydisperse nanoparticles and of TOAB.

In contrast to the sharp signals observed for the latter compounds, the polydisperse gold nanoparticles are characterized by broad and shifted signals. This observation leads us to conclude that after purification the sample is free from BINAS-cyclic disulphide and BINAS impurities. Previous ^{1}H NMR studies[26-30] of MPNs have also described significant peak

broadening and four main explanations have been put forward: (a) Rapid spin-spin relaxation from dipolar interaction; (b) dependence of chemical shifts on the size of nanoparticles and on the type of binding site (vertex, edges, terraces); (c) size-dependent rotation diffusion of the cluster leading to size-dependent spin-spin relaxation broadening; (d) the oxidation states of nanoparticles have a significant effect on NMR spectra of the monolayer ligand shell. The aliphatic part of ^{1}H NMR spectra reveals the presence of tetraoctylammonium groups, which have a NMR signature significantly different from the one of free TOAB. This shows that there is no free TOAB. It has been shown by mass spectroscopy that the tetraoctylammonium groups balance the negative charge on the Au-thiolate cores.[31]

4.4.3 UV-vis Spectra

The UV-vis spectra in **Figure 4.2** of the separated samples show no sign of a surface plasmon resonance characteristic for particles equal or larger to 3 nm, in agreement with TEM measurements. However, the absorption spectra of the different fractions **1-5** show considerable structure. Also, the absorption spectra are distinctly different from the ones observed for the free BINAS and BINAS-cyclic disulphide ligands. There is also a clear trend in the spectra as concerns the absorption onset, which shifts to longer wavelengths with increasing particle size. This trend was already observed for gold particles covered by glutathione[14, 25] and N-isobutyryl-cysteine,[11] respectively, separated into different compounds by gel electrophoresis. For example, the absorption onset was found at about 400 nm for particles containing 10-12 gold core atoms and at above 800 nm for 25 gold core atoms. This indicates that the particles investigated here are very small, containing ten to a

few tens of gold atoms only. Interestingly, the absorption onset of particles containing 10 or 12 gold atoms strongly depends on the nature of the ligand. For Au_{11} covered by phosphine ligands the absorption onset is found at around 600 nm,[17] whereas for gold particles of similar size covered by thiols it is found at around 400 nm.[25] This may be a consequence of the different nature of the gold – phosphorus and gold – sulfur bonds, the latter being considerably stronger. This has likely also an influence on the structure of the metal core. The structure of Au_{11} covered by phosphine ligands is well-known from X-ray crystallography,[32, 33] which reveals a compact metal core with a central gold atom surrounded by 10 peripheral gold atoms. The structure of gold particles of similar size covered by thiols might however be quite different. Indeed, density functional theory (DFT) calculations indicate that the structure of such small gold cores is strongly distorted by the adsorbing thiol. In particular, based on DFT calculations, the formation of cyclic thiolated gold clusters has been proposed.[34]

4.4.4 Optical Activity in the UV-Vis

Figure 4.5 shows the ECD spectra of the separated fractions. The ECD spectra of the gold particles covered by the BINAS are distinctly different from the ECD spectra of both the free BINAS and the BINAS-cyclic disulphide. It is therefore concluded that the optical activity observed for the gold particles covered by the BINAS is associated with electronic transitions within the metal core. It is also evident that the ECD spectra depend on the particle size.

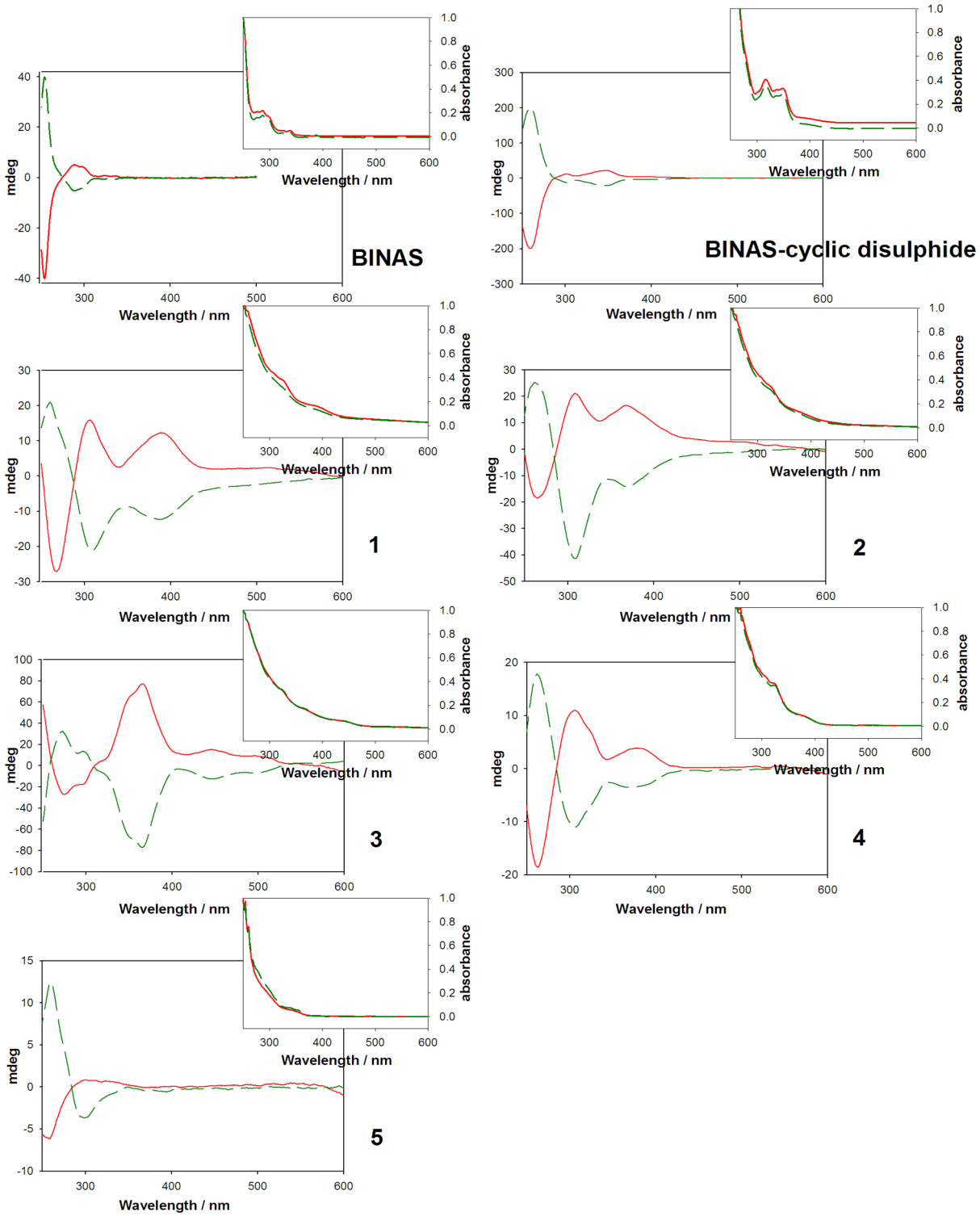

Figure 4.5 : ECD and UV-vis spectra of separated fractions **1-5** of gold particles covered with (*S*)-BINAS (dashed) and (*R*)-BINAS (solid line). The UV-vis spectra were scaled to 1 absorbance unit at 250 nm.

This is particularly apparent from a comparison between the ECD spectra of fractions **1** and **3**. None of the ECD spectra is similar to the ones reported for small gold particles covered by the water-soluble thiols glutathione,[14] penicillamine[15] and N-isobutyryl-cysteine,[11] respectively.

Optical activity in gold particles covered by BINAS has not been reported yet. However, two independent studies report the ECD spectra of gold nanoparticles protected by BINAP.[16, 17] The protocol for the preparation of these particles was quite different in the two cases. In one case, according to the procedure proposed by Hutchison *et al.*,[35] $HAuCl_4$ was reduced in the presence of the BINAP. This resulted in small particles with a size of 1.7 ± 0.4 nm, according to TEM. The other procedure started from a Au_2Cl_2(BINAP) precursor that was subsequently reduced. This resulted selectively in Au_{11} clusters, as supported by electrospray ionization (ESI) mass spectrometry and in agreement with TEM.[17] The ECD spectra reported for these two compounds are strikingly similar despite the fact that the average size of the particles in the former study is considerably larger. For the particles covered with the *R*-enantiomer of the BINAP the ECD spectra reported in both studies are characterized by a positive band at 440 nm, an about twice as strong positive band at 350 nm with a shoulder at longer wavelength and an even stronger negative band at slightly below 300 nm. The striking similarity of these spectra indicates that the optical activity originates from similar particles within the two samples. Since the average size of the two samples is rather different and since in one case the sample consisted predominantly of Au_{11} clusters, it is proposed that the sample with the larger average size particles contains Au_{11} clusters, which leads to the observed optical activity. This furthermore implies that the larger particles, around 1.7 nm in size, do not contribute much to the optical activity of the sample.

Comparison of the ECD spectra of the gold BINAP particles described above with the ones reported here for the gold BINAS particles shows that for example fraction **3** has a completely different ECD spectrum. On the other hand fraction **4** exhibits a ECD spectrum with similar shape and sign as the one for Au_{11} covered by BINAP, however shifted to shorter wavelength by about 50 nm. For the *R* enantiomer, a positive band at 380 nm, an about two and a half times as strong positive band at 300 nm with a shoulder at longer wavelengths and an even stronger negative band at 260 nm are observed. The corresponding UV-vis spectra also bear the same similarity with discrete bands shifted to longer wavelengths for the gold particles covered by the BINAS. For the gold particles covered by the BINAP (BINAS, fraction **4**) bands in the absorption spectra are observed at about 440 nm (380 nm), 370 nm (325 nm) and 350 nm (305 nm). These similarities could of course arise by chance, but they can also be an indication that fraction **4** contains Au_{11} clusters covered by BINAS and that these Au_{11} clusters have a similar structure as the ones covered by BINAP. The shift of the ECD and absorption spectra has likely to do with the different nature of the gold – sulfur and gold – phosphorus bond.

It has been proposed that the optical activity of the Au_{11} clusters covered by BINAP is due to an intrinsically chiral core.[17] It is known that the structure of the Au_{11} core depends on the type of the phosphine ligands.[36] This has probably to do with the fact that ten out of the eleven gold atoms reside on the surface of the metal core. The atoms are therefore unsaturated and relatively flexible. Adsorption of the BINAP leads to a deformation of the core to an asymmetric structure, which is at the origin of the optical activity in metal-based transitions. Such deformations are likely favored by molecules that contain two or more functional groups that can interact with the gold core. Our findings are in agreement with such

a model. Since the gold – sulfur bond is stronger than the gold - phosphorus bond the distortion of the gold core imposed by the adsorbed ligand is expected to be stronger in the case of adsorbed BINAS compared to adsorbed BINAP. This could also lead to a stronger deviation from a symmetric structure in the former case. Indeed, the anisotropy factors ($\Delta\varepsilon/\varepsilon$) found here for fraction **4** of gold particles covered by BINAS are about a factor of two stronger than the ones reported for Au_{11} covered by BINAP.[17] In both cases the band at the longest wavelength has the largest anisotropy factor (**Figure 4.6**), which is 1.2×10^{-3} in the latter and 2.5×10^{-3} in the former case. Note that anisotropy factors as large as 4.0×10^{-3} are found for fraction **3**. To the best of our knowledge such large anisotropy factors were never observed for optically active gold particles.

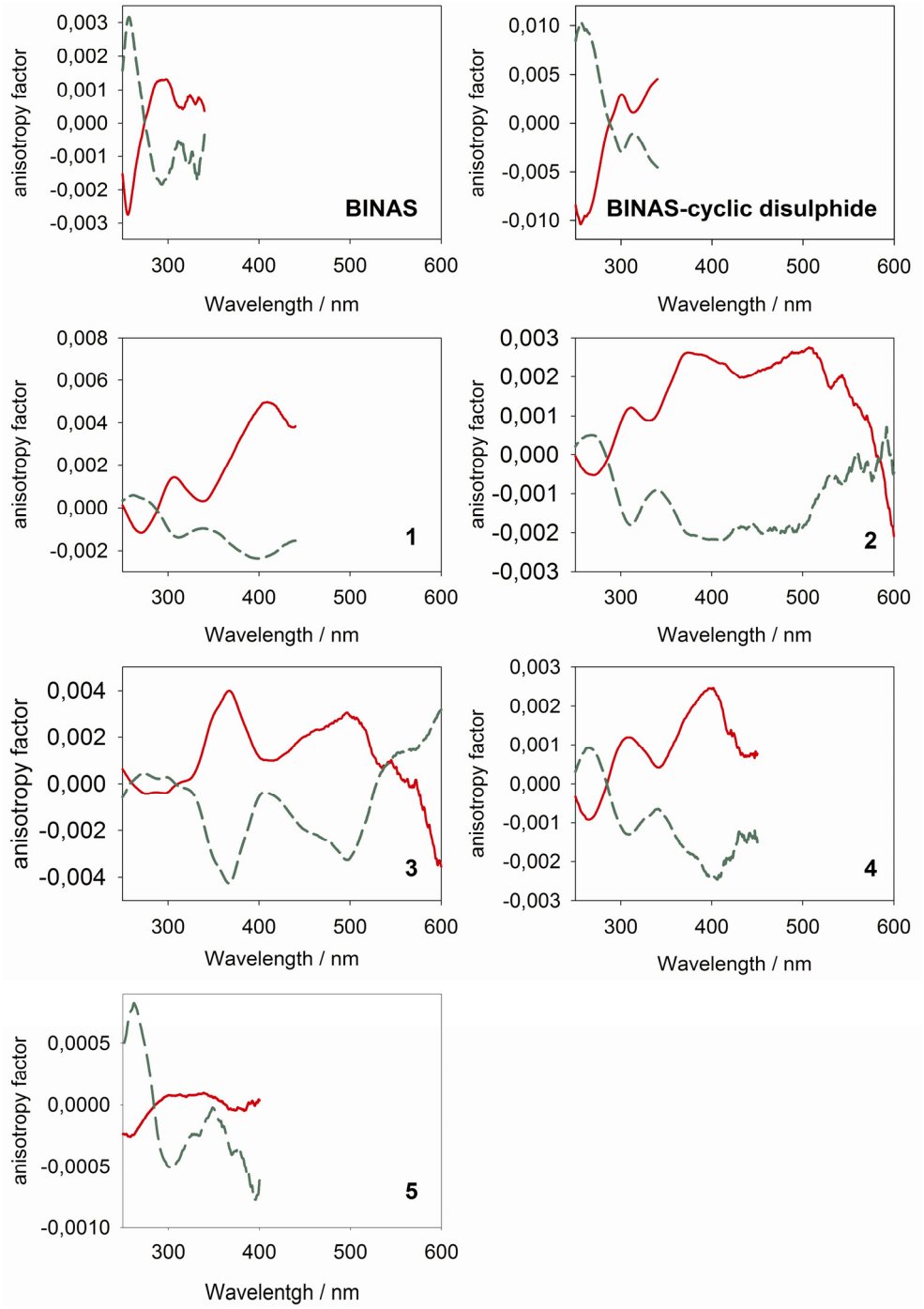

Figure 4.6 : Anisotropy factor of fractions **1-5** of BINAS gold nanoparticles, BINAS and BINAS-cyclic disulphide. Dashed (solid) spectra are for the (*S*)-enantiomer ((*R*)-enantiomer). The anisotropy factor of fractions **1** and **5** is not symmetric for the two enantiomers because these fractions contain mixtures of different particles.

4.5 Conclusion

In conclusion, we report the preparation of small gold particles passivated by BINAS. The as prepared and purified particles could be separated into several distinct fractions using size-exclusion chromatography. The different fractions exhibit different color, absorption and ECD spectra. The absorption and ECD spectra of one fraction bears some resemblance with the spectra previously reported for Au_{11} particles stabilized by BINAP although the spectra are shifted to shorter wavelength in the case of the thiol. The anisotropy factors are as large as 4×10^{-3}, which is the largest reported so far for gold particles covered by chiral thiols. This indicates that BINAS is particularly well-suited to bestow chirality onto gold particles. The results show that the optical activity is enhanced by using a stronger gold – ligand bond. This is in good agreement with a model that imputes the optical activity to an adsorbate-induced local deformation of the metal core, *i.e.* the formation of a "chiral-footprint".

4.6 References

[1] M. C. Daniel, D. Astruc, *Chem Rev* **2004**, *104*, 293.

[2] G. C. Bond, *Catalysis Today* **2002**, *72*, 5.

[3] J. J. Storhoff, R. Elghanian, R. C. Mucic, C. A. Mirkin, R. L. Letsinger, *J Am Chem Soc* **1998**, *120*, 1959.

[4] J. L. West, N. J. Halas, *Ann Rev Biomed Eng* **2003**, *5*, 285.

[5] V. P. Zharov, R. R. Letfullin, E. N. Galitovskaya, *J Phys D: Appl Phys* **2005**, *38*, 2571.

[6] S. Sun, C. B. Murray, D. Weller, L. Folks, A. Moser, *Science* **2000**, *287*, 1989.

[7] W. L. Barnes, A. Dereux, T. W. Ebbesen, *Nature* **2003**, *424*, 824.

[8] T. G. Schaaff, M. N. Shafigullin, J. T. Khoury, I. Vezmar, R. L. Whetten, W. G. Cullen, P. N. First, C. GutierrezWing, J. Ascensio, M. J. JoseYacaman, *J Phys Chem B* **1997**, *101*, 7885.

[9] S. W. Chen, R. S. Ingram, M. J. Hostetler, J. J. Pietron, R. W. Murray, T. G. Schaaff, J. T. Khoury, M. M. Alvarez, R. L. Whetten, *Science* **1998**, *280*, 2098.

[10] C. Gautier, T. Bürgi, *Chem Commun* **2005**, 5393.

[11] C. Gautier, T. Bürgi, *J Am Chem Soc* **2006**, *128*, 11079.

[12] M. Bieri, T. Bürgi, *J Phys Chem B* **2005**, *109*, 22476.

[13] T. G. Schaaff, G. Knight, M. N. Shafigullin, R. F. Borkman, R. L. Whetten, *J Phys Chem B* **1998**, *102*, 10643.

[14] T. G. Schaaff, R. L. Whetten, *J Phys Chem B* **2000**, *104*, 2630.

[15] H. Yao, K. Miki, N. Nishida, A. Sasaki, K. Kimura, *J Am Chem Soc* **2005**, *127*, 15536.

[16] M. Tamura, H. Fujihara, *J Am Chem Soc* **2003**, *125*, 15742.

[17] Y. Yanagimoto, Y. Negishi, H. Fujihara, T. Tsukuda, *J Phys Chem B* **2006**, *110*, 11611.

[18] T. H. Li, H. G. Park, H. S. Lee, S. H. Choi, *Nanotechnology* **2004**, *15*, S660.

[19] G. Shemer, O. Krichevski, G. Markovich, T. Molotsky, I. Lubitz, A. B. Kotlyar, *J Am Chem Soc* **2006**, *128*, 11006.

[20] I. L. Garzón, J. A. Reyes-Nava, J. I. Rodríguez-Hernández, I. Sigal, M. R. Beltrán, K. Michaelian, *Phys. Rev. B* **2002**, *66*, 073403.

[21] M. R. Goldsmith, C. B. George, G. Zuber, R. Naaman, D. H. Waldeck, P. Wipf, D. N. Beratan, *Phys Chem Chem Phys* **2006**, *8*, 63.

[22] A. S. K. Hashmi, G. J. Hutchings, *Angew Chem Int Ed* **2006**, *45*, 7896.

[23] D. Fabbri, G. Delogu, O. De Lucchi, *J Org Chem* **1993**, *58*, 1748.

[24] M. Brust, M. Walker, D. Bethell, D. J. Schiffrin, R. Whyman, *J Chem Soc, Chem Commun* **1994**, 801.

[25] Y. Negishi, K. Nobusada, T. Tsukuda, *J Am Chem Soc* **2005**, *127*, 5261.

[26] R. L. Donkers, D. Lee, R. W. Murray, *Langmuir* **2004**, *20*, 1945.

[27] M. J. Hostetler, J. E. Wingate, C. J. Zhong, J. E. Harris, R. W. Vachet, M. R. Clark, J. D. Londono, S. J. Green, J. J. Stokes, G. D. Wignall, G. L. Glish, M. D. Porter, N. D. Evans, R. W. Murray, *Langmuir* **1998**, *14*, 17.

[28] A. Badia, W. Gao, S. Singh, L. Demers, L. Cuccia, L. Reven, *Langmuir* **1996**, *12*, 1262.

[29] A. Badia, R. B. Lennox, L. Reven, *Acc Chem Res* **2000**, *33*, 475.

[30] Y. Song, A. S. Harper, R. W. Murray, *Langmuir* **2005**, *21*, 5492.

[31] R. C. Price, R. L. Whetten, *J Am Chem Soc* **2005**, *127*, 13750.

[32] V. G. Albano, P. L. Bellon, Manassero M., M. Sansoni, *J Chem Soc, Chem Commun* **1970**, 1210.

[33] W. Bos, R. P. F. Kanters, C. J. Vanhalen, W. P. Bosman, H. Behm, J. M. M. Smits, P. T. Beurskens, J. J. Bour, L. H. Pignolet, *J Organomet Chem* **1986**, *307*, 385.

[34] H. Hakkinen, M. Walter, H. Gronbeck, *J Phys Chem B* **2006**, *110*, 9927.

[35] W. W. Weare, S. M. Reed, M. G. Warner, J. E. Hutchison, *J Am Chem Soc* **2000**, *122*, 12890.

[36] K. Nunokawa, S. Onaka, T. Yamaguchi, T. Ito, S. Watase, M. Nakamoto, *Bull Chem Soc Jpn* **2003**, *76*, 1601.

5

Vibrational Circular Dichroism of BINAS-Stabilized Gold Clusters

5.1 Introduction

Adsorption of molecules on surfaces is of fundamental importance for many processes comprising separation, (bio-)sensing, surface processing, lubrication and heterogeneous catalysis. The conformation of the molecules at the surface can have a pronounced effect on surface properties. However, such information is rather difficult to obtain. A special class of surfaces results from modification by chiral molecules. The resulting chirally modified surfaces have potential for applications in enantioselective separation, detection of enantiomers and heterogeneous enantioselective catalysis.[1, 2] The latter effects strongly rely on intermolecular interactions, which depend on the conformation of the adsorbed molecule.

A powerful method for obtaining conformational information is vibrational circular dichroism (VCD), *i.e.* the differential absorption of left- and right-circularly polarized light by

a chiral sample.[3] VCD is more sensitive to conformation than conventional infrared absorption spectroscopy. In order to extract that structural information the experimental VCD spectrum has to be compared with theoretical spectra calculated for different conformers. Density functional theory (DFT) calculations have predictive character for VCD spectra of organic molecules.[4] An experimental challenge of VCD spectroscopy is the relatively small signals. The anisotropy factors $\Delta A/A = \Delta\varepsilon/\varepsilon$ are typically on the order of 10^{-4} to 10^{-6}. As a consequence measurements on flat surfaces are very challenging, since monolayers give typically rise to absorbance signals of less than 10^{-2}. One way to overcome this obstacle is the use of a high specific surface area material, such as nanoparticles. The latter can be viewed as the nanometer-size analogues of extended flat surfaces. Indeed, we have shown recently that VCD spectra of molecules adsorbed on small metal particles can be measured.[5, 6]

We have prepared in the past gold nanoparticles covered by N-acetyl-cysteine[5] and N-isobutyryl-cysteine[6] and measured their VCD spectra in D_2O (Chapters 1 and 3). We have also calculated VCD spectra of these thiols adsorbed on small gold particles. As expected the calculated VCD spectra strongly depend on the conformation of the thiol and on the way the latter interacts with the gold particle. Comparison between experimental and calculated VCD spectra indicated an adsorption mode where both the N-acetyl-cysteine and N-isobutyryl-cysteine interacted via the thiolate and the carboxylate with the gold particle, in agreement with ATR-IR work and orientation measurements.[7]

The two reports mentioned above are so far the only ones on VCD of molecules adsorbed on metal nanoparticles, to the best of our knowledge. The results are promising, and the technique may become a versatile tool also in view of the fact that chemically modified metal nanoparticles are considered as building blocks in nanotechnology. Compared to VCD

of molecules additional aspects may play a role for VCD of molecules adsorbed on metal nanoparticles. For example, the nanoparticles have low-lying electronic states that might have an influence, similar to what was reported for metal complexes.[8] In addition, the electromagnetic field in the vicinity of a metal particle might be amplified. Also, the role of the structure of the metal particle on the VCD of the adsorbed molecule is unclear. Finally, calculations including metal particles are more difficult and it is not clear yet if the same quality of agreement between calculations and experiment can be obtained as for free organic molecules. Further examples need to be studied to clarify the importance of these effects.

The two systems investigated up to now are challenging for mainly two reasons and are therefore not ideal to learn more about intrinsic aspects of the technique. First of all N-acetyl-cysteine and N-isobutyryl-cysteine are quite flexible molecules with considerable conformational freedom. Therefore, several conformers might contribute to the experimental spectrum. Second, the particles that were studied up to now are soluble in water. It is very likely that water specifically interacts with N-acetyl-cysteine and N-isobutyryl-cysteine via hydrogen bonding and this will influence the VCD at least to a certain extent.[9] This should be included in the calculation of the VCD spectra.

Here we apply VCD spectroscopy to another system with much less conformational freedom and which is soluble in organic solvents, thus avoiding specific intermolecular interactions. This should allow us to shed some light on the potential and limitations of the approach. In particular, we have prepared small gold nanoparticles covered with (*R*)-1,1'-binaphthyl-2,2'-dithiol [(*R*)-BINAS] and (*S*)-1,1'-binaphthyl-2,2'-dithiol [(*S*)-BINAS] (see **Chart 4.1**), respectively, and the particles were separated into different sizes by size

exclusion chromatography (SEC).[10] Then the VCD spectra of the samples were measured and compared with calculated spectra for different models of gold clusters.

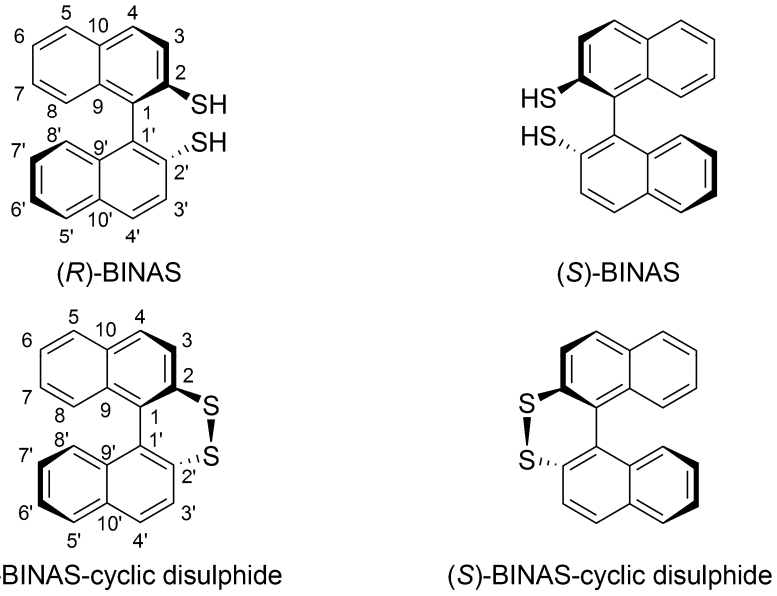

Chart 5.1 : Structure of (*R*)-BINAS, (*S*)-BINAS, (*R*)-BINAS-cyclic disulphide and (*S*)-BINAS-cyclic disulphide.

5.2 Materials and Methods

5.2.1 VCD and IR Spectroscopy

The preparation of enantiomerically pure (*R*)- and (*S*)-BINAS was reported elsewhere.[11] Deuterated chloroform (99.8%) and CD_2Cl_2 (99.9%) were received from Cambridge Isotope Laboratories.

IR and vibrational circular dichroism (VCD) spectra were recorded on a Bruker PMA 50 accessory coupled to a Tensor 27 Fourier transform infrared spectrometer. A photoelastic modulator (Hinds PEM 90) set at l/4 retardation was used to modulate the handedness of the

circular polarized light. Demodulation was performed by a lock-in amplifier (SR830 DSP). An optical low-pass filter (< 1800 cm^{-1}) in front of the photoelastic modulator was used to enhance the signal/noise ratio. All solutions of BINAS-stabilized gold particles (monolayer protected nanoparticles, MPNs) were prepared in CD_2Cl_2. Solutions of (*R*)- and (*S*)-BINAS MPNs, of the corresponding free dithiol and of the tetraoctylammonium bromide (TOAB) were prepared in CD_2Cl_2 with a concentration of 150 $mg.ml^{-1}$, 19 $mg.ml^{-1}$ and 15 $mg.ml^{-1}$, respectively, whereas (*R*)- and (*S*)-BINAS-cyclic disulphide were prepared in $CDCl_3$ at 25 $mg.ml^{-1}$. VCD reference spectra were recorded for racemic mixtures of the samples. Alternatively, the pure solvents served as references.

All spectra were recorded at 10 °C to avoid evaporation of the solvent with a resolution of 8 cm^{-1} (4 cm^{-1} for BINAS) in a cell equipped with CaF_2 windows and 100 μm, 500 μm and 1,000 μm Teflon spacers for the separated MPNs**,** BINAS and BINAS-cyclic disulphide, respectively. Both samples and references were measured for two hours in time slices of 30 minutes, corresponding to about 16'000 scans in total for sample and reference, respectively. The spectra are presented without smoothing or further data processing.

5.2.2 Computational Methods

Density functional theory (DFT) as implemented in Gaussian03 was used to study the structure of BINAS, BINAS-cyclic disulphide and BINAS adsorbed on gold particles and to calculate the corresponding IR and VCD spectra. For the gold atoms an effective core potential was used. The calculations were performed using the b3pw91[12, 13] functional and a LanL2DZ basis set[14] for Au and a 6-31G(d,p) basis set[15] for all other atoms. Prior to

the calculation of the spectra all degrees of freedom were completely relaxed unless otherwise stated. Vibrational frequencies were scaled by a factor of 0.965. IR and VCD spectra were constructed from calculated dipole and rotational strengths assuming Lorentzian band shape with a half-width at half-maximum of 5 cm^{-1}.

5.3 Results and Discussion

5.3.1 Separation and Characterization of Particles

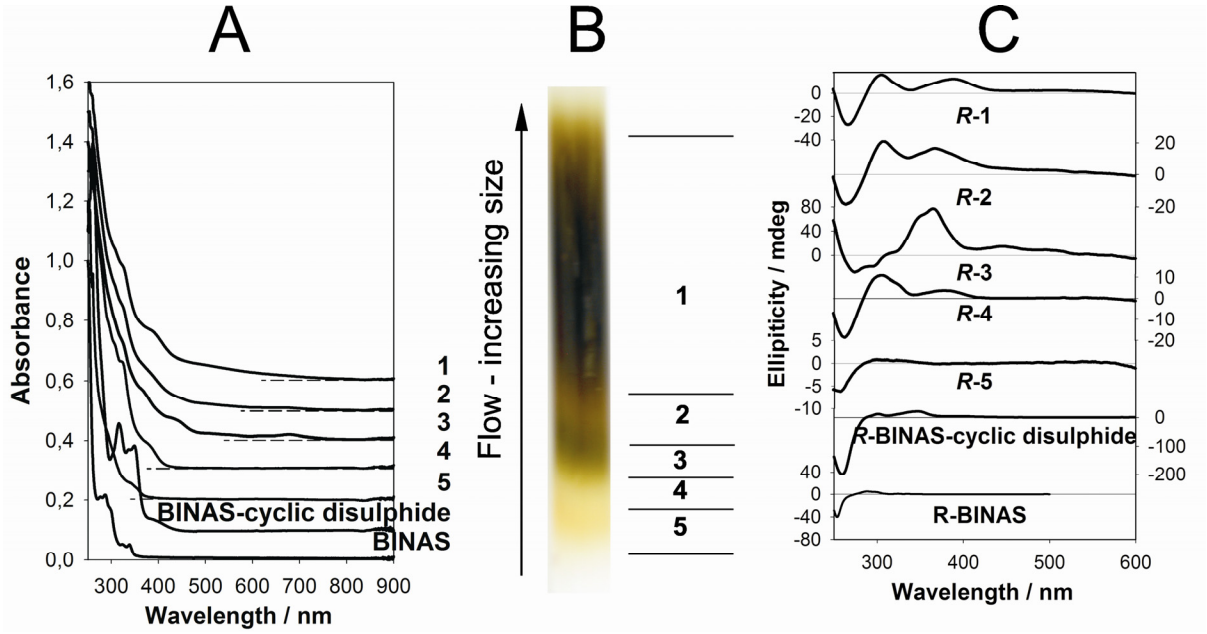

Figure 5.1 : (A) UV-vis spectra and (C) ECD spectra of the size-separated nanoparticles **1-5,** of (*R*)-BINAS and (*R*)-BINAS-cyclic disulphide. (B) Size exclusion chromatography separation of BINAS protected gold particles. The separated fractions are numbered from **1-5** according to their decreasing elution mobility. Horizontal lines show roughly the limit between adjacent fractions.

The as prepared BINAS-stabilized gold nanoparticles have an average size smaller than 2 nm as shown by the TEM,[10] which is consistent with the absence of a surface plasmon band at around 520 nm. Nuclear magnetic resonance (NMR) reveals no detectable free BINAS and BINAS-cyclic disulphide in solution. We have reported before[10] that these nanoparticles can be separated according to their size by SEC. **Figure 5.1** shows such a separation. In total five fractions with different color could be separated and were numbered **1-5** according to their elution order or their decreasing size. The observed color-dependence on particle size is a direct consequence of a quantum size effect. The latter is also responsible for the systematic red shift of the absorption onset for increasing particle size (from **5** to **1**). Fractions **1**, **3** and **5** are respectively brown, green and yellow. **Figure 5.1** also reveals that both the UV-vis and ECD spectra change significantly with the size of the particles. These spectra reflect the electronic structure of the particles, which strongly changes with their size in the size regime relevant here.

5.3.2 IR and VCD

5.3.2.1 BINAS and BINAS-cyclic disulphide

Before turning our attention to the spectra of the BINAS-stabilized gold particles the vibrational properties of the free ligand are presented. In particular BINAS but also the oxidized cyclic disulfide (BINAS-cyclic disulphide) form were studied. The latter is rigid, whereas the former has three conformational degrees of freedom, namely the two S-H groups and the angle between the naphthyl planes. There is only one minimum for this degree of freedom, whereas there are three possible combinations for the position of the two S-H groups

(see **Figure 5.2**, both in, both out, one in and one out). The S-H groups pointing inwards are slightly more stable than the ones pointing outwards, which might result from electrostatic interactions between these groups. The S-H groups are coplanar to the corresponding naphthyl groups. The angle between the naphthyl groups as measured by the torsion angle α comprising carbon atoms 2, 1, 1' and 2' (**Chart 4.1**) is in all cases very close to 90°. In contrast, for the cyclic disulphide form the angle α is only 46.3°. This angle is in good agreement with torsion angle of 50.04° measured in the solid state by X-ray diffraction (not shown).

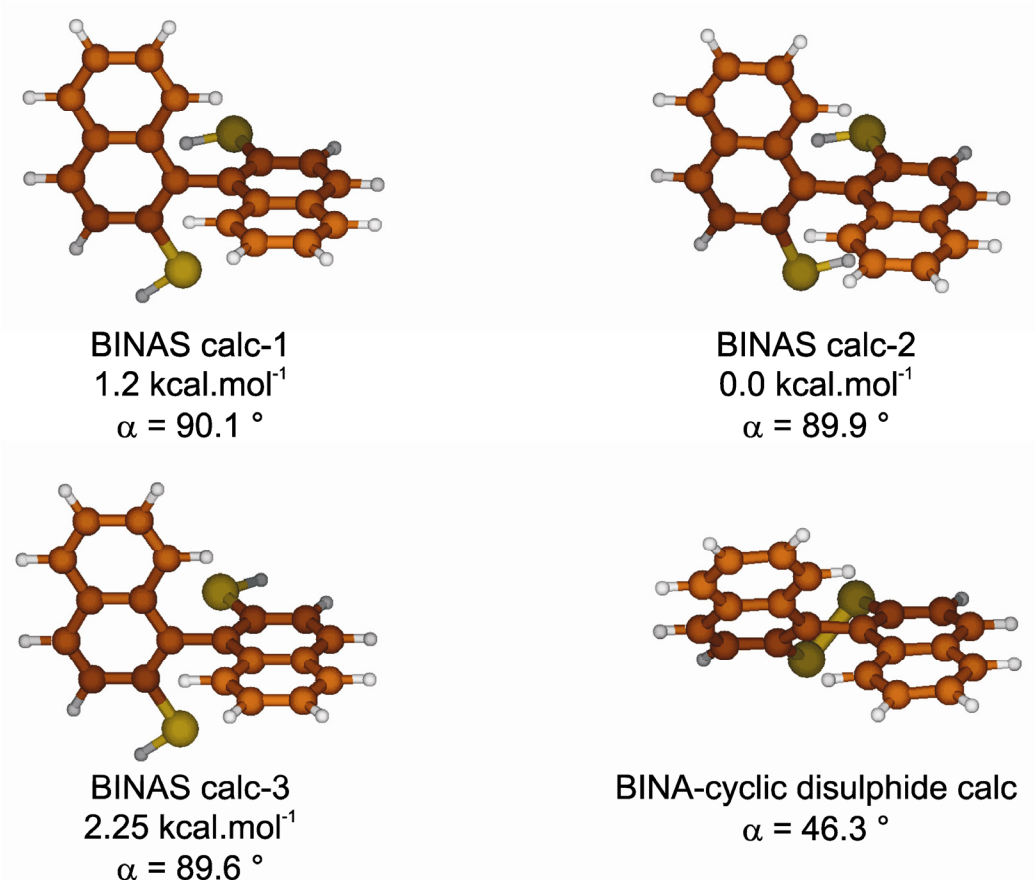

Figure 5.2 : Calculated conformers of BINAS and of BINAS-cyclic disulphide. For computational details see the experimental part.

For all the structures shown in **Figure 5.2** the IR and VCD spectra were calculated. For the three conformers of BINAS the VCD and IR spectra are very similar (not shown). In the following we therefore concentrate on the vibrational properties of the most stable conformer (BINAS calc-2) only. **Figure 5.3** and **Figure 5.4**, respectively, show the experimental and calculated IR and VCD spectra of BINAS and BINAS-cyclic disulphide, respectively. The spectra of the two forms are significantly different. Note that the quality of the BINAS-cyclic disulphide VCD spectra is not as good as the one for the dithiol due to the much lower solubility of the former.

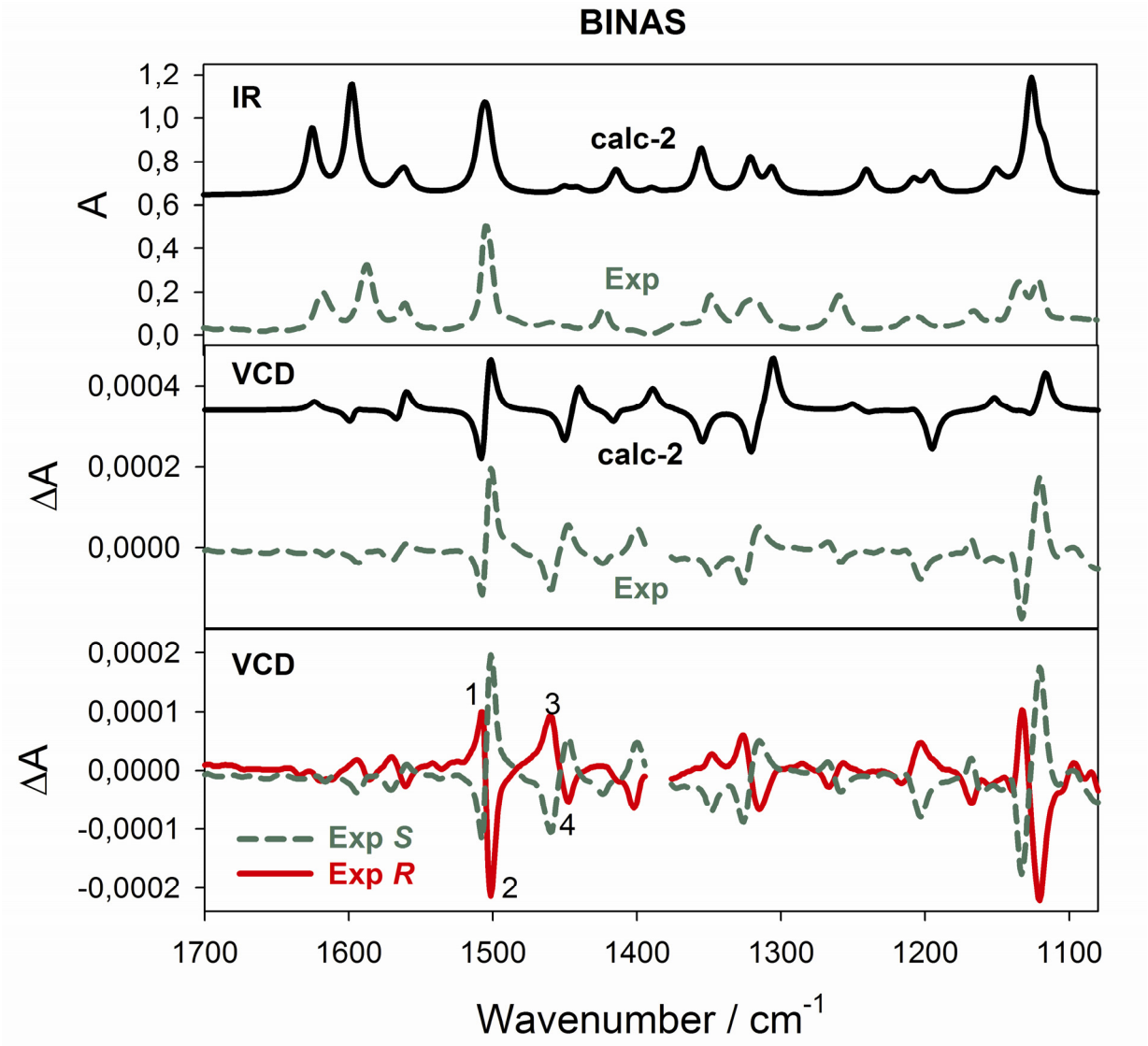

Figure 5.3 : Experimental and simulated IR and VCD spectra for BINAS. Calculated spectra for (*S*)-BINAS calc-2 are plotted in black, experimental spectra for (*R*)- and (*S*)-BINAS are plotted in red(solid line) and green (dashed line), respectively. In the experimental VCD spectra the small part below 1400 cm^{-1} is not accessible due to strong solvent absorption.

The VCD spectra of some 1,1'-binaphthyl derivatives have been reported before.[16] There are some bands associated with the binapthyl core that are characteristic, *e.g.* bands 1 – 4 (see **Figure 5.3**). The VCD spectrum of BINAS is dominated by pairs of bands with opposite sign. These patterns arise from the splitting of bands due to the C_2 symmetry and the

dipolar excitation coupling of the naphthyl chromophores. For example modes 1 and 2 are ring deformation modes localized around C_6, $C_{6'}$, C_7 and $C_{7'}$ of the binaphtyl part, whereas modes 3 and 4 are localized around C_2 and $C_{2'}$ and thus expected to be influenced by substitution at these positions. In general the agreement between experimental and calculated VCD and IR spectra for BINAS is excellent, except for the part at and below around 1200 cm^{-1}.

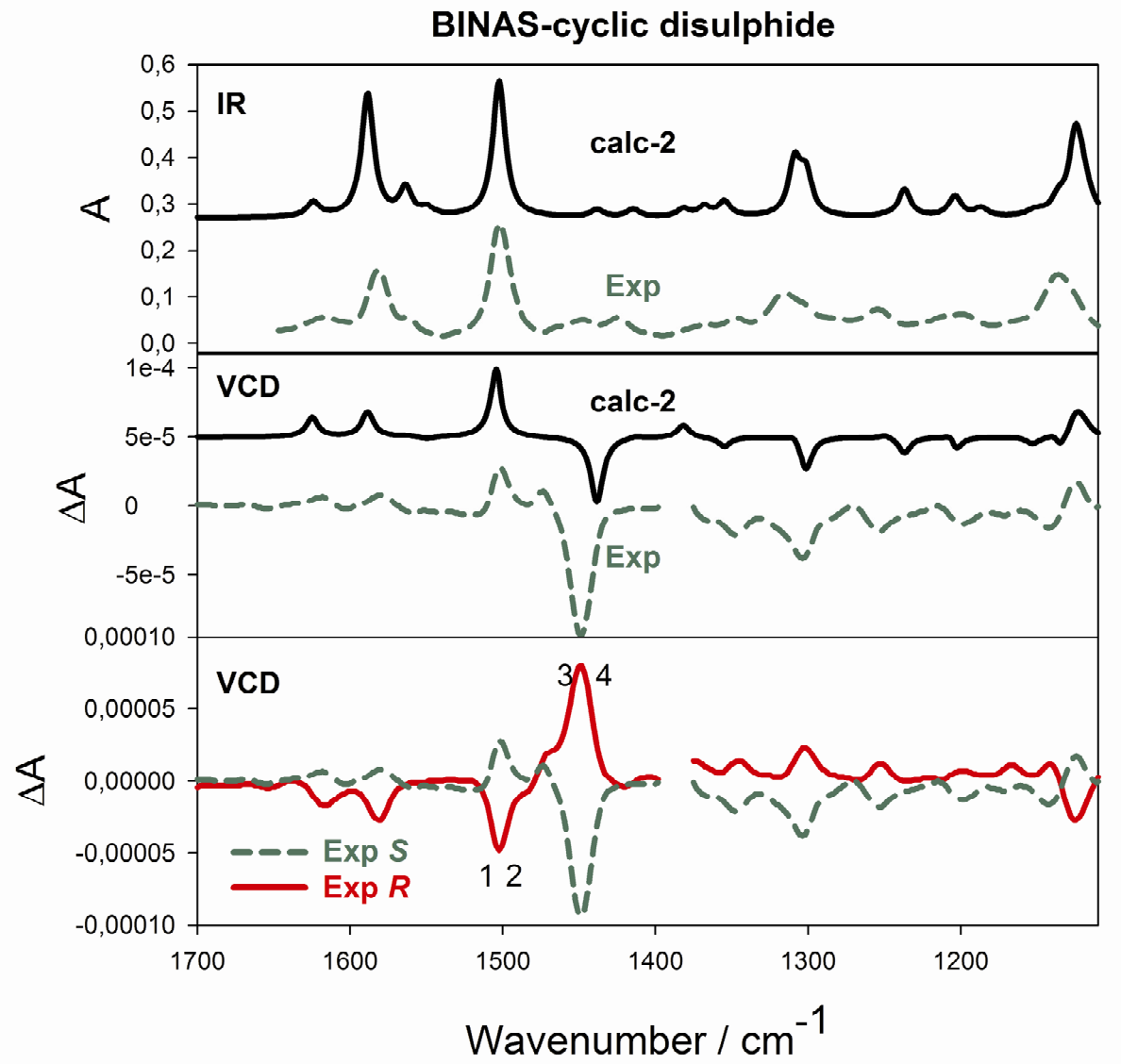

Figure 5.4 : Experimental and simulated IR and VCD spectra for BINAS-cyclic disulphide. Calculated spectra for BINAS-cyclic disulphide are plotted in black, experimental spectra for (*R*)- and (*S*)-BINAS-cyclic disulphide are plotted in red (solid line) and green (dashed line), respectively. In the experimental VCD spectra the small part below 1400 cm^{-1} is not accessible due to strong solvent absorption.

The potential energy surface of the angle α between the two naphthyl parts is quite shallow and calculations on parent 1,1'-binaphthol have shown that some of the modes in the VCD, including modes 1-4, are quite sensitive to that angle.[16] Fore example modes 1 and 2

at around 1500 cm^{-1} can turn from a (+/-) couplet at small angles (40°) to a (-/+) couplet at angles around 90° going through only one single band in between. Also modes 3 and 4 can merge into one strong band (negative for (*S*)-enantiomer) at small angles around 40°. Such behavior is for example observed for BINAS disulfure with a calculated angle of 46.3°. **Figure 5.4** shows that there is only one band in the VCD for modes 1 and 2 and one (strong) with opposite sign for modes 3 and 4. The calculated and experimental IR and VCD spectra are again in excellent agreement. Also the VCD spectrum above about 1400 cm^{-1} strongly resembles the one reported for the one of 1,1'-binaphthyl-2,2'-diyl-hydrogenphosphate.[16] In the latter the angle between the naphthyl planes is fixed by the phosphate bridge at around 55°. In general, the VCD spectra of the dithiol and the disulphide are distinctly different from each other, particularly also for the characteristic modes 1-4.

5.3.3 Conformational study of BINAS adsorbed on NPs

5.3.3.1 IR Spectroscopy

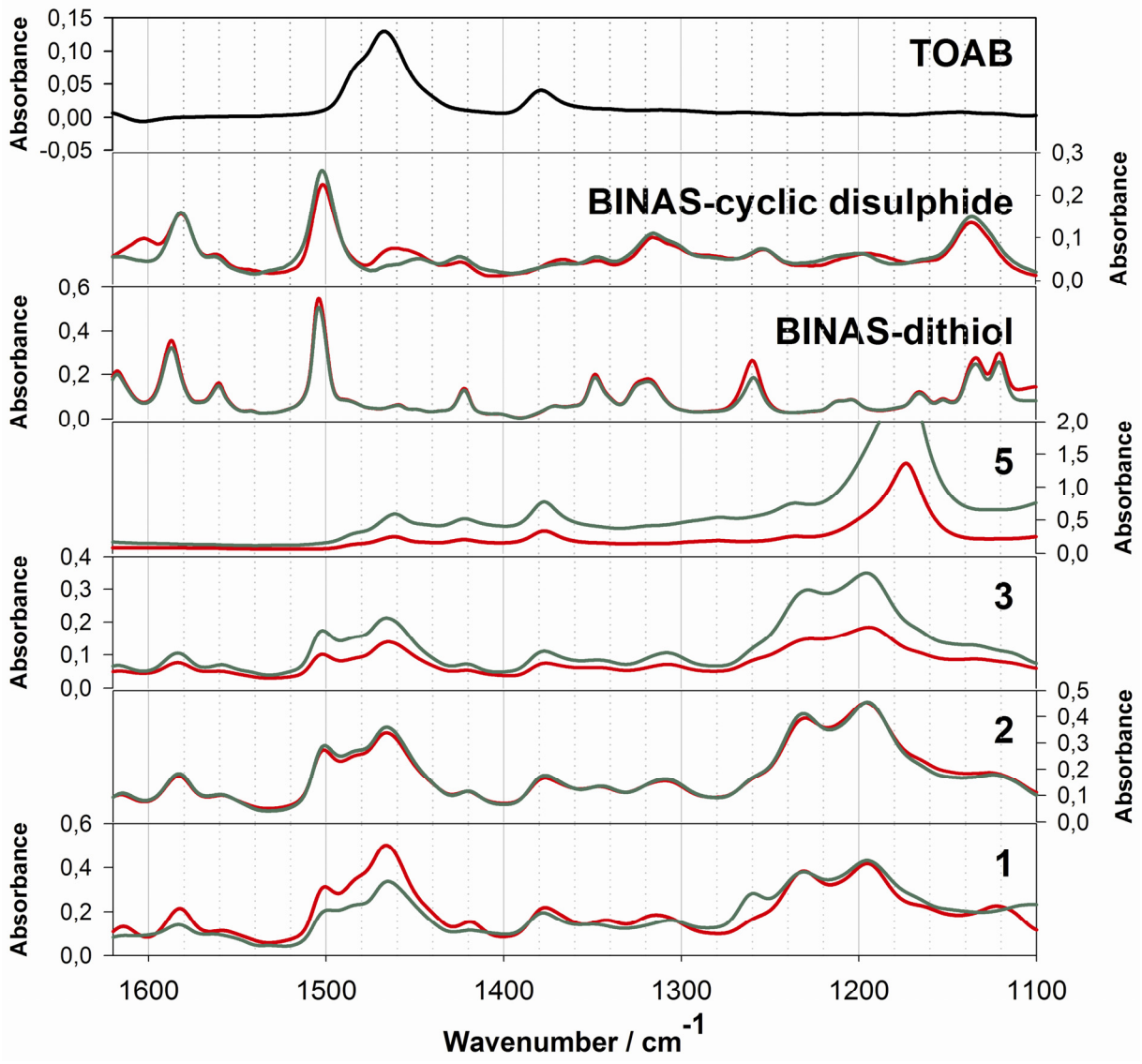

Figure 5.5 : Infrared spectra of separated fractions **1-3** and **5**, of BINAS, BINAS-cyclic disulphide and TOAB in CD_2Cl_2 ($CDCl_3$ for BINAS-cyclic disulphide). Red curves and green curves correspond to the (*R*)- and (*S*)-enantiomers of the chiral compounds, respectively.

Figure 5.5 shows that the IR spectra of the separated fractions **1-3** covered either by the (*R*)- or the (*S*)-BINAS are very similar whereas fraction **5** is drastically different. This may be explained by the fact that fraction **5** corresponds to the smaller nanoparticles and can be polluted by organic residues or Au-thiolate oligomers. The IR spectra of the fractions **1-3** show clearly a superposition of the IR signals of BINAS and TOAB. This result is in good agreement with the ^{1}H NMR spectrum of the crude nanoparticles (Chapter 5).[10] TOAB is used during the synthesis of the particles as a phase transfer agent[17] and is removable neither by SEC nor by precipitation. TOAB is strongly attached to the particles trough charge compensation of the negative gold particles.[18] At this stage, a contribution of the BINAS-cyclic disulphide in the IR signal can not be excluded due to the similarity of the IR spectra of both dithiol and disulphide. Surprisingly, the IR spectra of the nanoparticles reveal a strong and broad signal at around 1200 cm^{-1} which can be attributed neither to the TOAB nor to the two BINAS forms (dithiol and disulfide). This signal can be explained by the presence of sulfonate species formed via oxidation of disulphide upon exposure to air in presence of halide ions.[19] However, such species have not been evidenced by NMR and might be effectively removed by SEC. Another origin can be a modification of the C-S dipolar moment upon adsorption of the BINAS on gold.

5.3.3.2 VCD Spectroscopy

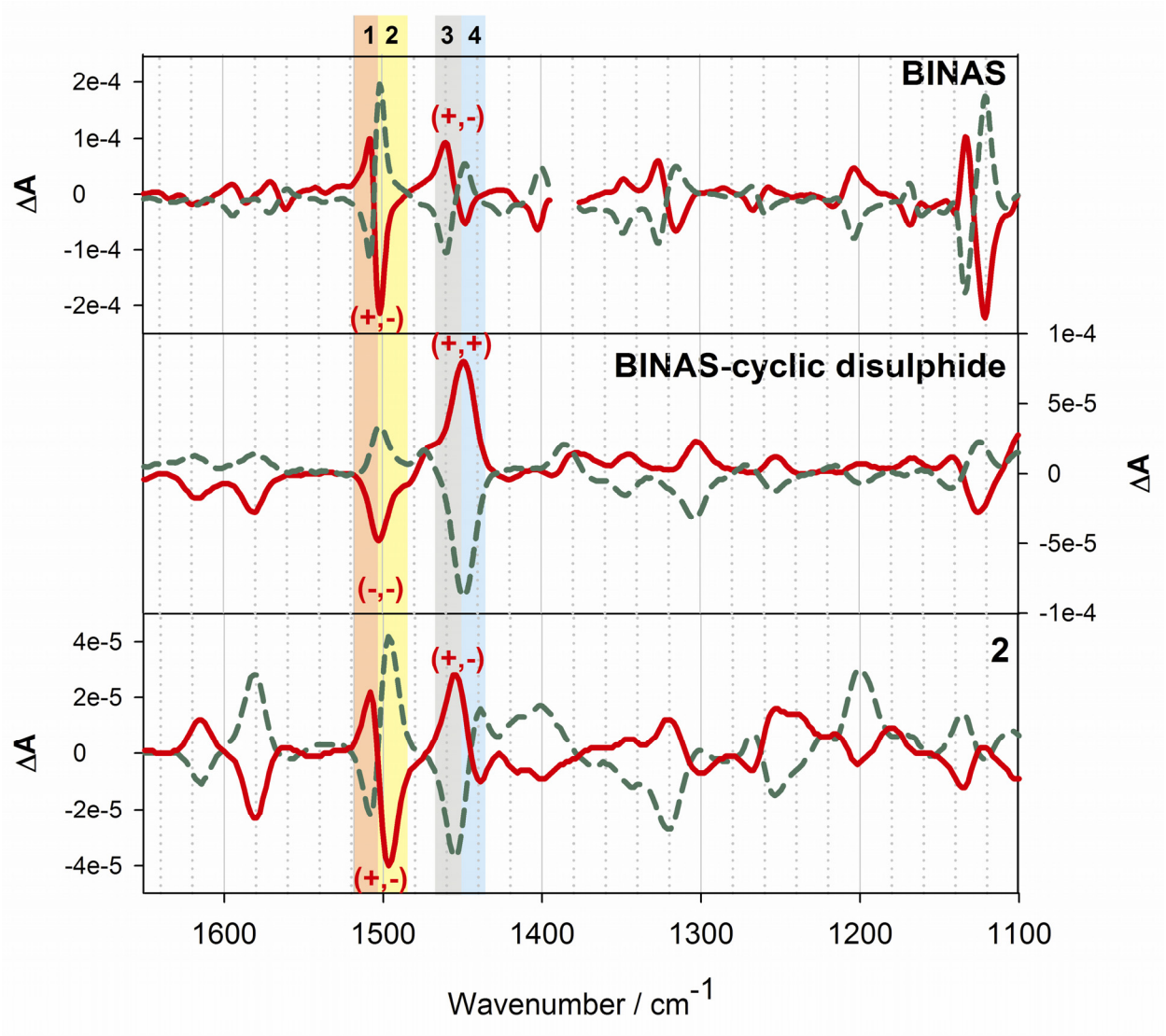

Figure 5.6 : VCD spectra of the fraction **2** of the size separated nanoparticles protected with the (*R*)- and (*S*)-BINAS, of the free (*R*)- and (*S*)-BINAS and of the (*R*)- and (*S*)-BINAS-cyclic disulphide. The spectra of the (*R*)- and (*S*)-enantiomers are plotted in red (solid line) and green (dashed line), respectively.

The VCD spectra of the two enantiomers of BINAS-cyclic disulphide, of BINAS and of the BINAS adsorbed on gold nanoparticles **2** show good mirror image relationships and

good signal-to-noise ratios as shown in **Figure 5.6**. On the one hand, the modes 1-2 and 3-4 of fraction **2** and of BINAS are very similar and form two (+/-) couplets whereas the modes 1 and 2 merge in one strong negative band and 3 and 4 merge in one strong positive band for (*R*)-BINAS-cyclic disulphide as discussed before. In the case of the particles **2**, the relative intensity of the mode 3 with respect to mode 1 is slightly higher than for the BINAS. This can be attributed to a slight reduction of the torsion angle of the BINAS upon adsorption[16] but also only to the contribution of the gold in this mode since this mode is mainly located close to the C_2 and $C_{2'}$ atoms which are directly bonded to the thiol groups. Extension of the discussion above of bands 1-4 for parent 1,1'-binaphthol to BINAS adsorbed on gold nanoparticles, indicates a torsion angle close to 90°. On the other hand, the rest of the spectra are largely different for the three compounds in term of sign and intensity. This clearly shows that the optical activity does not arise from free BINAS but also that the conformation of the adsorbed BINAS needs to be investigated by DFT calculations (*vide infra*).

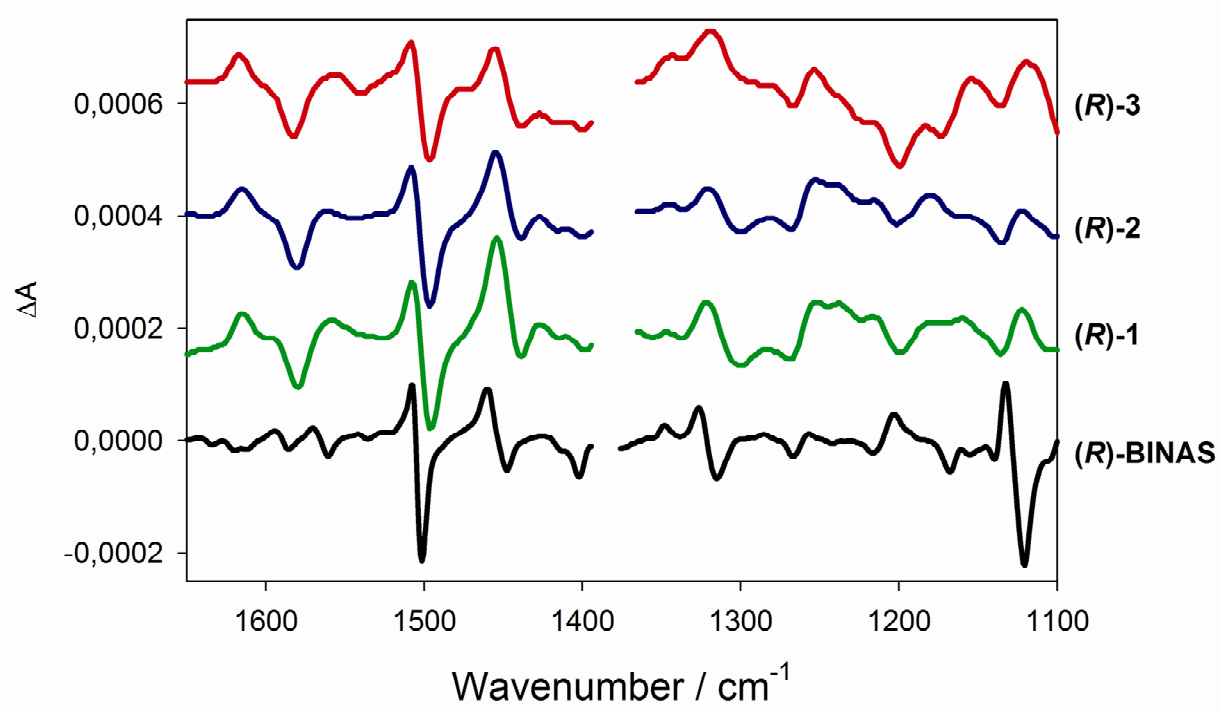

Figure 5.7 : VCD spectra of the size-separated nanoparticles protected with (*R*)-BINAS **1-3**.

Figure 5.7 shows the VCD spectra of the size separated nanoparticles **1-3** covered with the (*R*)-BINAS and of the free (*R*)-BINAS for comparison. Whereas the size of the particle has strong effects on UV-vis and even more on ECD spectra (see **Figure 5.1**), the size has less effects on IR and VCD spectra. Indeed, the different sizes of particles display very similar VCD spectra. The small differences for fraction **3** are rather attributed to the lower quality of the spectra due to the smaller quantity of particles available than to a different conformation of the absorbed BINAS. This result demonstrates that the conformation of the adsorbed dithiol is not drastically modified by the size of the particle even in the subnanometer range. This is even more surprising because at these scales, one could thinks that size modifications of a few atoms would drastically change the structure of the particle surface and thus the conformation of the adsorbate.

5.3.3.3 DFT Calculations

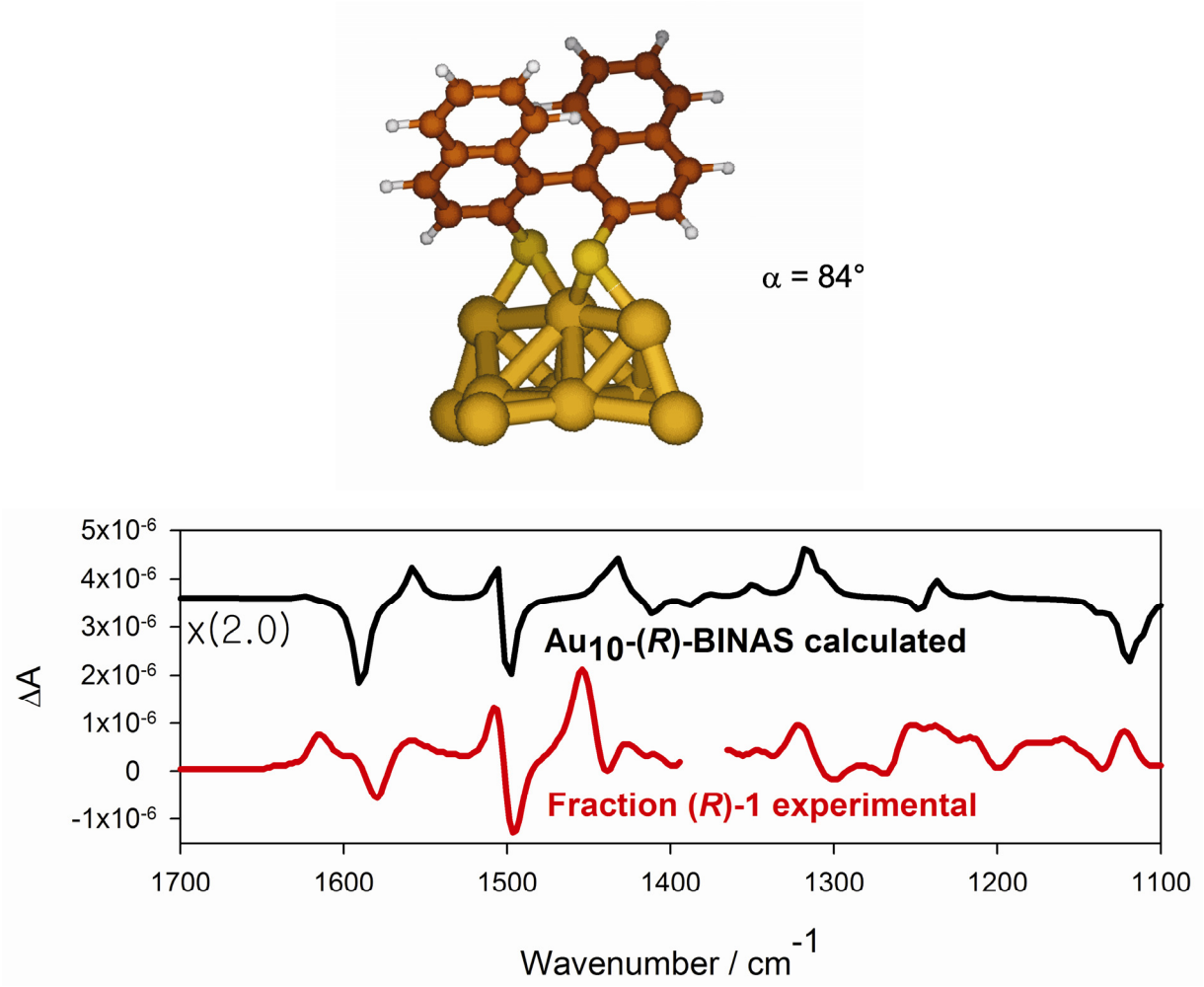

Figure 5.8 : Calculated conformer of (*R*)-BINAS adsorbed on a Au_{10} cluster. The structure was optimized using Gaussian03.[20] Simulated VCD spectrum of the calculated conformer of adsorbed (*R*)-BINAS (black) and measured VCD spectrum for the fraction (*R*)-**1** (red).

We have chosen a Au_{10} cluster to study the conformation of adsorbed BINAS. **Figure 5.8** shows a calculated low energy conformer of the (*R*)-BINAS adsorbed on the latter cluster. In this conformation, (*R*)-BINAS is adsorbed through the two thiolates. Each thiolate is attached to two gold atoms in a bridge site and one of these two gold atoms is shared between

the two thiolates of the BINAS. This adsorption motif, one thiolate adsorbed between two gold atoms with one of the two gold atoms linked to a second thiolate, is very similar to the adsorption motif of *p*-mercaptobenzoic acid on a 102 gold atoms nanoparticles which has been determined by Jadzinsky *et al.* by X-ray diffraction.[21] However, in our calculated conformation the gold atom attached to the two thiolates is not detached from the surface and the S-Au-S motif is not linear as described by Jadzinsky. The torsion angle between the two naphtyl groups is 84° in our calculated conformation. This angle is relatively close to the torsion angle determined for the free BINAS in solution (*vide supra*). The simulated spectra for the calculated conformation is in good agreement with the experimental spectrum especially between 1600 and 1400 cm^{-1} (see **Figure 5.8**). Indeed, both simulated and experimental spectra, show (+,-) couplets for band 1-2 and 3-4. As discussed before, these signals are strongly dependant on the torsion angle of binaphtyl compounds and characteristic of an angle close to 90° in this case. This reveals that BINAS is not adsorbed in its oxidized (disulfide) form. The strong correlation between the torsion angle determined by DFT calculations and by the qualitative experimental observations of VCD spectra on very similar compounds shows the sensitivity of the DFT-VCD approach for the determination of the conformation of adsorbed molecules on nanoparticles. However, the two regions above 1600 cm^{-1} and below 1300 cm^{-1} are rather different in experimental and simulated spectra. These regions may be dominated by the vibrations localized outside of the biphenyl rings.

5.4 Conclusion

Both qualitative interpretation based on knowledge of the VCD spectra of binaphtyl compounds and the DFT-VCD approach conclude to a torsion angle close to 90° for BINAS adsorbed on gold clusters. This correlation emphasizes the validity and the sensitivity of the latter approach for the conformational study of absorbates on nanoparticles. The comparison between experimental and calculated spectra shows that BINAS is not adsorbed in its disulphide form. The VCD spectra of the size separated fractions are very similar. This demonstrates that the conformation of the adsorbed BINAS is not dependent on the size of the nanoparticles. However, a better simulation of the structure of the underlaying metal atoms may greatly enhance the correlation between the simulated and the experimental spectra and help to a better understanding of the surface reconstruction upon adsorption of organic molecules.

5.5 References

[1] Y. Izumi, *Adv. catal.* **1983**, *32*, 215.

[2] Y. Orito, S. Imai, S. Niwa, *J. Chem. Soc. Japan* **1979**, 1118.

[3] L. A. Nafie, T. A. Keiderling, P. J. Stephens, *J. Am. Chem. Soc.* **1976**, *98*, 2715.

[4] L. A. Nafie, *Annu. Rev. Phys. Chem.* **1997**, *48*, 357.

[5] C. Gautier, T. Bürgi, *Chem. Commun.* **2005**, *43*, 5393.

[6] C. Gautier, T. Bürgi, *J. Am. Chem. Soc.* **2006**, *128*, 11079.

[7] M. Bieri, T. Bürgi, *J. Phys. Chem. B* **2005**, *109*, 22476.

[8] L. A. Nafie, *J. Phys. chem. A* **2004**, *108*, 7222.

[9] K. J. Jalkanen, I. M. Degtyarenko, R. M. Nieminen, X. Cao, L. A. Nafie, F. Zhu, L. D. Barron, *Theor. Chem. Account* **2008**, *119*, 191.

[10] C. Gautier, R. Taras, S. Gladiali, T. Bürgi, *Chirality* **2007**, *20*, 486.

[11] D. Fabbri, G. Delogu, O. De Lucchi, *J Org Chem* **1993**, *58*, 1748.

[12] A. D. Becke, *J. Chem. Phys.* **1993**, *98*, 5648.

[13] J. P. Perdew, J. A. Chevary, S. H. Vosko, K. A. Jackson, M. R. Pederson, D. J. Singh, C. Fiolhais, *Phys. Rev. B* **1992**, *46*, 6671.

[14] P. J. Hay, W. R. Wadt, *J. Chem. Phys.* **1985**, *82*, 270.

[15] R. Ditchfield, W. J. Hehre, J. A. Pople, *J. Chem. Phys.* **1971**, *54*, 724.

[16] V. Setnicka, M. Urbanova, P. Bour, V. Kral, K. Volka, *J Phys Chem A* **2001**, *105*, 8931.

[17] M. Brust, M. Walker, D. Bethell, D. J. Schiffrin, R. Whyman, *J. Chem. Soc., Chem. Commun.* **1994**, 801.

[18] R. C. Price, R. L. Whetten, *J. Am. Chem. Soc.* **2005**, *127*, 13750.

[19] M. Dasog, R. W. J. Scott, *Langmuir* **2007**, *23*, 3381.

[20] M. J. Frisch, *et al.* , Rev. C.01 ed., Gaussian, Inc., Wallingford CT, **2003**.

[21] P. D. Jadzinsky, G. Calero, C. J. Ackerson, D. A. Bushnell, R. D. Kornberg, *Science* **2007**, *318*, 430.

6

Chiral Inversion of Gold NPs

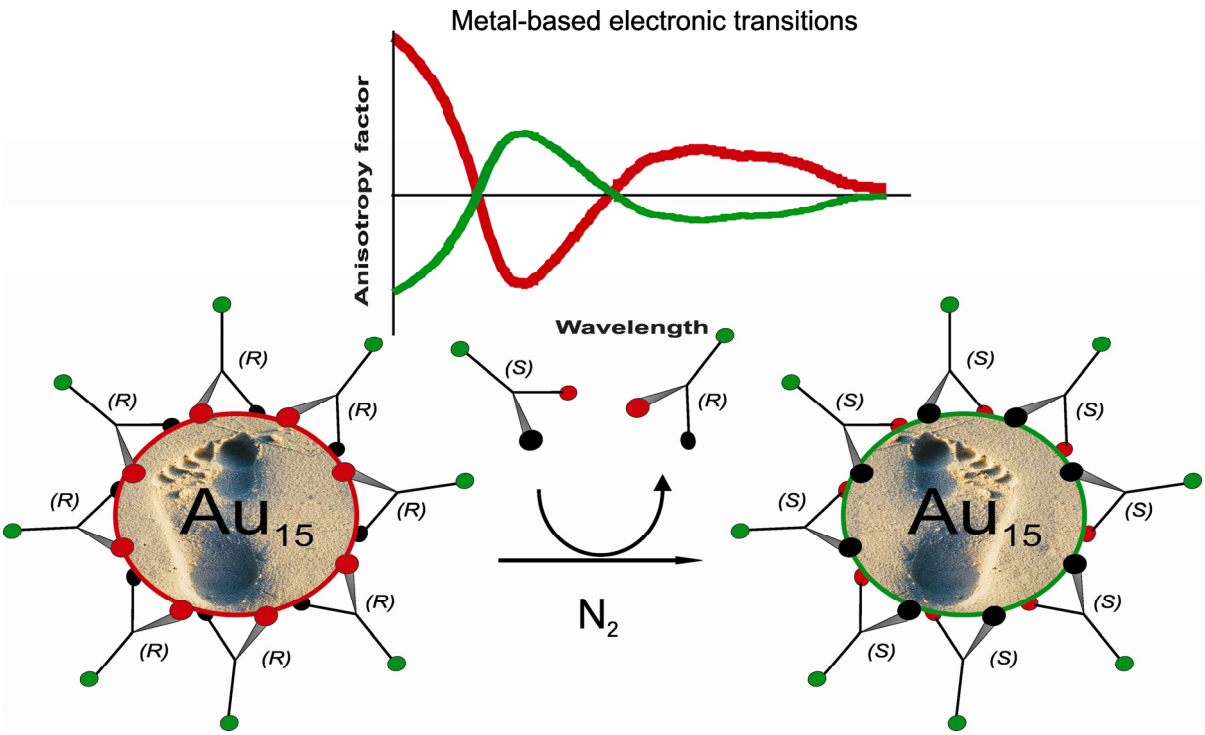

6.1 Abstract

The thiolate-for-thiolate ligand exchange was performed on well-defined gold nanoparticles under inert atmosphere without any modification of the core-size. This reaction is faster than the well known core-etching. Surprisingly, if a chiral thiol is exchanged for its opposite enantiomer, the optical activity in the metal-based electronic transitions is reversed although the form of the ECD spectra remains largely unchanged. The extent of inversion corresponds to the overall ee of the chiral ligand in the system. This shows that the chiral arrangement of metal atoms in the metal particle (surface) can not withstand the driving force imposed by the ligand of opposite absolute configuration. If the incoming thiol has a different structure, the electronic transitions in the metal core are slightly modified whereas the absorption onset remains unchanged. These results emphasized the influence of the thiols on the structure of the gold nanoparticles and give insight on the ligand exchange pathways.

6.2 Introduction

Chirality of extended metal surfaces and of their nanometer size analogues, metallic nanoparticles (NPs), has become an emerging field of research in recent years triggered by potential applications in heterogeneous enantioselective catalysis,[1, 2] enantiodiscrimination,[3] enantioseparation, enantioselective crystallization,[4, 5] liquid crystal displays,[6] and nonlinear optic. On the one hand, bare high Miller index metal surfaces such as Ag(643) are naturally and intrinsically chiral. The chirality of these surfaces is associated with kinked steps. Similarly, density functional theory (DFT) calculations have shown that small naked metallic NPs can also be intrinsically chiral.[7-9] On the other hand,

the adsorption of a chiral or even a achiral/prochiral molecule (the modifier) on a surface can break reflection symmetry of both the molecule and the surface and thus strengthens asymmetry of a chiral surface or imparts chirality onto an achiral surface. This phenomenon is the first basic manifestation of chirality at surfaces. One modifier can have different ionic forms and conformations,[10] which can lead to different expressions of local chirality. The different chiral motifs can furthermore self-assemble at the nano- or at the micro-scale in a single phase or in a cascade of chiral or achiral phases. The adsorption of an achiral/prochiral compound can lead to a racemic mixture of domains with opposite chirality,[11-13] whereas the adsorption of a chiral compound can create a local handedness, which is sustained over the entire surface.[14, 15] Of course, this global organization is dictated by a balance of molecule – molecule interactions such as hydrogen bonds, π stacking, van der Waals forces, charge-transfer and dipole-dipole interactions and molecule – metal interactions such as thiol –, amine –, carboxylate – and phosphine – metal interactions. In addition, the adsorption of a modifier can distort the structure of extended metal surfaces.[11, 15] For example, the adsorption of (*R*, *R*)-tartaric acid on Ni(110) goes along with a local relaxation of the metal surface atoms.[15] This chiral stress imparted on the surface upon adsorption of a molecule is known as chiral footprint. Chirality transfer through metal interactions represents a key parameter for the propagation of the local chirality to the macroscale, as has been proposed for the chiral organization of (*R,R*)-bitartrate molecules in long chains on the Cu(110) surface.[14]

Gold NPs in the nanometer-size range covered by enantiopure chiral thiols or phosphines such as *L*-glutathione (GSH),[16-19] and the two enantiomers of penicillamine,[20] N-isobutyryl-cysteine (NIC),[21] 2,2’-bis(diphenylphosphino)-1,1’-

biphenyl (BINAP)[22, 23] and 1,1'-binaphthyl-2,2'-dithiol (BINAS)[24] exhibit optical activity in metal-based electronic transitions (MBETs), which shows that the electronic structure of the gold particle is chiral. The findings reported so far for optically active NPs can be summarized as follows: Optical activity differs with the size of the NPs and generally decreases as the size is increasing. As for classical chiral molecules, the electronic circular dichroism (ECD) spectra of NPs display a mirror image relationship when covered with the two opposite enantiomers and no optical activity is observed when a racemique mixture of ligand is used. A common feature of the modifiers inducing ECD signals reported up to now is that they contain several functional groups able to coordinate to the gold particle.[21, 25]

Interestingly, calculations have shown that the optical activity in the MBETs can arise from an intrinsically chiral gold core[8, 9] as well as from an achiral one if the latter is placed in a chiral environment. The latter possibility includes the chiral arrangement of the ligands and the influence of the stereocenter of the chiral ligands (through space or through bonds) on the electronic structure of the metal. For example, it has been demonstrated recently by using a dissymmetrically-perturbed particle-in-a-box model that ECD signals can arise from chiral adsorbates on symmetric particles.[26] These two different origins of optical activity can act concurrently but their own contribution remained to be determined. Very recently an intermediate model corresponding to the local chiral distortion of the surface atoms involved in the adsorption of the ligand (similar to a chiral footprint) was evidenced for NPs composed of 102 gold atoms and 44 *p*-mercaptobenzoic acids (*p*-MBA) molecules. Note that the *p*-MBA ligand is achiral. Indeed, the first total structure determination by X-ray crystallography of a small gold-thiolate NPs was recently accomplished by Jadzinsky *et al.*.[27] Each NP is chiral and the crystal is composed of a racemic mixture of both enantiomers. The gold atoms in the

core of the NPs are packed in a symmetric Marks decahedron (MD) structure, which is very similar to the fcc structure of bulk gold. The chirality of the overall particle arises at two levels. First, the adsorbate forms dimers on the NP surface connected through a gold atom that is somewhat detached from the gold core.[27, 28] In these structures the sulfur atoms represent chiral centers. It should be noted that each enantiomer of the NPs posses a small enantiomeric excess (ee) in the absolute configuration of the adsorbed *p*-MBA. Second, chirality also arises from the arrangement of equatorial gold atoms on the surface of the gold NPs. The asymmetric structure of the surface of the NPs reflects the interaction with the prochiral thiol. This important X-ray study confirms the theoretical prediction that upon adsorption, an achiral compound does not only decorate the surface of the NPs but also distorts locally the structure of the surface.[29] Furthermore, the local distortion may be comparable to some extend to the chiral footprint observed on extended metal surfaces.

It is likely that similar structural motifs, as the ones elucidated by the X-ray study mentioned above, are also found for the small gold particles[29] exhibiting optical activity in MBETs, although the latter consist much less than 102 gold atoms and therefore the achiral core, if existing at all, would be very small. Evidently the chiral arrangement of surface gold atoms plays a major role for the optical activity of the NPs. Covering the latter by one enantiomer of a chiral ligand may favor one chiral motif on the surface over its enantiomer and this transfer of chirality from the adsorbate to the metal particle (surface) is favored by multiple adsorbate – particle interactions. However, the behavior of this chiral distortion has not been studied yet. A key question remains whether the chiral arrangement of the metal surface atoms is stable enough to withstand a ligand exchange reaction. This would, for example, allow the fine tuning of a surface in view of its use in heterogeneous asymmetric

catalysis. One could also imagine that the chiral imprint left by the outgoing ligand can influence the adsorption of a prochiral incoming ligand. Indeed, DFT calculations have shown a difference of ~100 meV in the adsorption energy of the right-handed and the left-handed enantiomers of cysteine on a Au_{55} cluster.[30]

Here we investigate the behavior of monodisperse NPs covered with one enantiomer when exposed to the free thiol of the opposite absolute configuration, to a racemic mixture of thiols and to an achiral thiol under inert atmosphere. The retention of the core size, the evolution of the absorption in UV-vis and of the optical activity in the MBETs are followed by electrophoresis, UV-vis and ECD spectroscopy, respectively. The results give new insight into the chiral properties of these particles and furthermore provide information on thiolate-for-thiolate ligand exchange reactions.

6.3 Experimental

6.3.1 Materials

Gold(III) chloride trihydrate ($HAuCl_4.3H_2O$, 99.99%), N-isobutyryl-*L*-cysteine (NILC, 99.5%), N-isobutyryl-*D*-cysteine (NIDC, 99.5%), N-acetyl-*L*-cysteine (NALC, > 99%), 3-mercaptopropionic acid (MPA, > 99%), tiopronin (Tp, ≥ 98%) sodium borohydride ($NaBH_4$, 98%), acrylamide (> 99%), N,N'-methylenebisacrylamide (Bis, > 99%), ammonium persulfate (APS, 98%), 0.01 M phosphate buffered saline solution (PBS, NaCl 0.138 M, KCl 0.027 M, pH 7.4, powder) and N,N,N',N'-tetramethylethylenediamine (TEMED, > 99.5%) were purchased from Aldrich, concentrated (10X) premixed tris(hydroxymethylaminomethane) (Tris)/glycine buffer (250 mM Tris, 1920 mM glycine),

0.5 M Tris-HCl buffer pH 6.8 and 1.5M Tris-HCl buffer pH 8.8 were purchased from BIO-RAD. Water was purified with a Milli-Q system (≥18 MΩ.cm^{-1}). All other chemicals were analysis grade and used as received.

6.3.2 Synthesis of the thiolate-protected NPs

NILC, NIDC, NALC and Tp protected gold NPs were prepared following previous reports.[21, 25] Briefly, 400 mg of tetrachloroauric acid (1.0 mmol) and 4.0 mmol of the corresponding thiol were dissolved in 200 ml of a methanol : acid acetic solution 6 : 1 (v : v). The solution rapidly turned red before yielding a cloudy white suspension. This indicates the formation of a Au(I)thiolate polymers. After 30 minutes, the polymer was reduced by slow addition of a freshly prepared aqueous $NaBH_4$ solution (70 ml, 2.13 mol.l^{-1}) under vigorous stirring. The mixture was allowed to react for 90 minutes. The resulting dark solution was filtered using a 0.2 μm PTFE membrane to remove insoluble materials and subsequently evaporated under vacuum at a temperature inferior to 40 °C to near dryness. The NPs were precipitated several times with a large excess of ethanol and filtered using the same 0.2 μm PTFE membrane. The removal of remaining unreacted thiols or disulfides was finally completed by dialysis (Spectra/Por CE) in a bag with a molecular weight cut-off of 3500 Daltons. Particles were dissolved in 30 ml of water and loaded into the membrane which was then placed in a 2 liter beaker of water and slowly stirred. The water was changed every 10 hours over the course of 96 hours. The black solution was evaporated under vacuum to yield 300-340 mg of a black powder.

6.3.3 Separation of MPNs by PAGE

PAGE was performed with a Biorad Protean II XI system with gels of 3 mm thickness. The experimental conditions for PAGE are close to those employed in previous works.[19] The total content of the acrylamide monomers were 3% (acrylamide/Bis, 94 : 6) and 25% (acrylamide/Bis, 93 : 7) for the stacking gel and separation gel, respectively. The staking and the separating gels were buffered at pH = 6.8 and 8.8, respectively, with Tris-HCl solution. The eluting buffer consisted of a solution of glycine (192 mM) and Tris (25 mM) in 80 : 20 (v/v) water : methanol. The purified NPs were dissolved in a 5% glycerol solution in water to a concentration of 4 $mg.ml^{-1}$. The NPs solutions (2 ml) were loaded on a 3 mm gel without lanes and eluted for 17 hours at a constant voltage of 150 V to achieve separation. Parts of the gel containing each separated fraction were cut out and placed in Milli-Q water overnight. The gel lumps suspended in the solution were removed by filtration. NPs were finally further purified by dialysis in the same way as described above. For each ligand exchange reaction described below, 6 to 8 gels are necessary in order to get sufficient quantities of size separated NPs.

6.3.4 Ligand Exchange Reactions

The size separated and purified gold NPs protected with either NILC, NIDC or NALC (2.7-3.6 mg) were dissolved in 3 ml of a PBS solution (pH 7.4). For the reactions under inert atmosphere, the solution was treated with N_2 for 20-30 min. The solution was rapidly transferred via a syringe to a quartz cell containing the corresponding incoming thiol for in

situ ECD measurements. For the reaction under inert atmosphere the syringes and the quartz cells containing the thiols were purged by a flow of N_2 and sealed with a septum, prior to use.

6.3.5 Ultrafiltration

After 20 minutes the reactions were quenched by ultrafiltration using the Ultra-4 centrifugal device of Millipore with a cutoff of 5 kDa at 6500 RCF for 16 minutes at 5°C. The ultrafiltration was performed 5 times after dissolution in 3 ml of MilliQ-water.

6.3.6 UV-vis and ECD

UV-vis and ECD spectra of the separated particles were collected respectively on a Cary 300 and a Jasco 710 spectrometer using a quartz cell of 1 cm path length and solutions of approximately 0.3 $mg.ml^{-1}$ in H_2O (or 1 $mg.ml^{-1}$ for the in situ ECD measurements).

6.4 Results and Discussion

6.4.1 Effect of Dissolved Oxygen on Core-Size Retention

The first set of experiments was performed with the gold NPs covered by either NILC or NIDC. These particles were separated by PAGE into eight well-defined compounds, *i.e.* compounds with a precise number of gold atoms and ligands.[21] Separated NPs were referred to as compounds **1-8** (see **Figure 6.1** (A)) according to their electrophoretic mobility with the yellowish compound **2** being the second most mobile species. In a previous report,[21] it was shown that the UV-vis spectra are strikingly similar for analogous

compounds **1-3** covered by NIC and GSH.[16] This comparison allowed us to assign the three smallest compounds **1**, **2** and **3** to $Au_{10}(NIC)_{10}$, $Au_{15}(NIC)_{13}$ and $Au_{18}(NIC)_{14}$, respectively. The NPs covered with NALC also contain the species **1-3** (see later). The isolated and dialyzed compounds could be stored for weeks without noticeable degradation, as verified by PAGE and UV-vis spectroscopy.

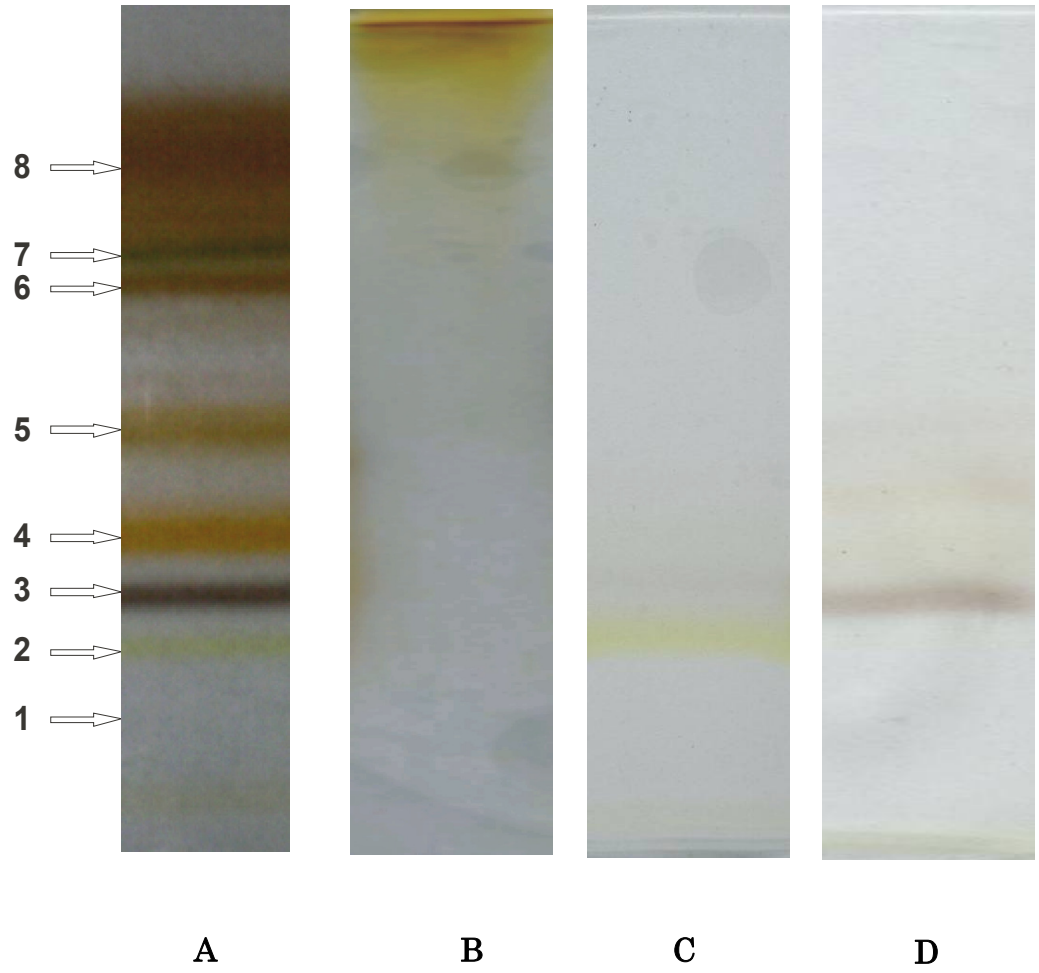

Figure 6.1 : PAGE separation of NPs protected with NIC after synthesis (A). The separated compounds are numbered from **1**-**8** according to their decreasing electrophoretic mobility. The smallest compound **1** is only visible under UV irradiation. Isolation of compound **2**, $Au_{15}(NIC)_{13}$, after reaction with the opposite enantiomer in PBS under aerobic condition (B) and under inert atmosphere (C). Isolation of compound **3**, $Au_{18}(NILC)_{14}$, after reaction with NIDC under inert atmosphere (D).

We noticed a pronounced effect of dissolved oxygen on the evolution of the ECD signals of the gold particles upon addition of further thiol. **Figure 6.2** (A) shows ECD spectra recorded after addition of NIDC to **2** ($Au_{15}(NILC)_{13}$) under aerobic condition, whereas (B) shows the evolution of the optical activity after addition of NILC to $Au_{15}(NIDC)_{13}$ under inert

condition. The ratio between the incoming and the outgoing ligands is around 9 for the two experiments. In both cases the signals at 420 and 336 nm were quickly inverted during the first 20 minutes to an extent of 56% under aerobic condition (C) and 70% under inert atmosphere (D). At 336 nm, the optical activity is not reversed (reduced to 44%) under aerobic condition whereas it is reversed at 82% under inert atmosphere. The shape of the full ECD spectra is more preserved under inert atmosphere. The larger differences in term of shape (difference of inversion at 336 and 420 nm) for the spectra under aerobic condition might be explained by the formation of particles of different size and by the formation of Au(I)thiolate species (*vide infra*). Indeed, in presence of oxygen the signals subsequently decreased with time and the solution was no more optically active after less than one hour, whereas the signal was stable in the absence of oxygen.

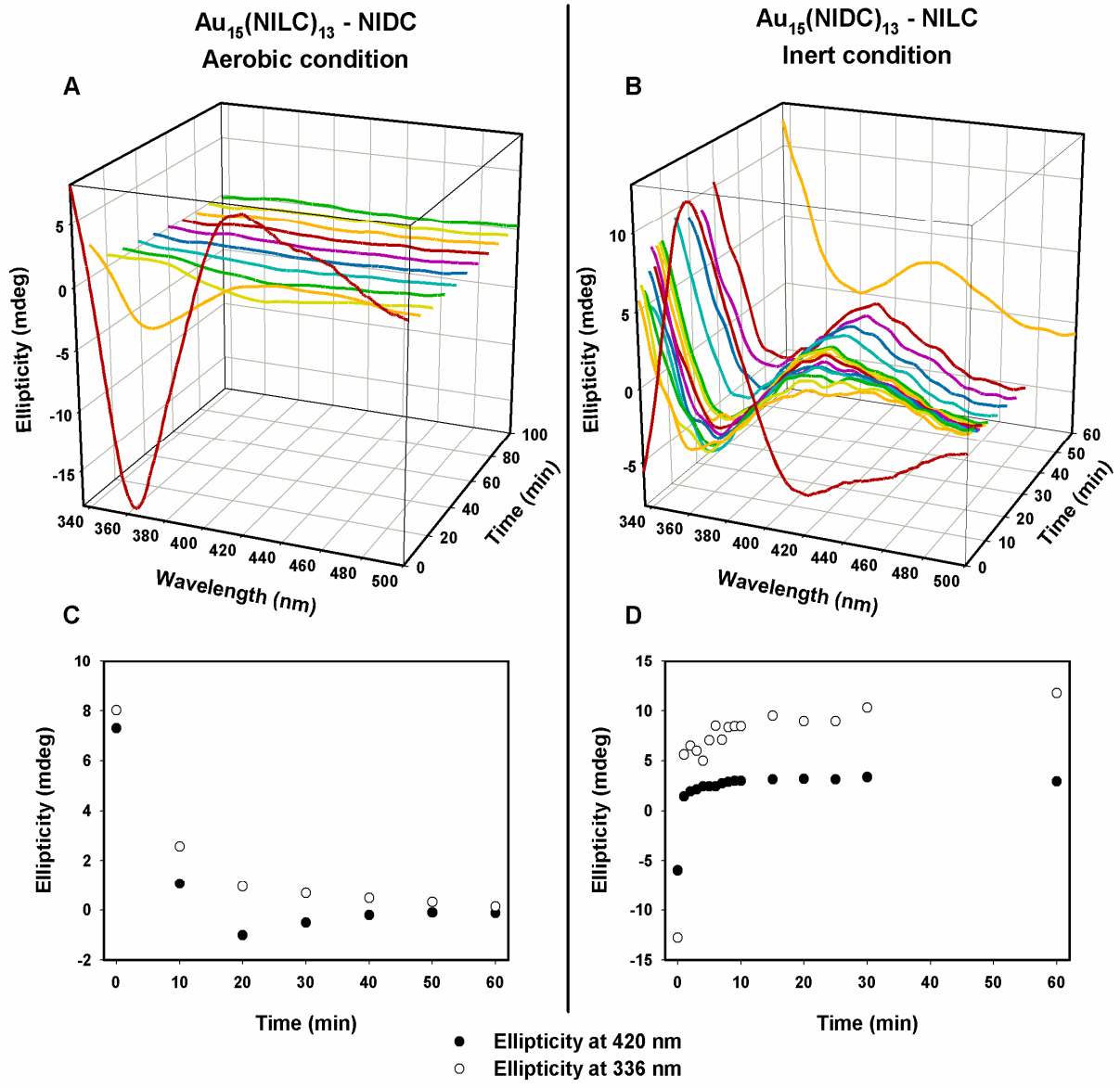

Figure 6.2 : Time evolution of ECD spectra after addition of 14.7 mg of NIDC (A) or 11 mg of NILC (B) to 3 ml of PBS pH 7.4 containing respectively, 3.6 mg of $Au_{15}(NILC)_{13}$ under aerobic condition and 2.7 mg of $Au_{15}(NIDC)_{13}$ under inert atmosphere. Time evolution of the ellipticity at 420 nm (black circles) and 336 nm (white circles) during the ligand exchange reaction: $Au_{15}NILC_{13}$ – NIDC under aerobic condition (C) and $Au_{15}(NIDC)_{13}$ - NILC under inert atmosphere (D).

The size distribution after exchange was monitored by PAGE. For the experiment under aerobic conditions compound **2** was not observed by PAGE and the sample showed a drastic reduction of electrophoretic mobility after 1 day (see **Figure 6.1** (B)). The batch under inert atmosphere was rapidly quenched by removing excess of free thiols and PBS by UF. PAGE (see **Figure 6.1** (C)) showed almost exclusively compound **2** with minor presence of the larger compounds **3-5**. A similar behavior was observed for the same type of reaction on compound **3** with the discrete apparition of the adjacent species **2** and **4**, which are very similar in term of size (D). It should be noted that UF was not performed rigorously under inert atmosphere and thus some influence of oxygen on the size distribution observed in **Figure 6.1** (C, D) is possible even for the reaction under anaerobic condition. The intensity of the inverted signals in **Figure 6.2** (B) is smaller (70% of optical inversion) than the one that could be expected from the ee of NIC in the system (80%), which is probably due to the formation of larger particles, as evidenced by PAGE (**Figure 6.1** (C)). The larger compounds **3-5** have considerably smaller anisotropy factors[21] and thus the ECD spectrum is dominated by compound **2** $Au_{15}(NIDC)_{13}$.

6.4.2 Inversion of the Absolute Configuration of the Ligands

Further experiments were performed under inert atmosphere with the species **2** and **3** of the gold NPs protected with NILC, which correspond respectively to $Au_{15}(NILC)_{13}$ and $Au_{18}(AuNILC)_{14}$. These compounds can be isolated again after one hour of reaction with the ligand of opposite absolute configuration by UF and PAGE in order to eliminate the small contribution of NPs of different size. The ratio between NIDC (incoming) and NILC

(outgoing) enantiomers is 9 for these two experiments. **Figure 6.1** shows that the electrophoretic mobility of **2** (C) and **3** (D) are not modified after the reaction with NIDC.

In addition, **Figure 6.3** (A) shows that both UV-vis spectra of the isolated NPs **2** and **3** after exchange reaction with NIDC remain unchanged. This confirms that the size and the total number of ligands are preserved during the reaction, in agreement with electrophoresis. More interestingly, the ECD spectra are reversed with a quasi-perfect mirror image relationship. The signals are blue shifted by one to two nanometers after exchange and the ratio of the signals at 360 and 420 nm is slightly different (see **Figure 6.3** (B)). The anisotropy factor, $\Delta\varepsilon/\varepsilon$, shows that the optical activity is reversed at 78% (at 360 nm) for the reaction of $Au_{15}(NILC)_{13}$ with NIDC (see **Figure 6.3** (C)). This percentage of inversion, about 80% (magnitude of the inverted signal is 80% of the initial signal), corresponds very well to the overall ee of NIC in the system (added NIDC plus NILC adsorbed on the NPs). The observations are similar for the reaction on **3** $Au_{18}(NILC)_{14}$. Due to the weaker optical activity the relatively large noise prevents accurate quantification. However, it is evident that the form of the ECD spectrum does not change drastically upon inversion for these two compounds **2** and **3**.

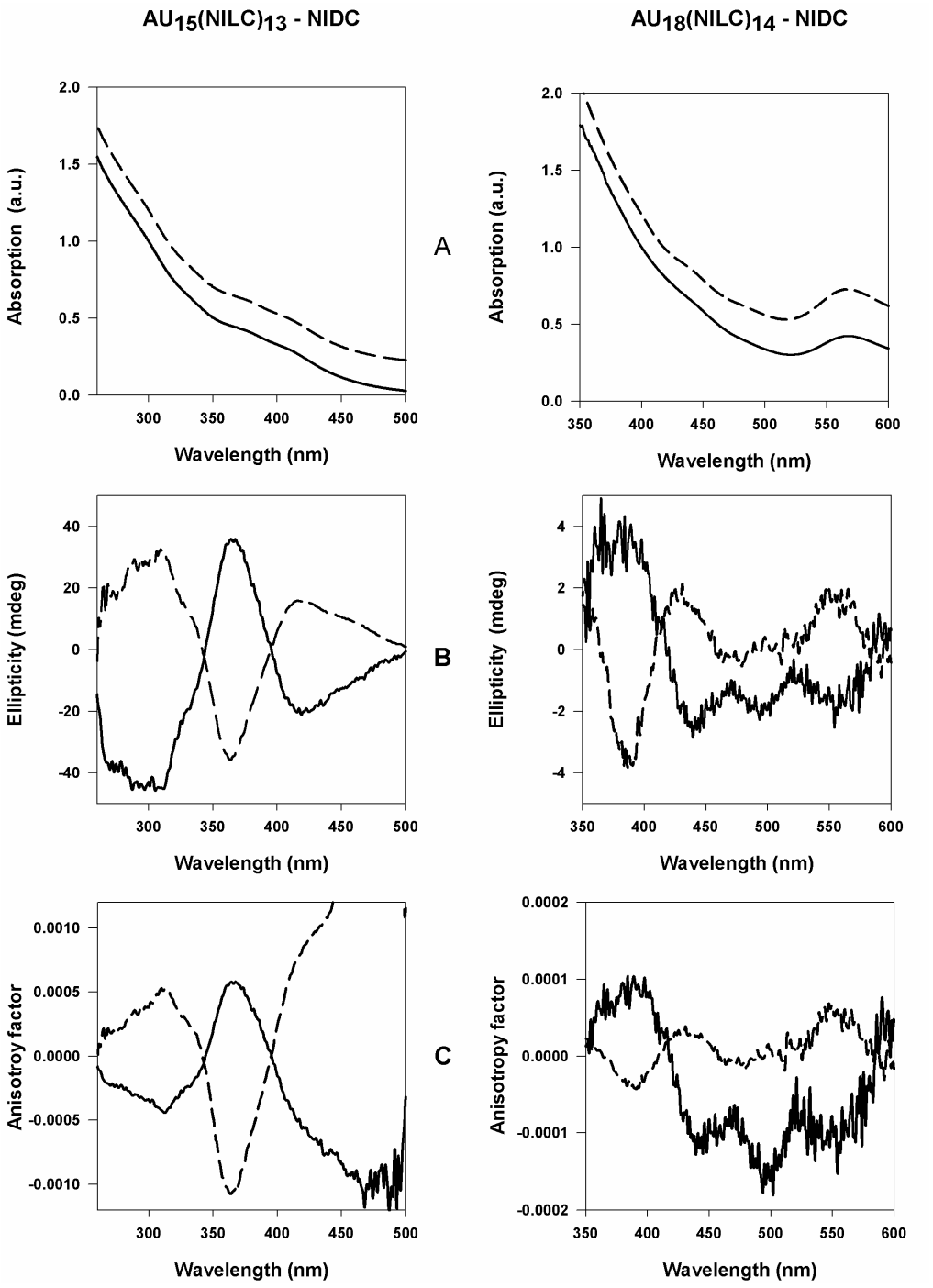

Figure 6.3 : UV-vis spectra normalized at 300 nm and offset for clarity (A), ECD spectra (B) and anisotropy factor (C) of $Au_{15}(NILC)_{13}$ (left) and $Au_{18}(NILC)_{14}$ (right) before (dashed line) and after ligand exchange reaction with NIDC (solid line).UV-vis spectra of $Au_{15}(NILC)_{13}$ and $Au_{18}(NILC)_{14}$ are offset and normalized to one in absorbance at 300 and 400 nm, respectively and ECD spectra of $Au_{15}(NILC)_{13}$ are normalized to 35.8 mdeg at 364 nm for clarity.

The observed inversion of the ECD signal indicates rapid ligand exchange and has interesting implications on the nature of chirality of the gold particles. The fact that the shapes of the ECD spectra are unchanged and that their intensity corresponds to the overall ee of the ligand in the system is an argument against the model which attributes the optical activity in MBETs to a symmetric core perturbed by a dissymmetric or chiral field. In fact, Beratan *et al.*[26] have shown that the computed chiroptical response changes significantly when the chiral field is modified. The latter is influenced by the number and arrangement of point charges (charged functional groups of NIC). The chiral field changes under our conditions where one to two ligands per particle have opposite absolute configuration (assuming a statistical distribution of NIC enantiomers on the particles).

Therefore the findings in **Figure 6.3** contradict a model based mainly on the chiral arrangement of the thiols on an achiral metal core. The other proposed model is based on the assumption that the core of small metal particles can adopt intrinsically chiral structures.[9] If such particles grow in the presence of a passivating chiral enantiopure thiol then one enantiomeric form of the chiral core could be stabilized over the other, which would explain the observed optical activity in the MBETs. One could then imagine that this enantiomeric form of the metal core is prevented, even if the thiol ligand is exchanged for example by the opposite enantiomer. The observed inversion of the optical activity for species **2** and **3** shows that this is not the case. Hence, the metal core, if it is intrinsically chiral, relaxes to the other enantiomer, when the absolute configuration of the ligand is changed. In other words, still under the assumption of an intrinsically chiral metal core, the barrier between the two enantiomeric forms of the metal core is too small compared to the driving force imposed on it by the change in absolute configuration of the thiol ligand. Assuming an analogous structure

as the one reported by Jadzinsky *et al.* it seems clear that the chiral local distortion of the gold atoms involved in the adsorption of the chiral thiol (*e.g.* "chiral footprint") is the key parameter for the optical activity in the MBETs. The findings reported here thus show that this chiral footprint does not support a ligand exchange reaction and the incoming chiral thiol finally imposes its own chiral footprint. This implies that the resolution of a racemic mixture of NPs might not be possible using derivatization with a chiral thiol.

6.4.3 Exchange with a Racemic Mixture or with an Achiral Thiol

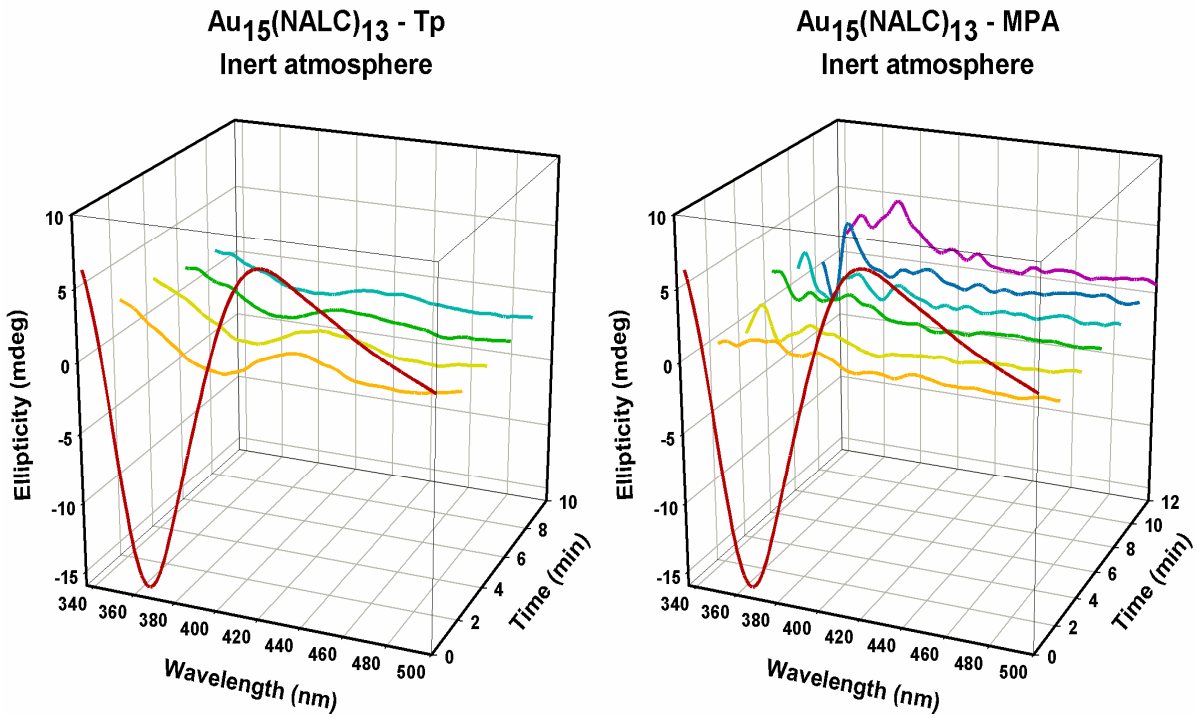

Figure 6.4 : Time evolution of ECD spectra after addition of 5.4 mg of Tp (left) and 3.5 mg MPA (right) to 3.2 mg of $Au_{15}(NALC)_{13}$ in 3 ml of PBS pH 7.4 under inert condition.

These experiments are performed under inert atmosphere with $Au_{15}(NALC)_{13}$ in presence of either a racemic mixture of Tp or of the achiral MPA with a molar ratio between the incoming ligands and NALC limited to 4. **Figure 6.4** shows the evolution of the optical activity in the MBETs of $Au_{15}(NALC)_{13}$ during the thiolate-for-thiolate exchange reaction with racemic Tp (left) and MPA (right). The former reaction leads to a large diminution of the optical activity and a qualitative change of the ECD spectra, whereas the latter annihilates completely the ECD signal. The size evolution is monitored by PAGE. **Figure 6.5** compares the results of PAGE for the crude gold NPs protected with either NALC (A) or Tp (B) as well as the size evolution of $Au_{15}(NALC)_{13}$ (**2**) upon exchange with the Tp (C) and the MPA (D). The ligand exchange reaction with Tp leads to two main species which do not correspond to the isolated species for the crude gold NPs protected with either the NALC or with the Tp. However, the electrophoretic mobility of the products and of the starting material are quite similar. Furthermore, Tp and NALC have similar chemical formula and the same charges (see **Chart 2**). This implies that the resulting NPs might be very similar in size despite their different colors. The situation is similar for the exchange reaction involving MPA. In this case three distinct fractions are isolated. The most mobile fraction is yellow as the starting NALC NPs **2** but has a higher electrophoretic mobility probably due to the smaller size of the incoming MPA.

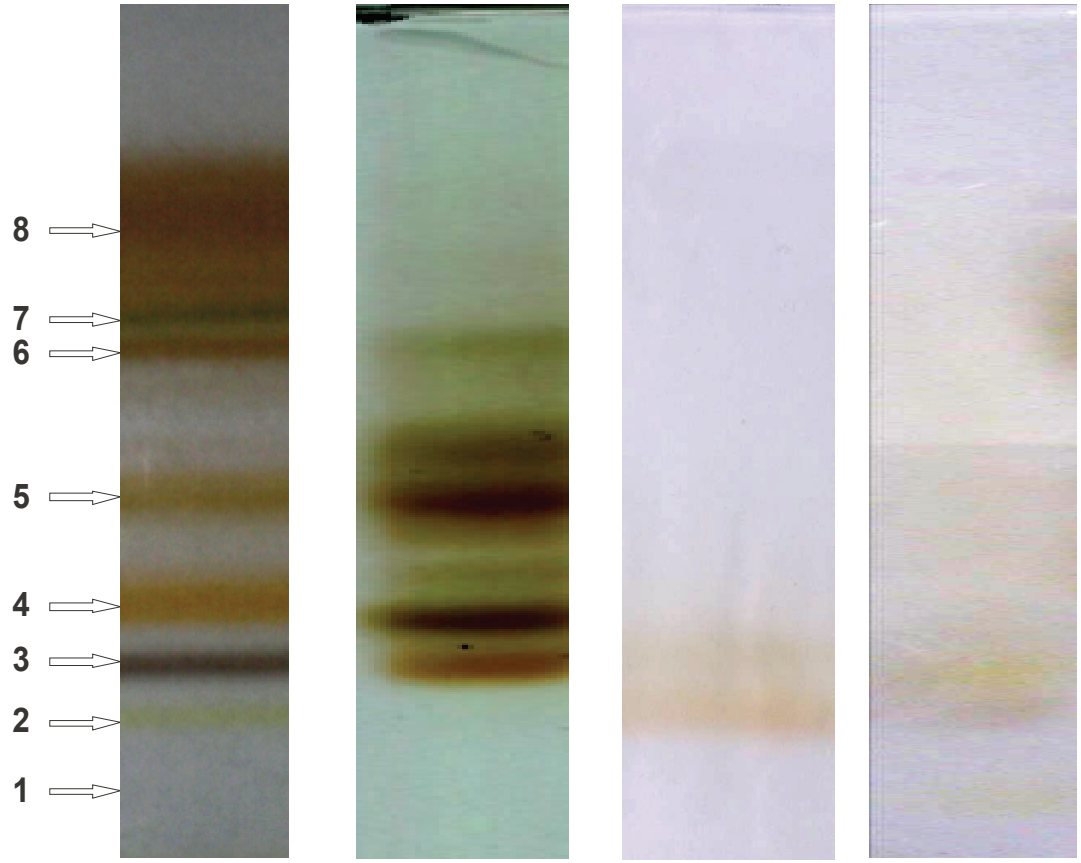

Figure 6.5 : PAGE separation of NPs protected with NALC (A) and racemic Tp (B) after syntheses. Separation of compound **2** ($Au_{15}(NALC)_{13}$) after reaction with racemic Tp (C) and MPA (D) in PBS pH 7.4 under inert atmosphere.

Enantiopure leaving and incoming thiols

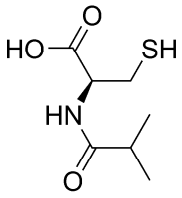

N-isobutyryl-*D*-cysteine
(NIDC)

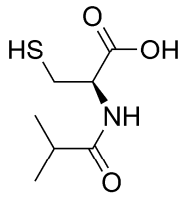

N-isobutyryl-*L*-cysteine
(NILC)

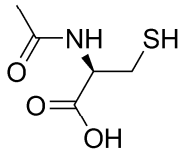

N-acetyl-*L*-cysteine
(NALC)

Racemic incoming thiol

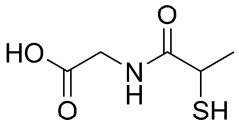

Tiopronine
(Tp)

Achiral incoming thiol

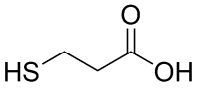

mercaptopropionic acid
(MPA)

Chart 2 : Chemical structures of the thiols used.

The two species resulting from the ligand exchange with Tp were furthermore isolated in order to control their size and their individual optical activity. **Figure 6.6** shows the UV-vis (right) and ECD (left) spectra of the two isolated fractions. The UV-vis spectra of the products and of **2** are different in term of shape but the absorption onsets are very similar for the three species (~700 nm). This implies that the sizes of these compounds are very close[31] and that the variation of the electronic structure may not be attributed to a variation of the size but rather to a difference in the surface structure (*i.e.* footprint). The optical activity is very weak for the two species and may still be attributed to the non exchanged NALC rather than due to enantioselective adsorption.[30] These findings emphasize once more the flexibility of

the NPs structure and the effect of the adsorbates onto the electronic structure of the cluster. For example, NALC and NILC which have been shown to have the same type of adsorption on gold NPs by VCD and DFT calculations,[21, 25] present similar UV-vis spectra for many fractions (unpublished results). Furthermore, the electrophoretic separation of these two types of NPs leads to very similar fractions with higher mobility for the NPs covered with NALC due to its smaller size (see **Figure 6.1** (A) and **Figure 6.5** (B)).

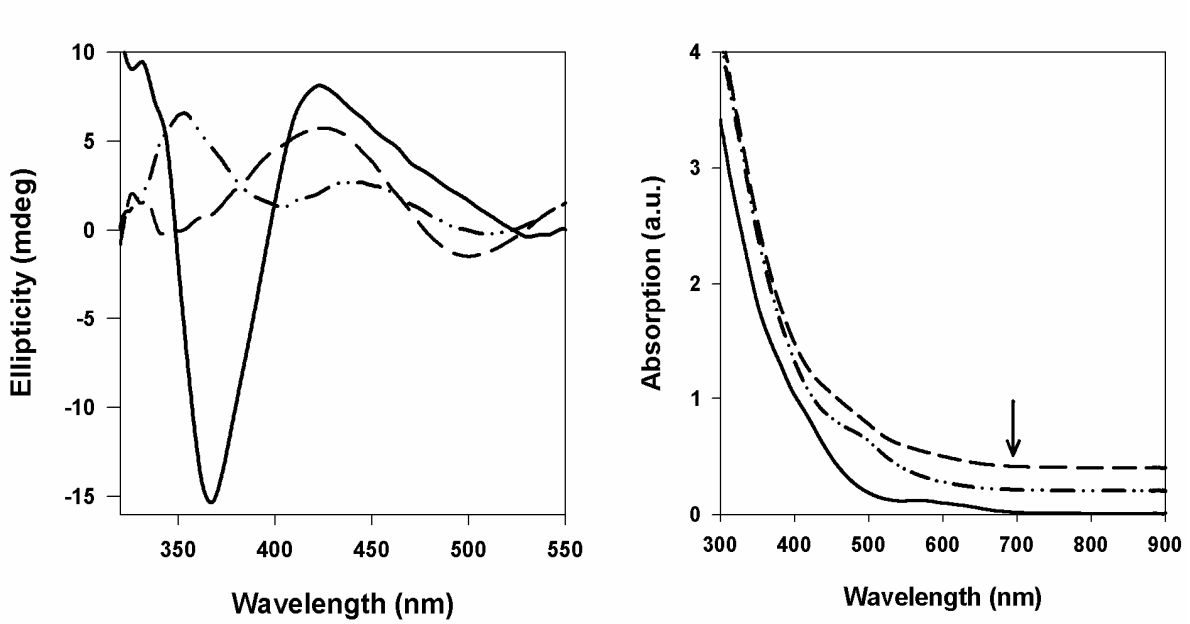

Figure 6.6 : ECD (left) and UV-vis (right) spectra of the species isolated by PAGE after the reaction of $Au_{15}(NALC)_{13}$ with Tp. The spectra of $Au_{15}(NALC)_{13}$ before reaction, the most mobile and the second isolated fraction correspond respectively to the solid, the dash point and the dash lines. ECD spectra of the two products isolated after the reaction are multiplied by a factor five and UV-vis spectra are normalized at 400 nm and offset for clarity. The vertical arrow indicates the absorption onset for the three UV-vis spectra.

6.4.4 Insight on the thiolate-for-thiolate ligand exchange

These experiments further contain interesting information about thiolate-for-thiolate ligand exchange in subnanometer particles and the different evolutions of the core-size in the presence of excess thiol under inert atmosphere or in aerobic condition. So far, the reports dealing with the core size evolution during ligand exchange are not in complete agreement. On the one hand some reports, mainly relying on transmission electron microscopy (TEM), indicate that thiolate-for-thiolate ligand replacements on Au NPs lead to retention of the Au core size.[32-34] On the other hand, Murray *et al.*[35] have recently demonstrated by mass spectrometry that reaction of $Au_{55}(PPh_3)_{12}Cl_6$ with hexanethiol under argon yields Au_{75} clusters. In the same way, Tsukuda and Teranishi[36] reported recently the large scale synthesis of thiolated Au_{25} cluster under N_2 atmosphere via ligand exchange reaction with phosphine-stabilized Au_{11} clusters as starting materiel. They also suggested that the population of the smaller particles decreased after aeration. The two latter studies deal with phosphine-for-thiol exchange reaction. This may differ from the thiolate-for-thiolate exchange studied here but in both cases the exchange was done in presence of an excess of incoming thiol. Tsukuda and Teranishi have recently demonstrated the extremely high stability of the $Au_{25}(SG)_{18}$ clusters against core etching in presence of a large excess of GSH even in aerobic condition.[37] This study demonstrates that in aerobic condition, the glutathionate protected clusters smaller than Au_{25} are etched into Au(I)thiolate polymers and very small clusters, whereas the bigger clusters are converted to Au_{25} by etching. As discussed above, for both $Au_{15}(NILC)_{13}$ and $Au_{18}(NILC)_{14}$, the present study provides strong evidence that the size memory can be kept to a large extent during the ligand exchange reaction under inert atmosphere. The ECD measurements also demonstrate that this reaction is very fast. The

mechanism of thiolate-for-thiolate ligand exchange is not established but Murray *et al.*[38] have shown that the exchange is inhibited when conducted under N_2 and in the absence of Au(I)thiolate species. Their results imply participation of an oxidized form of Au probably in the form of Au(I)thiolate. Some of these Au(I)thiolate and especially ringlike units have been predicted by DFT calculations[29, 39, 40] and have been observed by electrospray mass spectrometry[16, 17, 41] and might be a general structural motif of very small clusters composed of 10 to 50 gold atoms which is the size-range of the NPs studied here. The X-ray study of Jadzinsky has brought to light that for slightly bigger NPs (102 gold atoms) the Au(I)thiolate motif is present but mainly in the form of dimers.[27] These predicted building blocks could also play a significant role for the relatively fast kinetic of the described exchanges and for the optical activity in the MBETs described before. According to **Figure 6.2** (B and D) the reaction in the absence of O_2 and without Au(I)thiolate catalyst was almost complete in about 5 minutes, whereas ligand exchange on gold particles takes few hours according to published work.[38] Furthermore, we observed that even under aerobic condition, the optical activity is reversed within 20 min without a drastic modification of the signal (see **Figure 6.2** A and C). However, after that the ECD spectra progressively decreased and its shape was modified. This implies that two different processes are involved. On the one hand, the first process involves ligand exchange without modification of the size of the clusters. This very fast ligand exchange without alteration of the core size can be explained for example by a radical mechanism, which does not involve Au(I)thiolate leaving groups and which has been evidenced by the spin trapping technique.[42] On the other hand, the second process, the core etching, is slower, catalysed by O_2 and leads to a modification of the size distribution probably by the formation of Au(I)thiolate polymers. Interestingly, the yield of

the ligand exchange reaction in the absence of oxygen (first process) calculated from the anisotropy factor (**Figure 6.3** (C)) is close to the ee of the ligand in the system, which indicates an equilibrium. This would mean that adsorption and desorption are reversible and that the two enantiomers of NIC have similar affinity for the NPs.

6.5 Conclusions

In conclusion, the thiolate-for-thiolate ligand exchange under inert condition can be performed on nanoclusters without degradation of the core-size. The optical activity in the MBETs of small monodisperse gold particles covered by one enantiomer of NIC is reversed when exposed to the opposite enantiomer. This shows that the optical activity is dictated by the chiral thiol. If the particles exhibit an intrinsically chiral structure, the results furthermore imply that this structure is not stable enough in one of its enantiomeric forms to withstand a switch of the absolute configuration of the passivating thiol. This observation reveals the influence of the adsorbed thiols on the structure of the cluster surface and demonstrates its key role in the optical activity. The extent of ligand exchange of NILC for its opposite enantiomer corresponds to the ee of overall NIC in the system. When the incoming thiol is different from the leaving one, the electronic structure of the cluster can be slightly different even if the size of the resulting clusters is similar. This shows the influence of the nature of the thiols on the electronic structure of the cluster.

6.6 References

[1] H. Bönnemann, G. A. Braun, *Angew. Chem. Int. Ed.* **1996**, *35*, 1992.

[2] M. Studer, H. U. Blaser, C. Exner, *Adv. Synth. Catal.* **2003**, *345*, 45.

[3] M. Bieri, C. Gautier, T. Bürgi, *Chem. Phys. Phys. Chem.* **2007**, *9*, 671.

[4] Y. M. David H. Dressler, *Chirality* **2007**, *19*, 358.

[5] D. H. Dressler, Y. Mastai, *J. Colloid Interface Sci.* **2007**, *310*, 653.

[6] H. Qi, T. Hegmann, *J. Mater. Chem.* **2006**, *16*, 4197.

[7] T. L. Wetzel, A. E. DePristo, *J. Chem. Phys.* **1996**, *105*, 572.

[8] I. L. Garzón, M. R. Beltran, G. Gonzalez, I. Gutierrez-Gonzalez, K. Michaelian, J. A. Reyes-Nava, J. I. Rodriguez-Hernandez, *Eur. Phys. J. D* **2003**, *24*, 105.

[9] I. L. Garzón, J. A. Reyes-Nava, J. I. Rodríguez-Hernández, I. Sigal, M. R. Beltrán, K. Michaelian, *Phys. Rev. B* **2002**, *66*, 073403.

[10] S. M. Barlow, R. Raval, *Curr. Opin. Colloid Interface Sci.* **2007**, *13*, 65.

[11] M. Schunack, E. Lægsgaard, I. Stensgaard, I. Johannsen, F. Besenbacher, *Angew. Chem. Int. Ed.* **2001**, *40*, 2623.

[12] R. Viswanathan, J. A. Zasadzinski, D. K. Schwartz, *Nature* **1994**, *368*, 440.

[13] G. P. Lopinski, D. J. Moffatt, D. D. M. Wayner, R. A. Wolkow, *Nature* **1998**, *392*, 909.

[14] M. Ortega Lorenzo, C. J. Baddeley, C. Muryn, R. Raval, *Nature* **2000**, *404*, 376.

[15] V. Humblot, S. Haq, C. Muryn, W. A. Hofer, R. Raval, *J. Am. Chem. Soc.* **2002**, *124*, 503.

[16] Y. Negishi, K. Nobusada, T. Tsukuda, *J. Am. Chem. Soc.* **2005**, *127*, 5261.

[17] Y. Negishi, Y. Takasugi, S. Sato, H. Yao, K. Kimura, T. Tsukuda, *J. Am. Chem. Soc.* **2004**, *126*, 6518.

[18] T. G. Schaaff, G. Knight, M. N. Shafigullin, R. F. Borkman, R. L. Whetten, *J. Phys. Chem. B* **1998**, *102*, 10643.

[19] T. G. Schaaff, R. L. Whetten, *J. Phys. Chem. B* **2000**, *104*, 2630.

[20] H. Yao, K. Miki, N. Nishida, A. Sasaki, K. Kimura, *J. Am. Chem. Soc.* **2005**, *127*, 15536.

[21] C. Gautier, T. Bürgi, *J. Am. Chem. Soc.* **2006**, *128*, 11079.

[22] M. Tamura, H. Fujihara, *J. Am. Chem. Soc.* **2003**, *125*, 15742.

[23] Y. Yanagimoto, Y. Negishi, H. Fujihara, T. Tsukuda, *J. Phys. Chem. B* **2006**, *110*, 11611.

[24] C. Gautier, R. Taras, S. Gladiali, T. Bürgi, *Chirality* **2007**, *20*, 486.

[25] C. Gautier, T. Bürgi, *Chem. Commun.* **2005**, *43*, 5393.

[26] M. R. Goldsmith, C. B. George, G. Zuber, R. Naaman, D. H. Waldeck, P. Wipf, D. N. Beratan, *Phys. Chem. Chem. Phys.* **2006**, *8*, 63.

[27] P. D. Jadzinsky, G. Calero, C. J. Ackerson, D. A. Bushnell, R. D. Kornberg, *Science* **2007**, *318*, 430.

[28] R. L. Whetten, R. C. Price, *Science* **2007**, *318*, 407.

[29] H. Häkkinen, M. Walter, H. Gronbeck, *J. Phys. Chem. B* **2006**, *110*, 9927.

[30] X. López-Lozano, L. A. Pérez, I. L. Garzón, *Phys. Rev. Lett.* **2006**, *97*, 233401.

[31] R. B. Wyrwas, M. M. Alvarez, J. T. Khoury, R. C. Price, T. G. Schaaff, R. L. Whetten, *Eur. Phys. J. D* **2007**, *43*, 91.

[32] G. H. Woehrle, M. G. Warner, J. E. Hutchison, *J. Phys. Chem. B* **2002**, *106*, 9979.

[33] G. H. Woehrle, J. E. Hutchison, *Inorg. Chem.* **2005**, *44*, 6149.

[34] Y. Yang, S. Chen, *Nano Lett.* **2003**, *3*, 75.

[35] R. Balasubramanian, R. Guo, A. J. Mills, R. W. Murray, *J. Am. Chem. Soc.* **2005**, *127*, 8126.

[36] Y. Shichibu, Y. Negishi, T. Tsukuda, T. Teranishi, *J. Am. Chem. Soc.* **2005**, *127*, 13464.

[37] Y. Shichibu, Y. Negishi, H. Tsunoyama, M. Kanehara, T. Teranishi, T. Tsukuda, *Small* **2007**, *3*, 835.

[38] Y. Song, T. Huang, R. W. Murray, *J. Am. Chem. Soc.* **2003**, *125*, 11694.

[39] H. Grönbeck, M. Walter, H. Häkkinen, *J. Am. Chem. Soc.* **2006**, *128*, 10268.

[40] T. Iwasa, K. Nobusada, *J. Phys. Chem. C* **2007**, *111*, 45.

[41] A. P. Gies, D. M. Hercules, A. E. Gerdon, D. E. Cliffel, *J. Am. Chem. Soc.* **2007**, *129*, 1095.

[42] P. Ionita, B. C. Gilbert, V. Chechik, *Angew. Chem. Int. Ed.* **2005**, *44*, 3720.

7

General Conclusions and Outlook

From a synthetic point of view, new gold nanoparticles functionalized with polar and apolar chiral molecules have been prepared using three different approaches: (i) the one-phase direct synthesis, (ii) the two-phase direct synthesis and (iii) the indirect ligand exchange pathway. The mean diameter of the nanoparticles obtained by the direct syntheses has been controlled mainly by the metal-to-ligand molecular ratio. However the direct syntheses have inevitably yielded to a discrete size distribution whereas the thiolate-for-thiolate ligand exchange pathway has allowed a surprisingly fast modification of the organic layer with a perfect size-memory of the initial nanoparticle under anaerobic condition. This latter pathway is very interesting for the fine tuning of strictly monodispersed nanoparticles. The size-separation of the negatively charged polar and of the apolar nanoparticles have been performed with a molecular precision by polyacrylamide gel electrophoresis and size exclusion chromatography, respectively.

From a fundamental point of view, we have focused our interest on the chiroptical signature of subnanometer thiol-stabilized gold nanoparticles. At this scale, almost all gold atoms are involved in the surface. The size separated nanoparticles have shown a systematic bathochromic shift in their optical spectra as their size was increasing. This trend is due to the quantum size effects and shows that in this size-range gold nanoparticles behave as semiconductors. As for common organic molecules, the vibrational circular dichroism (VCD) and the electronic circular dichroism (ECD) spectra of the nanoparticles covered by thiols of opposite absolute configurations have shown a mirror image relationship whereas their UV-vis and their IR spectra were identical. The optical activity in the UV-vis have been shown to be size dependant and stronger for the smaller particles whereas the size had less influence on the VCD spectra. These results and the density functional theory (DFT) calculations have demonstrated that ECD selectively probes electronic transitions located in the metal core, while VCD is much more sensitive towards molecular vibrations within the organic shell.

In this thesis, we have combined for the first time VCD and DFT calculations in order to study the conformation of the chiral thiols adsorbed on gold nanoparticles by comparison between experimental and calculated spectra. In particular, the conformations of two cysteine derivatives were elucidated and characterized by an interaction between the carboxylate and the gold cluster. This interaction represents a second anchoring point beside the strong gold – sulfure bond. According to our results and to the data reported untill now in the literature, this two-point interaction is a common characteristic of the thiols able to impart optical activity to the metal core. In addition, the size-separated gold nanoparticles protected with a chiral atropisomeric dithiol have revealed the highest anisotropy factor reported so far for the electronic transitions located in the gold core.

We have finally demonstrated that the optical activity in the metal-based electronic transitions of well defined gold nanoparticles protected by one chiral thiol is reversed with a quasi-perfect mirror image relationship when this thiol is exchanged for its opposite enantiomer.

The results described in this thesis have particularly emphasized the influence of the adsorbed thiol, of its bonding with the surface, of its conformation and finally of its configuration on the structure of the gold particle. When all the results are considered, it seems clear that the thiol does not only decorate the surface of the particles but also distorts its structure and in the case of a chiral bidentate thiol creates a "chiral footprint" which is surely the main origin of the strong optical activity in the metal-based electronic transitions. Such distortions have already been very reasonably speculated on extended surfaces and recently strongly suggested on gold nanoparticles by X-ray total structure determination.

Further information has been pointed out about the flexibility and the reversability of the chiral footprint and in general of the surface reconstruction imposed by a thiol. This information is very useful for a better understanding of the metal-molecule interaction on surfaces and of the properties of both nanoparticles and extended surfaces. The evolution of the computational methods in the future combined with the chiroptical study of further metal-ligand nanoparticles systems may greatly help the development of surface science and particularly the development of heterogeneous enantioselective catalysis because surface – molecule interactions and conformation of molecules at surfaces are very difficult to probe with the other spectroscopic methods.

Appendix

A

Supplementary information of Chapter 2

A.1. Materials

D_2O (99.9%) was received from Cambridge Isotope Laboratories. $HAuCl_4 \cdot 3H_2O$ (99.99%), N-acetyl-*L*-cysteine (>99%) and sodium borohydride (98%) were purchased from Aldrich. Water was purified with a Milli-Q system (≥18 $M\Omega.cm^{-1}$). All other chemicals were analysis grade and used as received.

A.2. Characterization of the Particles by TEM, UV-vis and NMR

^{1}H and ^{13}C and DEPT NMR spectra were measured on a Brucker Avance 400 spectrometer at room temperature. Solutions were prepared in D_2O at a concentration of 50 $mg.ml^{-1}$. A relaxation delay of 5 s was used to allow adequate signal decay between pulses.

Transmission Electron Microscopy (TEM) images were recorded with a Philips C200 electron microscope operated at 200 kV. TEM samples were prepared by casting a drop of a 1 $mg.ml^{-1}$ solution in water onto a carbon-coated copper grid. UV-vis spectra of the particles in water were collected on a Cary 300 spectrometer.

A.3. IR and VCD Spectroscopy

IR and vibrational circular dichroism (VCD) spectra were recorded on a Bruker PMA 50 accessory coupled to a Tensor 27 Fourier transform infrared spectrometer. A photoelastic modulator (Hinds PEM 90) set at l/4 retardation was used to modulate the handedness of the circular polarized light. Demodulation was performed by a lock-in amplifier (SR830 DSP). An optical low-pass filter (< 1800 cm^{-1}) put before the PEM was used to enhance the signal/noise ratio. All solutions of N-acetyl-*L*-cysteine and N-acetyl-*L*-cysteine MPNs were prepared in D_2O. NaOD was added to deprotonate the carboxylic acid group. A VCD reference spectrum of D_2O containing the same amount of NaOD was subtracted from the VCD spectrum of the dissolved molecules and MPNs, respectively. All spectra were recorded at room temperature with a resolution of 8 cm^{-1} in a cell equipped with CaF_2 windows and a 50 μm Teflon spacer. Both sample and reference were measured for three hours in time slices

of one hour, corresponding to about 24'000 scans in total for sample and reference, respectively. The spectra are presented without smoothing or further data processing. More information about the experimental procedure can be found elsewhere.[1, 2]

A.4. Density Functional Theory Calculations

The adsorption of deprotonated N-acetyl-*L*-cysteine on a gold 19 cluster was investigated using the Amsterdam Density Functional (ADF) program.[3] The inner electrons were frozen for Au (up to 4f), S (2p), N (1s), O (1s) and C (1s). The core was modeled by a relativistically corrected pseudopotential using the ZORA (zero order regular approximation) method. A double–ζ basis set was used. The local part of the exchange and correlation functional was modeled using a Vosko, Wilk, Nuisar parametrization of the electron gas,[4] whereas the non-local part of the functional was modeled using the Becke correction for the exchange[5] and the Perdew correction for the correlation.[6] More computational details can be found elsewhere.[7] The adsorption of deprotonated N-acetyl-*L*-cysteine on Au_4 clusters was studied using Gaussian03.[8] For the gold atoms an effective core potential was used. The calculations were performed using the b3pw91[9, 10] functional and a LanL2DZ basis set[11] for Au and 6-31G(d,p) basis set[12] for all other atoms. Vibrational frequencies were scaled by a factor of 0.98. IR absorption and VCD spectra were constructed from calculated dipole and rotational strengths assuming Lorentzian band shape with a half-width at half-maximum of 4 cm^{-1}.

A.5. References (including full references 16 and 17)

[1] T. Bürgi, A. Vargas, A. Baiker, *J. Chem. Soc. Perkin Trans. 2* **2002**, 1596.

[2] T. Bürgi, U. Urakawa, B. Behzadi, K.-H. Ernst, A. Baiker, *New. J. Chem.* **2004**, *28*, 332.

[3] E. J. Baerends, J. Autschbach, Bérces, A., B. C., P. M. Boerrigter, L. Cavallo, D. P. Chong, L. Deng, R. M. Dickson, D. E. Ellis, L. Fan, T. H. Fischer, C. Fonseca Guerra, S. J. A. van Gisbergen, J. A. Groeneveld, O. V. Gritsenko, M. Grüning, F. E. Harris, P. van den Hoek, H. Jacobsen, G. van Kessel, F. Kootstra, E. van Lenthe, D. A. McCormack, V. P. Osinga, S. Patchkovskii, P. H. T. Philipsen, D. Post, C. C. Pye, W. Ravenek, P. Ros, P. R. T. Schipper, G. Schreckenbach, J. G. Snijders, M. Sola, M. Swart, D. Swerhone, G. te Velde, P. Vernooijs, L. Versluis, O. Visser, E. van Wezenbeek, G. Wiesenekker, S. K. Wolff, T. K. Woo, T. Ziegler, 2004.01 ed., SCM, Amsterdam, **2004**.

[4] S. H. Vosko, L. Wilk, M. Nusair, *Can. J. Phys.* **1980**, *58*, 1200.

[5] A. D. Becke, *Phys. Rev. A* **1988**, *38*, 3098.

[6] J. P. Perdew, *Phys. Rev. B* **1986**, *33*, 8822.

[7] A. Vargas, T. Bürgi, A. Baiker, *J. Catal.* **2004**, *222*, 439.

[8] M. J. Frisch, G. W. Trucks, H. B. Schlegel, G. E. Scuseria, M. A. Robb, J. R. Cheeseman, J. A. Montgomery, T. Vreven, K. N. Kudin, J. C. Burant, J. M. Millam, S. S. Iyengar, J. Tomasi, V. Barone, B. Mennucci, M. Cossi, G. Scalmani, N. Rega, G. A. Petersson, H. Nakatsuji, M. Hada, M. Ehara, K. Toyota, R. Fukuda, J. Hasegawa, M. Ishida, T. Nakajima, Y. Honda, O. Kitao, H. Nakai, M. Klene, X. Li, J. E. Knox, H. P. Hratchian, J. B. Cross, C. Adamo, J. Jaramillo, R. Gomperts, R. E. Stratmann, O. Yazyev, A. J. Austin, R. Cammi, C. Pomelli, J. W. Ochterski, P. Y. Ayala, K. Morokuma, G. A. Voth, P. Salvador, J. J. Dannenberg, V. G. Zakrzewski, S. Dapprich, A. D. Daniels, M. C. Strain, O. Farkas, D. K. Malick, A. D. Rabuck, K. Raghavachari, J. B. Foresman, J. V. Ortiz, Q. Cui, A. G. Baboul, S. Clifford, J. Cioslowski, B. B. Stefanov, G. Liu, A. Liashenko, P. Piskorz, I. Komaromi, R. L. Martin, D. J. Fox, T. Keith, M. A. Al-Laham, C. Y. Peng, A. Nanayakkara, M.

Challacombe, P. M. W. Gill, B. Johnson, W. Chen, M. W. Wong, C. Gonzalez, J. A. Pople, Rev. C.01 ed., Gaussian, Inc., Wallingford CT, **2003**.

[9] A. D. Becke, *J. Chem. Phys.* **1993**, *98*, 5648.

[10] J. P. Perdew, J. A. Chevary, S. H. Vosko, K. A. Jackson, M. R. Pederson, D. J. Singh, C. Fiolhais, *Phys. Rev. B* **1992**, *46*, 6671.

[11] P. J. Hay, W. R. Wadt, *J. Chem. Phys.* **1985**, *82*, 270.

[12] R. Ditchfield, W. J. Hehre, J. A. Pople, *J. Chem. Phys.* **1971**, *54*, 724.

Appendix

B

Supporting Information of Chapter 3

B.1. Percentage by Weight

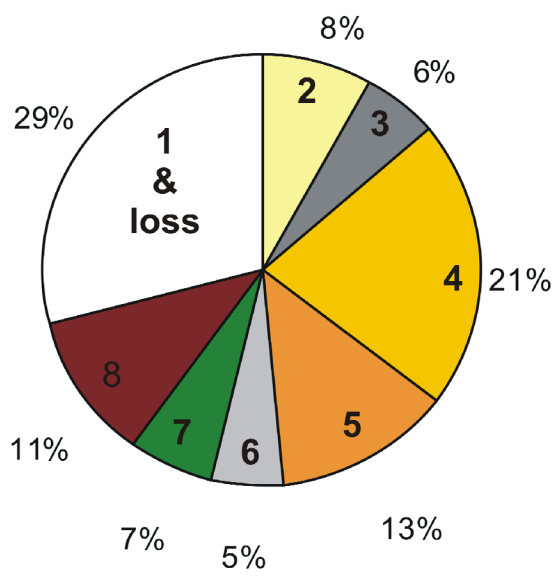

Figure B.1 : (Top) Percentage by weigth of the gold nanoparticles protected with NILC after size separation by PAGE. (Bottom) Photography of the size separated componds **2-8** in ultrafiltration devices which were used for fast purification.

B.2. UV-vis and CD Spectra

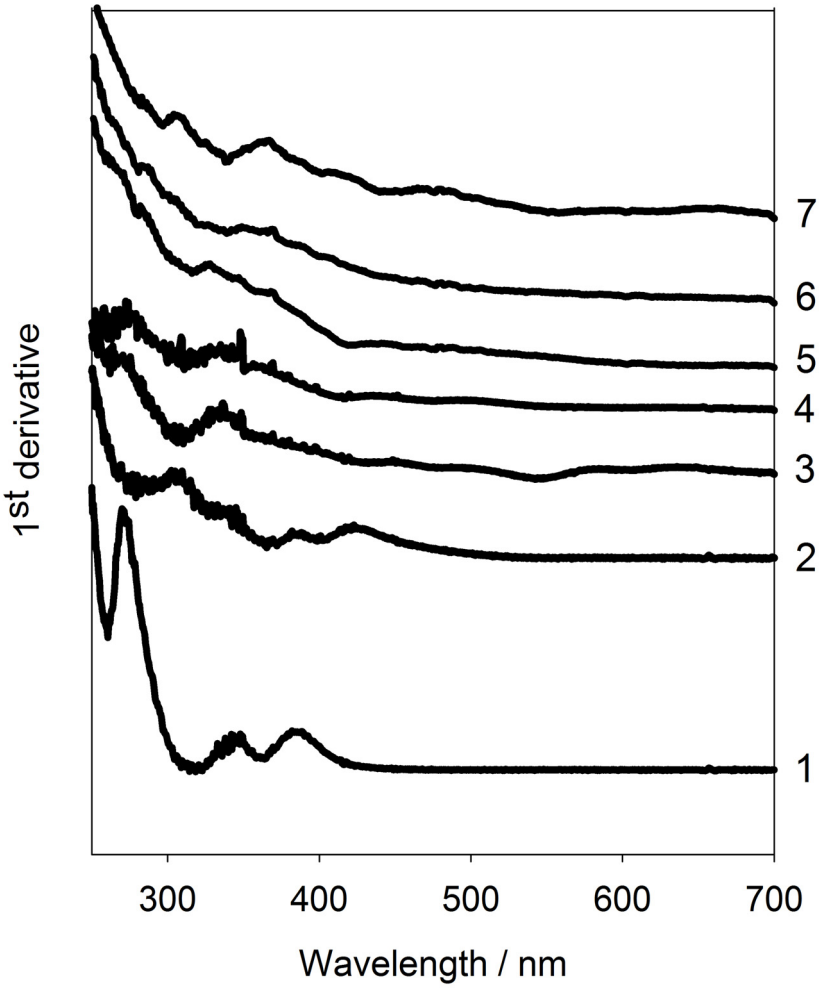

Figure B.2 : First derivative of the UV-vis spectra of separated compounds **1-7** of gold particles protected with N-isobutyryl-*L*-cysteine. The curves were derived from the spectra given in **Figure 3.7**.

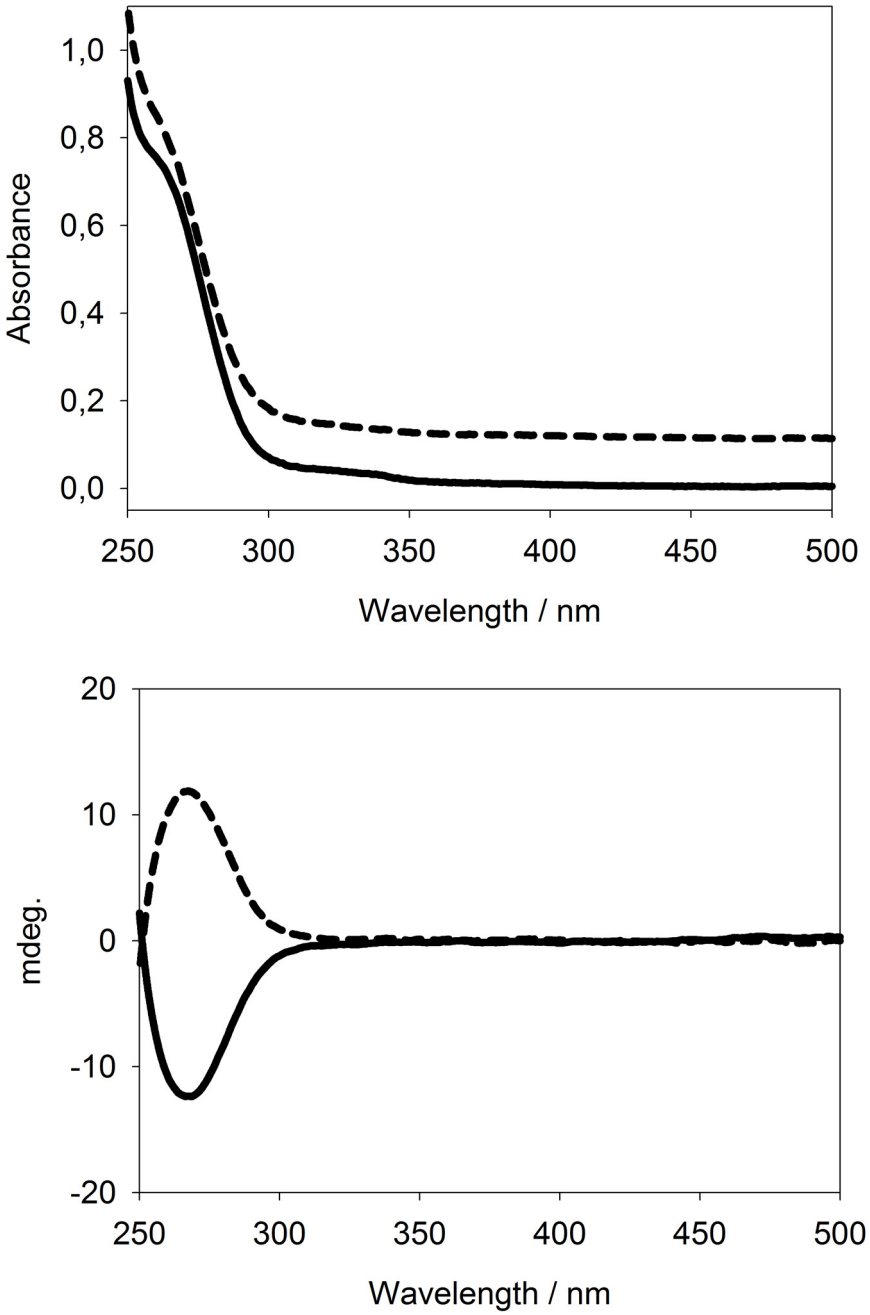

Figure B.3 : UV-vis and ECD spectra of N-isobutyryl-*L*-cysteine (dashed line) N-isobutyryl-*D*-cysteine (solid line). The UV-vis spectra were normalized to one absorbance unit at 250 nm.

B.3. Anisotropy Factor

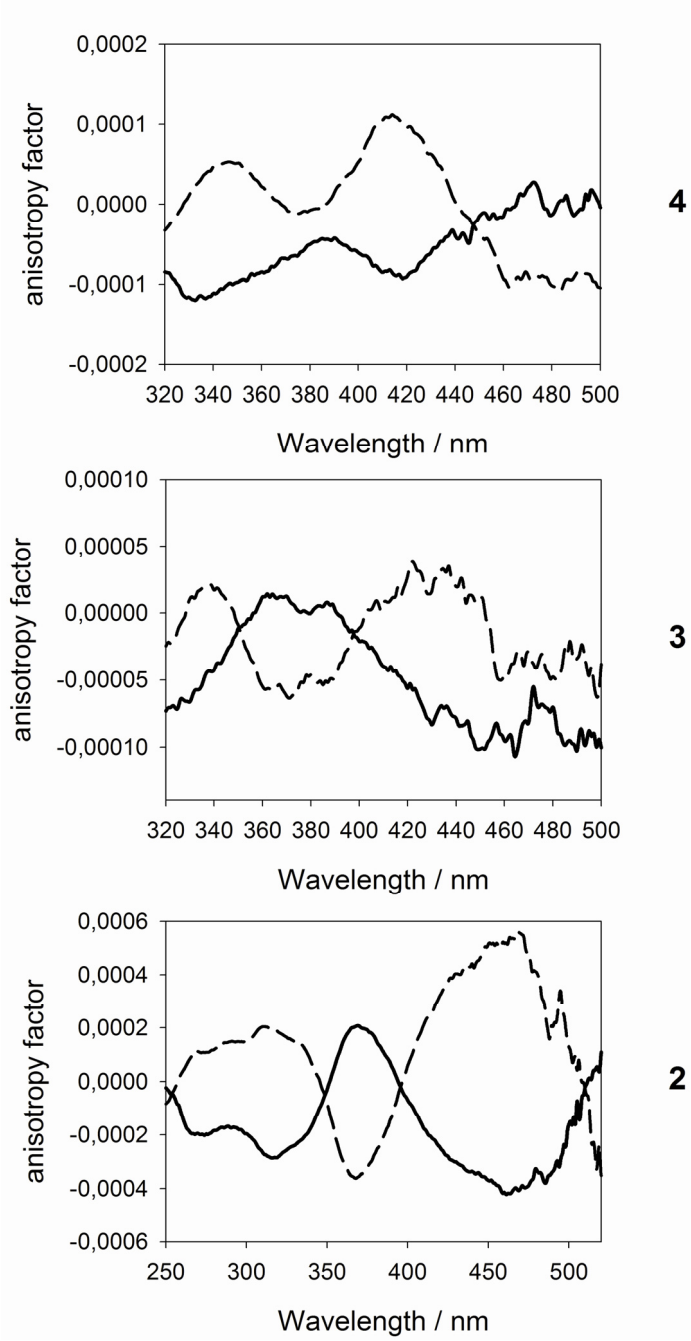

Figure B.4 : Anisotropy factors g for compounds **2-4**. $g = \Delta\varepsilon/\varepsilon \approx \theta/(33*A)$, where ε is the extinction coefficient, A is the absorbance and θ is the ellipticity.

B.4. NMR

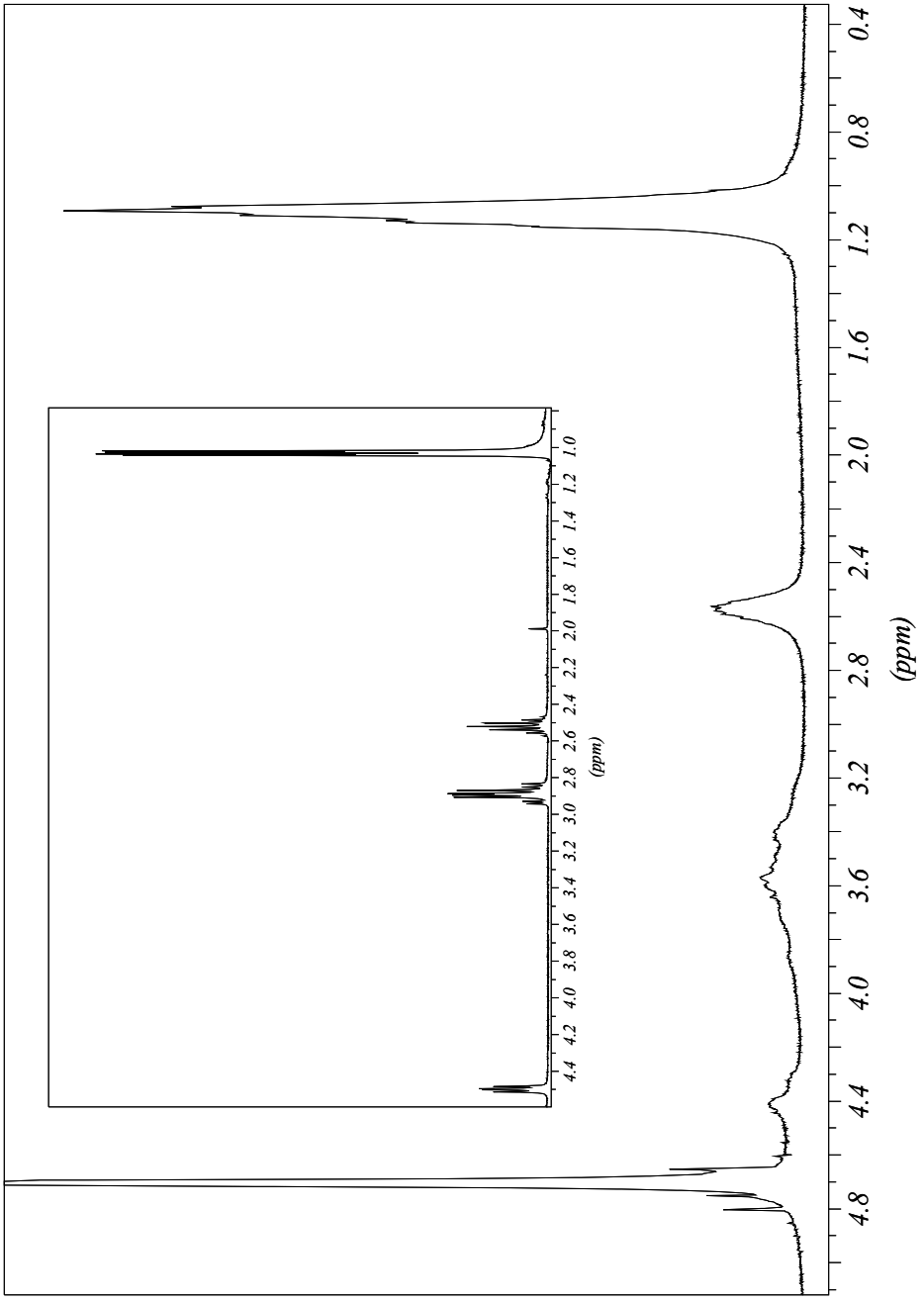

Figure B.5 : 400 MHz ^{1}H NMR spectrum of N-isobutyryl-*L*-cysteine MPNs in D_2O at 298 K before separation by gel electrophoresis. The inset shows the free ligand for comparison.

B.5. TEM

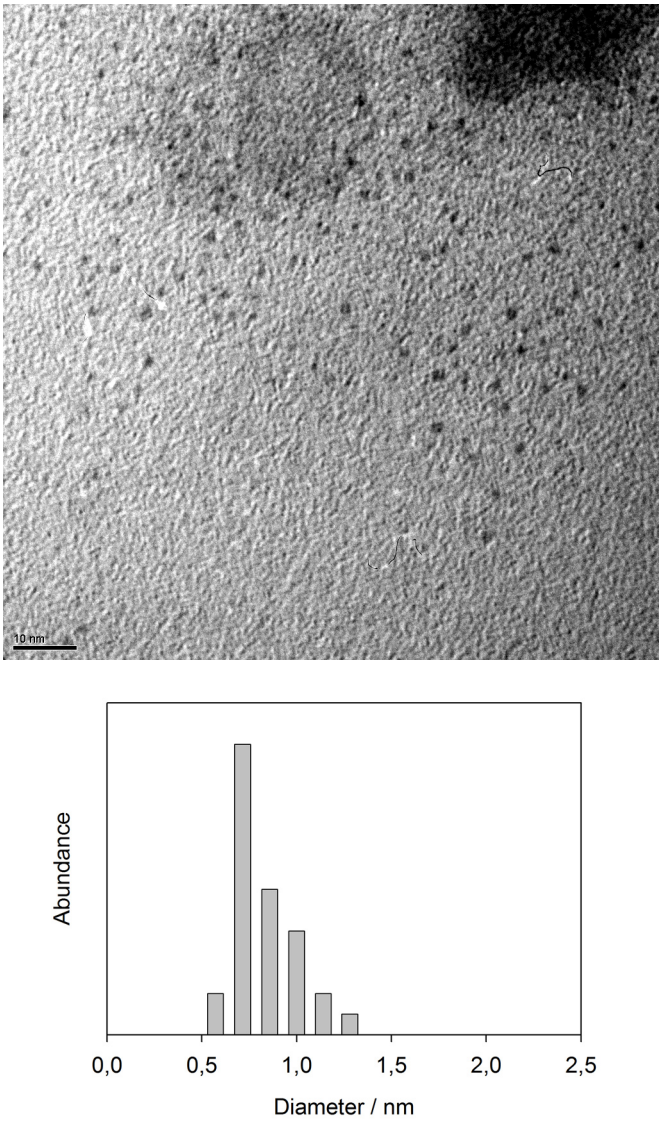

Figure B.6 : TEM of compound **2** of N-isobutyryl-*L*-cysteine MPNs after gel electrophoresis separation (top). The bar corresponds to 10 nm. Particle size distribution derived from the TEM graphs (bottom).

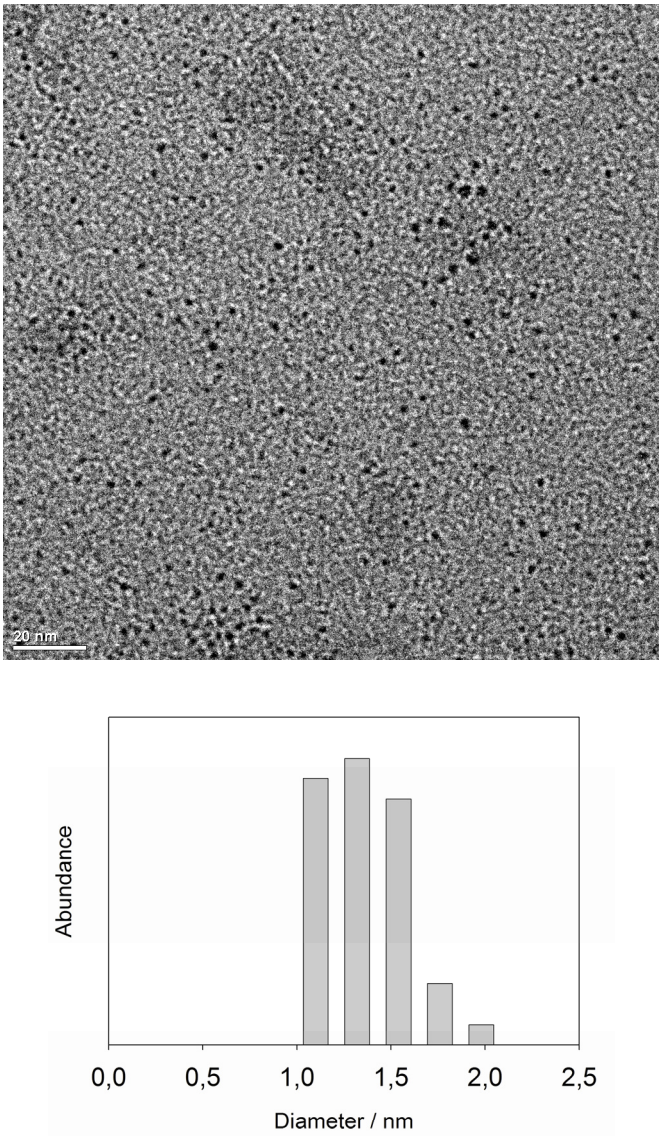

Figure B.7 : TEM of compound **7** of N-isobutyryl-*L*-cysteine MPNs after gel electrophoresis separation (top). The bar corresponds to 20 nm. Particle size distribution derived from the TEM graphs (bottom).

B.6. Model of Chiral Footprint

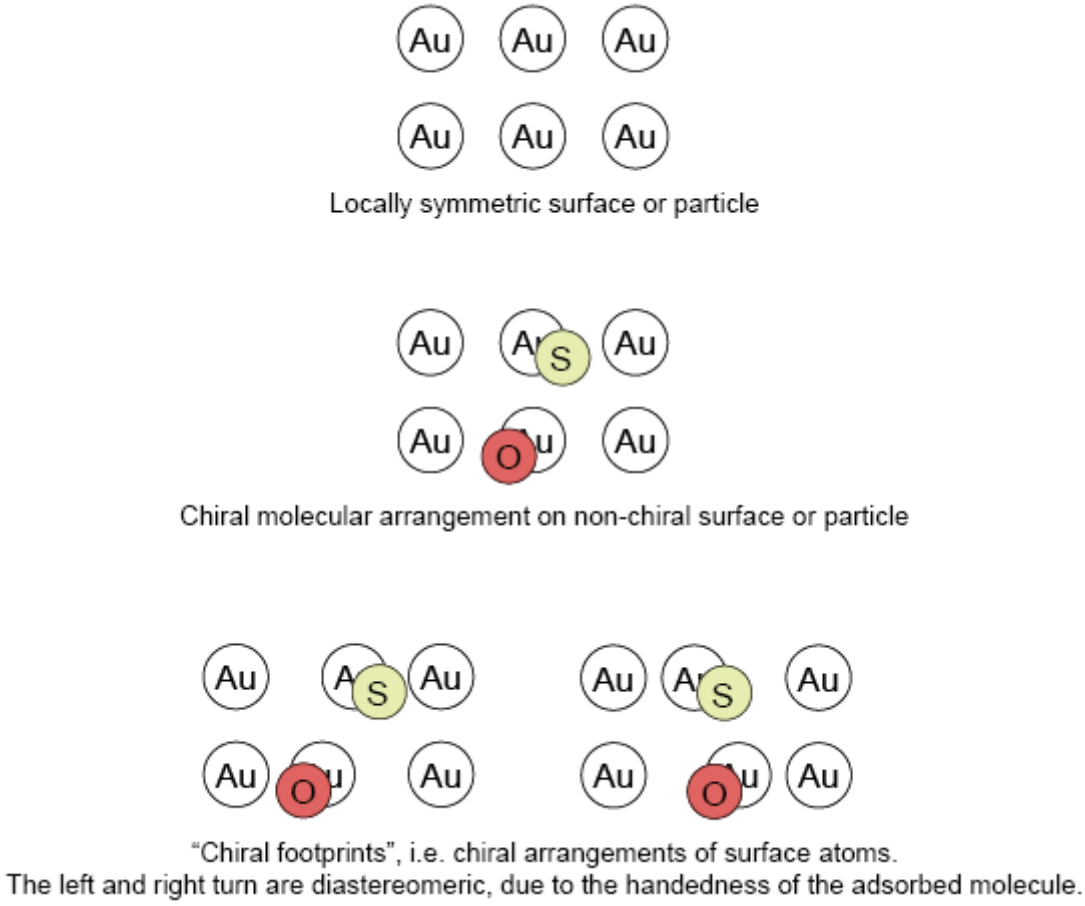

Figure B.8 : Model of inducing a chiral "footprint" on a surface or on a particle. The yellow and red circles represent the sulfur and oxygen atoms of a chiral molecule, which interacts with the surface via a twofold interaction. Top: locally non-chiral surface or particle. Middle: A chiral molecular arrangement on a non-chiral surface or particle. Bottom: Chiral "footprint" induced by the chiral molecular arrangement. The situations on the left and on the right correspond to mirror image situations as concerns the arrangement of the gold atoms. Because the adsorbed molecule is chiral, the left- and right-handed twist of the surface atoms for one enantiomer of the molecule yields diastereomeric situations, which have, in the general case, different energy and therefore one turn is preferred over the other.

B.7. Reference (complete Ref. 34)

[34] Frisch, M. J.; Trucks, G. W.; Schlegel, H. B.; Scuseria, G. E.; Robb, M. A.; Cheeseman, J. R.; Montgomery, J. A.; Vreven, T.; Kudin, K. N.; Burant, J. C.; Millam, J. M.; Iyengar, S. S.; Tomasi, J.; Barone, V.; Mennucci, B.; Cossi, M.; Scalmani, G.; Rega, N.; Petersson, G. A.; Nakatsuji, H.; Hada, M.; Ehara, M.; Toyota, K.; Fukuda, R.; Hasegawa, J.; Ishida, M.; Nakajima, T.; Honda, Y.; Kitao, O.; Nakai, H.; Klene, M.; Li, X.; Knox, J. E.; Hratchian, H. P.; Cross, J. B.; Adamo, C.; Jaramillo, J.; Gomperts, R.; Stratmann, R. E.; Yazyev, O.; Austin, A. J.; Cammi, R.; Pomelli, C.; Ochterski, J. W.; Ayala, P. Y.; Morokuma, K.; Voth, G. A.; Salvador, P.; Dannenberg, J. J.; Zakrzewski, V. G.; Dapprich, S.; Daniels, A. D.; Strain, M. C.; Farkas, O.; Malick, D. K.; Rabuck, A. D.; Raghavachari, K.; Foresman, J. B.; Ortiz, J. V.; Cui, Q.; Baboul, A. G.; Clifford, S.; Cioslowski, J.; Stefanov, B. B.; Liu, G.; Liashenko, A.; Piskorz, P.; Komaromi, I.; Martin, R. L.; Fox, D. J.; Keith, T.; Al-Laham, M. A.; Peng, C. Y.; Nanayakkara, A.; Challacombe, M.; Gill, P. M. W.; Johnson, B.; Chen, W.; Wong, M. W.; Gonzalez, C.; Pople, J. A.; Rev. C.01 ed.; Gaussian, Inc.: Wallingford CT, **2003**.

List of Publications

List of publications related to the thesis

1. Gautier, C.; Bürgi, T. Vibrational Circular Dichroism of N-acetyl-L-cysteine Protected Gold Nanoparticles. *Chem. Commun.* **2005,** 43, 5393-5395 (Chapter 2 of the thesis).

2. Gautier, C.; Bieri, M.; Dolamic, I.; Angeloni, S.; Boudon, J.; Bürgi, T. Probing Chiral Nanoparticles and Surfaces by Infrared Spectroscopy *Chimia* **2006,** 60, 777 - 7782 (invited article).

3. Gautier, C.; Bürgi, T. Chiral N-isobutyryl-cysteine Protected Gold Nanoparticles: Preparation, Size Selection, and Optical Activity in the UV-vis and Infrared. *J. Am. Chem. Soc.* **2006,** 128, 11079-11087 (Chapter 3 of the thesis).

4. Bieri, M.; Gautier, C.; Bürgi, T. Probing Chiral Interfaces by Infrared Spectroscopic Methods. *Chem. Phys. Phys. Chem.* **2007,** 9, 671-685 (invited article).

5. Gautier, C.; Taras, R.; Gladiali, S.; Bürgi, T. Chiral 1,1'-binaphthyl-2,2'-dithiol-Stabilized Gold Clusters: Size Separation and Optical Activity in the UV-vis. *Chirality* **2008,** 20, 486-493 (invited article chapter 5 of the thesis)

6. Dolamic, I.; Gautier, C.; Boudon, J.; Shalkevich, N.; Bürgi, T. Adsorption of Thiol-Protected Gold Nanoparticles on TiO_2 and their Behavior Under UV Light Irradiation. *J. Phys. Chem. C* **2008**, accepted.

7. Gautier, C.; Bürgi, T. Vibrationnel Circular Dichroisme of 1,1'-binaphthyl-2,2'-dithiol Protected Gold Nanoparticles. *J. Phys. Chem. B* **2008,** (in preparation, chapter 5 of the thesis).

8. Gautier, C.; Bürgi, T., Chiral Nanoparticles. In *Chirality at the Nanoscale: Nanoparticles, Surfaces, Materials and More*, Wiley-VCH Weinheim, **2008** (invited book chapter, accepted, chapter 1 of the thesis).

9. Gautier, C.; Bürgi, T. Chiral Inversion of Gold Nanoparticles. *J. Am. Chem. Soc.* **2008,** (accepted, chapter 6 of the thesis).

10. Gautier, C.; Bürgi, T. Chiral Metal Surfaces and Nanoparticles. *Chimia.* **2008,** (invited articles, submitted).

Other publication

11. Girard, N.; Gautier, C.; Malassene, R.; Hurvois, J.-P.; Moinet, C.; Toupet, L. Dearomatization of N-Phenyl-2,6-dialkylpiperidines: Practical Synthesis of (±)-Solenopsin A and (±)-Dihydropinidine. *Synlett* **2004,** 11, 2005-2009.

Curriculum Vitae

Cyrille Gautier, Born January, 1979, France.

Education

1998-2000	Bachelor in Material Sciences, Rennes I University, France.
2000-2003	Master in Molecular Chemistry, Rennes I University, France.
2004-2008	Ph.D. Thesis, Surface Spectroscopy and Nanosciences (SS&N) Lab., Microtechnique Institute, Neuchâtel, Switzerland. Thesis Advisor: Prof. T. Bürgi.

Professional

2008	Post-doct, SS&N and Metallor technologies SA, Neuchâtel, Switzerland. World Gold Council Fellowship, London, United Kingdom.

Internship

2001	Electrochemistry Lab., Institut de Chimie, Rennes I University, France. « Syntheses Toward Martinelline ». Advisor Prof. J-P. Hurvois.

Internship (continued)

2002	Organic Chemistry department, IISC, Bangalore, India. « Syntheses of Chiral Dendron Designed with Bile Acid ». Advisor Prof. U. Maitra.
2003	Electrochimistry Lab., Institut de Chimie, Rennes I University, France. « Diastereoselective Syntheses of 2,6-disubstitued Piperidin ». Prof. J-P. Hurvois.

Conferences

09/2004	Summer school on physical-chemistry, Villard-sur-Ollon, Switzerland. *Poster presentation*.
10/2005	Swiss Chemical Society (SCS) Fall Meeting, Lausanne, Switzerland. *Poster presentation*.
04/2006	Nanopowder-day, EMPA, Dubendorf, Switzerland. *Oral presentation*.
09/2006	Swiss National Supercomputing Centre (CSCS) User Day, Manno, Switzerland. *Poster presentation.*
10/2006	Swiss Chemical Society (SCS) Fall Meeting, Zurick, Switzerland. *Poster presentation*.
09/2007	Summer school on Nanochemistry, Villard-sur-Ollon, Switzerland. *Poster presentation*.
10/2007	Swiss Chemical Society (SCS) Fall Meeting, Lausanne, Switzerland. *Oral presentation*.

10/2007 International conference, Chirality at the Nanoscale, Barcelona, Spain. *Award for the best oral presentation*.